Leg 205 Preliminary Report

Fluid Flow and Subduction Fluxes across the Costa Rica Convergent Margin: Implications for the Seismogenic Zone and Subduction Factory

2 September–6 November 2002

Shipboard Scientific Party

Ocean Drilling Program
Texas A&M University
1000 Discovery Drive
College Station TX 77845-9547
USA

January 2003

PUBLISHER'S NOTES

This report was prepared from shipboard files by scientists who participated in the cruise. The report was assembled under time constraints and does not contain all works and findings that will appear in the *Initial Reports* of the ODP *Proceedings*. Reference to the whole or to part of this report should be made as follows:

Shipboard Scientific Party, 2003. Leg 205 Preliminary Report. *ODP Prelim. Rpt.,* 105 [Online]. Available from World Wide Web: <http://www-odp.tamu.edu/publications/prelim/205_prel/205PREL.PDF>. [Cited YYYY-MM-DD]

Distribution: Electronic copies of this series may be obtained from the Ocean Drilling Program's World Wide Web site at http://www-odp.tamu.edu/publications.

This publication was prepared by the Ocean Drilling Program, Texas A&M University, as an account of work performed under the international Ocean Drilling Program, which is managed by Joint Oceanographic Institutions, Inc., under contract with the National Science Foundation. Funding for the program is provided by the following agencies:

Australia/Canada/Chinese Taipei/Korea Consortium for Ocean Drilling
Deutsche Forschungsgemeinschaft (Federal Republic of Germany)
Institut National des Sciences de l'Univers–Centre National de la Recherche Scientifique (INSU-CNRS; France)
Ocean Research Institute of the University of Tokyo (Japan)
National Science Foundation (United States)
Natural Environment Research Council (United Kingdom)
European Science Foundation Consortium for Ocean Drilling (Belgium, Denmark, Finland, Iceland, Ireland, Italy, The Netherlands, Norway, Portugal, Spain, Sweden, and Switzerland)
Marine High-Technology Bureau of the State Science and Technology Commission of the People's Republic of China

DISCLAIMER

The following scientists and participants were aboard the *JOIDES Resolution* for Leg 205 of the Ocean Drilling Program:

SHIPBOARD SCIENTIFIC PARTY

Julie D. Morris
Co-Chief Scientist
Department of Earth and Planetary Sciences
Washington University
One Brookings Drive
CB 1169
St. Louis MO 63130-4899
USA
Work: (314) 935-6926
Fax: (314) 935-7361
jmorris@levee.wustl.edu

Heinrich W. Villinger
Co-Chief Scientist
Fachbereich Geowissenschaften
Universität Bremen
Postfach 330 440
28334 Bremen
Germany
Work: (49) 421-218-4509
Fax: (49) 421-218-7163
vill@uni-bremen.de

Adam Klaus
Staff Scientist
Ocean Drilling Program
Texas A&M University
1000 Discovery Drive
College Station TX 77845-9547
USA
Work: (979) 845-3055
Fax: (979) 845-0876
aklaus@odpemail.tamu.edu

Dawn M. Cardace
Sedimentologist
Department of Earth and Planetary Sciences
Washington University
Campus Box 1169, One Brookings Drive
St. Louis MO 63130-4899
USA
Work: (314) 935-9088
Fax: (314) 935-7361
cardace@levee.wustl.edu

Valerie M.C. Chavagnac
Petrologist
School of Ocean and Earth Sciences
Southampton Oceanography Centre
Isotope Geochemistry Unit
European Way
Southampton SO14 3ZH
United Kingdom
Work: (44) 23 8059 6546
Fax: (44) 23 8059 6554
vmcc@soc.soton.ac.uk

Peter D. Clift
Sedimentologist
Department of Geology and Geophysics
Woods Hole Oceanographic Institution
MS 22
Woods Hole MA 02543
USA
Work: (508) 289-3437
Fax: (508) 457-2187
pclift@whoi.edu

Matthias Haeckel
Organic Geochemist
Department of Oceanography
Dalhousie University
1355 Oxford Street
Halifax NS B3H 4J1
Canada
Work: (902) 494-3249
Fax: (902) 494-3877
matthias.haeckel@dal.ca

Toshio Hisamitsu
Paleomagnetist
Institute for Frontier Research on Earth Evolution (IFREE)
Japan Marine Science and Technology Center (JAMSTEC)
Marine and Core Research Center
Kochi University
2-5-1, Akebono-cho
Kochi 780-8520
Japan
Work: (81) 88-844-8629
Fax: (81) 88-844-8624
hisa@cc.kochi-u.ac.jp

Miriam Kastner
Inorganic Geochemist
Scripps Institution of Oceanography
University of California, San Diego
Geoscience Research Division
9500 Gilman Drive
La Jolla CA 92093-0212
USA
Work: (858) 534-2065
Fax: (858) 822-4945
mkastner@ucsd.edu

Marion Pfender
Physical Properties Specialist
Geowissenschaften 5
Universität Bremen
Postfach 33 04 40
28334 Bremen
Germany
Work: (49) 421- 2187165
Fax: (49) 421-2187163
pfender@uni-bremen.de

Demian M. Saffer
Physical Properties Specialist/Logging Scientist
Department of Geology and Geophysics
University of Wyoming
16th and Gibbon Streets
Laramie WY 82071-3006
USA
Work: (307) 766-2981
Fax: (307) 766-6679
dsaffer@uwyo.edu

Cara Santelli
Microbiologist
Department of Marine Chemistry and Geochemistry
Woods Hole Oceanographic Institution
McLean Laboratory
MS 8
Woods Hole MA 02543
USA
Work: (508) 289-3681
Fax: (508) 457-2183
csantelli@whoi.edu

Burkhard Schramm
Petrologist
Universität Bremen
FB 5-Geowissenschaften Klagenfurter Strasse
28334 Bremen
Germany
Work: (49) 421 218 7766
Fax: (49) 421 218 9460
bschramm@uni-bremen.de

Elizabeth J. Screaton
Physical Properties Specialist
Department of Geological Sciences
University of Florida
241 Williamson, Box 112120
Gainesville FL 32611
USA
Work: (352) 392-4612
Fax: (352) 392-9294
screaton@geology.ufl.edu

Evan A. Solomon
Inorganic Geochemist
Scripps Institution of Oceanography
University of California, San Diego
9500 Gilman Drive, Mail Stop 0208
La Jolla CA 92093-0208
USA
Work: (858) 822-0988
Fax: (858) 822-4945
esolomon@ucsd.edu

Moe Kyaw Thu
Logging Staff Scientist
Institute for Frontier Research on Earth Evolution (IFREE)
Japan Marine Science and Technology Center
2-15 Natsushima Cho
Yokosuka 237-0061
Japan
Work: (468) 67-9798
Fax: (468) 67-9775
moe@jamstec.go.jp

Paola Vannucchi
Structural Geologist
Dipartimento di Scienze della Terra
Università degli Studi di Modena
Piazzale S. Eufemia, 19
41100 Modena
Italy
Work: (39) 59-205-5863
Fax: (39) 59-205-5887
paolav@geo.unifi.it

Michael Strasser
Sedimentologist (Student Trainee)
Earth Science
Geology Diploma Student
Eidgenössische Technische Hochschule-Zentrum
8092 Zürich
Switzerland
Work: (41) 1 632 3701
michastr@student.ethz.ch

TRANSOCEAN OFFICIALS

Thomas Hardy
Master of the Drilling Vessel
Overseas Drilling Ltd.
707 Texas Avenue South, Suite 213D
College Station TX 77840-1917
USA

Jose Esteves
Drilling Superintendent
Overseas Drilling Ltd.
707 Texas Avenue South, Suite 213D
College Station TX 77840-1917
USA

ODP SHIPBOARD PERSONNEL AND TECHNICAL REPRESENTATIVES

Christopher Bennight
Marine Laboratory Specialist (Chemistry)

Lisa Brandt
Marine Laboratory Specialist (Chemistry)

Lisa Crowder
Marine Laboratory Specialist (Underway Geophysics)

John Davis
Marine Computer Specialist

Richard Dixon
Drilling Engineer

Charles Endris
Marine Laboratory Specialist (X-Ray)

Javier Espinosa
Schlumberger Logging Engineer

Randy Gjesvold
Marine Electronics Specialist

Ted Gustafson
Marine Laboratory Specialist (Downhole Tools/Thin Sections)

Burnette Hamlin
Laboratory Officer

Stan Hammon
Marine Laboratory Specialist (Physical Properties)

Scott Herman
Marine Laboratory Specialist (Paleomagnetism)

Michiko Hitchcox
Marine Laboratory Specialist (Yeoperson)

Michael Hodge
Marine Computer Specialist

Dwight Hornbacher
Programmer

Eric Jackson
Marine Laboratory Specialist (Core)

Michael Meiring
Marine Electronics Specialist

Soichi Moriya
Marine Works Japan, LTD. Marine Laboratory Specialist (Core)

Chieh Peng
Assistant Laboratory Officer/Storekeeper

Thomas Pettigrew
Operations Manager

Cyndi Prince
Marine Laboratory Specialist (Photographer)

Paula Weiss
Marine Laboratory Specialist (Curator)

ABSTRACT

The character of the incoming plate subducting at convergent margins and the processes affecting it as it passes below the shallow forearc may play a major role in the nature and extent of hazardous intraplate seismicity as well as the magnitude of volcanism and the chemistry of lavas produced in the overlying volcanic arc. The fate of incoming sediments and ocean crust and of their associated volatiles as they pass through the shallow levels of a subduction zone (0–50 km depth) has profound effects on the behavior of the seismogenic zone, which produces most of the world's destructive earthquakes and tsunamis. Fluid pressure and sediment porosity influence fault localization, deformation style, and strength and may control the updip limit of the seismogenic zone. Fluids within both fault zones and sediments underthrust at the trench affect early structural development and are a key agent in transport of chemical species. The mineralogy and chemistry of any subducted sediments and their dehydration reactions during subduction may control the physical properties of the deeper subduction interface and, hence, the updip and downdip limits of the seismogenic zone wherein interplate earthquakes are generated. The mineralogy, composition, and volatile content of the slab, transformed during its progress through the shallow subduction zone, will govern the flux of fluids or melts from slab to mantle wedge, which is an important control on the extent of mantle melting and formation of arc lavas.

Costa Rica is an important area for studies of the seismogenic zone and subduction factory for several reasons. As one of the few modern arcs subducting a carbonate-rich sediment section, Central America permits study of CO_2 recycling through a subduction zone. Changes along strike in seismicity, plate coupling, and volume and composition of the arc lavas (between Nicaragua and Costa Rica) appear to correlate with changes in sediment dynamics. This balance between sediment accretion, underplating, erosion, and subduction may ultimately result from changing bathymetry, thermal structure, or hydrological behavior along the margin.

Science objectives for Leg 205 have two primary foci, both related to seismogenic zone and subduction factory questions. The first is to determine the igneous and alteration history of the uppermost part of the downgoing plate at reference Site 1253, along with the inferred distribution of fracture permeability in the core and borehole. The second is to characterize and monitor two of the three hydrological systems inferred from Leg 170 results: in basement at Site 1253 and along the décollement (or upper fault zone) at Sites 1254 and 1255. These goals will be accomplished by (1) targeted coring of selected intervals, (2) downhole temperature and pressure measurements, (3) logging at Site 1253, and (4) installation of long-term observatories (modified CORK-IIs) to monitor temperature and pressure and to sample fluids and gases in each of the hydrologic systems. In the décollement zone, instruments will also be deployed to attempt to measure fluid flow rates. Temporal variation of fluid composition in the sealed-off intervals will be obtained by using osmotic fluid samplers. The samplers and temperature loggers will be recovered for analysis 1 to 2 years after installation, pressure data will be downloaded, and new samplers and temperature probes will be installed.

Science objectives specific to the reference Site 1253 center on mass flux to the subduction trench (and ultimately the volcanic arc) as well as the permeability and hydrology of the downgoing igneous section. In conjunction with Leg 170, the coring at Leg 205 provides samples that will allow an estimate of the sedimentary carbonate flux to the trench to be made. Although not a primary focus of the cruise, coring from the two legs also provides an extensive ash stratigraphy as the plate moved from near the Galapagos to outboard of the Middle America Trench. Leg 205 coring into the igneous section will be used to investigate the extent of sill emplacement and their origin and contribution to the bulk composition of the subducting plate along with their tectonic and magmatic implications. If a transition to basement is

recognized in the lower igneous section, the extensive recovery of Leg 205 can be used to determine the primary and secondary mineralogy and bulk chemistry of the uppermost part of the downgoing plate. These results can be integrated with those from the deep basement hole planned for Leg 206 (also on the part of the Cocos plate generated at the East Pacific Rise) to constrain the composition of the oceanic crust subducting at this margin. Microbial samples were taken (and contamination tests run) from the sedimentary horizons and from larger veins and fractures in the lower part of the igneous sections for postcruise studies. Logging, coring, and physical properties measured during Leg 205 establish key characteristics relevant to fluid flow and deformation, such as porosity, density, fracture distribution, orientation, and strength, ultimately to be used in conjunction with pressure, temperature, and chemical data from the CORK-II seafloor observatory.

Science objectives for the prism Sites 1254 and 1255 center on the development of the décollement, the use of pore fluid chemistry to infer local diagenetic and deeper dehydration reactions, and the installation of two CORK-IIs, ideally, in the region of maximum fluid flow within the décollement or related fault zones. Leg 205 coring intersected a thrust fault, as well as the décollement zone, in two locations slightly different from the two sites cored during Leg 170. Together, they provide the opportunity to examine variability over short distances in the development of the fault zones, the role of variable sediment lithology in strain partitioning and the style of décollement development, and the interplay between structural features and zones of fluid flow. Postcruise analysis of structural fabrics and experiments on whole-round samples will better constrain hydrological modeling and permit integration of fluid flow and deformation models. Sediments, gases and interstitial waters collected in the thrust fault and décollement during Legs 170 and 205 have some chemical features expected of deeply sourced fluids and provide samples for postcruise chemical and isotopic analyses, as well as for identifying key horizons for the CORK-II long-term seafloor observatory. Whole-round samples from the décollement and contamination testing allow for postcruise microbiological investigations to determine the resident microbial ecology of the zone for comparison to eventual microbial experiments on fluids collected from the décollement.

Installation of long-term seafloor observatories was a major focus of Leg 205. Briefly, the CORK-II design is built around and within a 4½-in casing string and monitors a single interval below a single packer. Deployments here combine pressure monitoring as used during Leg 196 with retrievable OsmoSamplers at the horizon of interest (containing osmotic fluid and gas samplers and temperature loggers.) At the prism site, OsmoFlow meters are included, which use the dilution of a chemical tracer injected at a constant rate to estimate flow rates.

At Site 1253 on the incoming plate, we cored 230 m, including ~170 m within two igneous units, where the upper unit is a 30-m-thick gabbro sill with sediments above and below. We also logged up to 150 m, primarily in the lower igneous section, and installed a CORK-II observatory. An exceptionally thick ash from Central America was recovered just above the sill, deposited when the plate was >1650 km from the arc; grain size and thickness imply an eruption comparable to the largest ever recorded from Toba Volcano. Interstitial water chemistry from above and below the sill indicates that there is fluid flow, of near-seawater composition, at depth in the igneous section. The lower igneous unit is composed of microgabbro with occasional layers of fine-grained gabbro and rare intervals with basaltic texture; all are of basaltic composition. It may be an exceptionally thick sill composed of multiple intrusions or a series of often thick and slowly cooled lava flows of oceanic crust created at the East Pacific Rise or represent a transition between extrusive and intrusive activity at the ridge. It is more extensively altered and fractured below ~510–513 meters below seafloor (mbsf). A CORK-II was installed, with temperature probes and osmotic fluid and gas samplers at 497–504 mbsf and also at 512–519 mbsf. Pressure monitoring is within the upper OsmoSampler zone and above the packer at ~453 mbsf.

At Site 1254 in the prism, we cored through a thrust fault zone at ~197–219 mbsf and the décollement zone at 338–365 mbsf. Despite drilling disturbance, it is possible to see that deformation, particularly brecciation and brittle shearing, generally increase downward in both zones but with concentration of shear along specific horizons. High concentrations of thermogenic hydrocarbons in the gases and sediments and unique pore water chemistry are seen within both zones, indicating advection of deeply sourced fluids preferentially along sandy horizons showing brittle fracture. The base of the décollement lies within the uppermost part of the underthrust section at Site 1254, as opposed to between the prism and underthrust sediment at Site 1040, which is 50 m away. Three attempts were made to install a CORK-II at Site 1254, twice into the décollement zone and once into the shallower thrust fault. All failed because of a combination of operational difficulties and hole conditions.

At Site 1255, ~0.4 km inboard of the deformation front, we conducted very limited coring and installed a CORK-II into the plate boundary fault. The base of the décollement was placed at 144 mbsf and corresponds to the lithologic boundary between prism and underthrust sediments. The chemical signature of deeply sourced fluids was observed just above the décollement, but is weaker than at Site 1254. The CORK-II was installed successfully, with the packer centered at 129 mbsf and the OsmoSampler centered at 140 mbsf, along with a temperature logger and pressure monitoring screen.

INTRODUCTION

The character of the incoming plate subducting at convergent margins and the processes affecting it as it passes below the shallow forearc may play a major role in the nature and extent of hazardous interplate seismicity as well as the magnitude of volcanism and the chemistry of lavas produced in the overlying volcanic arc. The fate of incoming sediments and ocean crust, and of their associated volatiles, as they pass through the shallow levels of a subduction zone (0–50 km depth) has profound effects on the behavior of the seismogenic zone, which produces most of the world's destructive earthquakes and tsunamis. Fluid pressure and sediment porosity influence fault localization and deformation style and strength and may control the updip limit of the seismogenic zone (e.g., Scholz, 1998; Moore and Saffer, 2001). Fluids within both fault zones and sediments underthrust at the trench affect early structural development and are a key agent in transport of chemical species. The mineralogy and chemistry of any subducted sediments and their dehydration reactions during subduction may control the physical properties of the deeper subduction interface and, hence, downdip limits of the seismogenic zone.

The escape of fluids to the surface from the downgoing plate at depth (return flow) may support a deep biosphere, contributes methane and higher molecular weight hydrocarbons for gas hydrate formation, affects seawater chemistry for selected elements, and is intimately linked to deformation, faulting, and the evolution of the décollement. The distillation and loss of some volatiles and fluid-soluble elements from the shallow slab not only record reactions and processes within the seismogenic zone, but they also play a central role in the supply of residual volatiles to the deeper Earth and change the composition of the slab delivered to the depths of magmatism beneath volcanic arcs. Processes operating in the shallow subduction zone thus affect the way the slab contributes to continent-building magmatism, explosive volcanism, ore formation and, ultimately, the evolution of the mantle through time (collectively known as the subduction factory). The subduction signature recorded in the chemistry of arc volcanics constrains the nature and sometimes the volume of the sediments transported through the seismogenic zone to the depths of magmatism. The arc thus acts as a flow monitor for the transport of sediments to depths greater than those that can be drilled or imaged seismically.

The Ocean Drilling Program (ODP) has identified deformation at convergent margins, fluid flow in the lithosphere, and subduction zone geochemical fluxes as important aspects of the JOIDES Long Range Plan (JOIDES Planning Committee, 1996). The Initial Science Plan for the Integrated Ocean Drilling Program includes an initiative focused on the seismogenic zone. The Central American convergent margin (see Fig. F1) has been a focus area for a number of national and international programs studying the seismogenic zone and subduction factory for several reasons. First, it is one of the few modern subduction zones that is subducting a significant carbonate section and thus provides an opportunity to investigate CO_2 cycling through convergent margins. Second, along strike from Nicaragua to Costa Rica (Fig. F2), the style and extent of seismicity and plate coupling changes. Third, along the same section, the style of arc volcanism changes as do volumes and the chemistry of the arc lavas. Changes in both the seismicity and volcanic chemistry have been proposed to result from changes in the balance between sediment underplating, erosion, and subduction (collectively referred to here as sediment dynamics), perhaps related to changing bathymetry, thermal structure, and hydrological behavior along the margin.

Leg 205, building on Leg 170 coring and logging while drilling (LWD) at the same sites (Fig. F3), is designed to investigate the composition of the downgoing plate together with the thermal structure and hydrological activity across the Costa Rica margin. This will be done through a combination of downhole measurements and long-term sampling of fluids and gases as well as monitoring of fluid pressure, temperature, and flow rate at critical horizons. First observations of temporal variations of fluid and gas chemistry will be available once the fluid and gas samples have been recovered 1 to 2 years postcruise. During the leg, we also drilled and cored into the subducting igneous section to characterize the mass and fluid fluxes to the volcanic arc together with their chemical compositions. The high recovery during coring through the décollement zone in the prism sites provided the opportunity to evaluate local heterogeneity in the development of the décollement (in conjunction with Leg 170 results) and to integrate the location and magnitude of pore fluid anomalies with structural fabrics observed in the cores.

The Central America Seismogenic Zone and Subduction Factory

A large body of work shows that there are differences in seismicity and arc magmatism along the length of the Central American margin (Fig. F1), with sharp contrasts seen between Nicaragua and immediately adjacent parts of Costa Rica. The Nicoya section of the Costa Rica margin appears to have earthquakes with a moment magnitude (M_w) of 7 or greater at a 40- to 50-year recurrence interval, with the last such event in 1950 (Guendel, 1986). Coupling between the downgoing and overriding plates is estimated from Global Positioning System data to be 40%–60% (T. Dixon, pers. comm., 2001) and appears to start ~15 km arcward of the trench. Nicaragua is characterized by a greater frequency of M_w of 7 or larger earthquakes, including the 1992 tsunamogenic earthquake. In detail, the updip limit of seismicity appears to be at ~20 km depth north of the fracture zone trace shown in Figure F4 and at ~10 km depth to the south (Newman et al., 2002).

There are also significant changes in volcanism between Nicaragua and Costa Rica. Figure F2 shows an offset in the volcanic chain just north of the northernmost Nicoya Peninsula. In Nicaragua, the arc-trench gap is 180–190 km and the volcanoes lie ~180–200 km above the Waditi-Benioff Zone of the downgoing slab. In Costa Rica, the arc-trench gap narrows to ~165 km and the seismic zone is ~120–130 km below the volcanoes (Protti et al., 1994). Nicaraguan volcanoes tend to be smaller than those of Costa Rica as shown in Figure F2; when averaged over the last 100–130 ka, magma production rates, compiled in Patino et al. (2000), are much lower in Nicaragua than Costa Rica (~14 and 44 km^3/km arc length per million years, respectively). In the chemistry of the arc volcanics, ^{10}Be data, radiogenic isotopes, and trace element

studies of Nicaragua lavas (Tera et al., 1986; Carr et al., 1990; Reagan et al., 1994; Patino et al., 2000) suggest that the entire sediment section is subducting to the depths of magma generation, producing in the lavas a strong signature from the hemipelagic sediments at the top of the incoming sediment section. In contrast, the Costa Rican lavas have a much smaller sediment signature, little contribution from the uppermost hemipelagic sediments of the incoming plate, and a proportionally larger contribution from the basal carbonate section.

The differences in arc chemistry along strike cannot be explained easily by variations in the lithology or chemistry of the incoming plate. Figure F5 shows the lithologic section entering the trench off Guatemala (DSDP 495) and Costa Rica (ODP Sites 1039 and 1253). The two sections show 150–180 m of diatom-rich hemipelagic sediments overlying 230–250 m of calcareous nannofossil oozes and chalks. Given the similarity of the subducting sediment sections along the Middle America Trench, differences in the sediment signature between the Nicaraguan and Costa Rican volcanoes are likely caused by variations in sediment dynamics.

Various workers have suggested that the changing nature of seismicity and arc volcanism along the Middle America Trench may be due to variations in the incoming plate, the fate of incoming sediments as they traverse the forearc of the overriding plate, or a combination of the two. The bathymetry and thermal structure of the incoming plate and the active fluid flow both outboard and inboard of the trench may play a key role in deformation and sediment dynamics across the margin. In addition, differences in origin and chemistry of the subducting oceanic crust may also contribute to changing chemistry of the arc lavas. These issues are addressed in more detail in the following section.

Geological and Geophysical Setting

Geophysical Database

The structure of the Middle America Subduction Zone (Fig. F1) has been intensively studied by North-American and German geophysicists since the early 1980s. The collected data sets comprise bathymetric and side-scan sonar surveys, seismic refraction and reflection studies, and passive seismological experiments (Christeson et al., 2000; McIntosh et al., 1993; Ranero et al., 2000a, 2000b; von Huene et al., 2000). Potential field investigations were mostly done in conjunction with seismic studies and bathymetric mapping. In Barckhausen et al. (1998, 2001), all marine magnetic data from Nicaragua south to the Carnegie Ridge were interpreted to unravel the tectonic history of the Cocos-Nazca spreading center (CNS) and the adjacent Cocos plate off Costa Rica. In addition, recent heat flow surveys at the margin of Costa Rica and Nicaragua (*METEOR* 54-2, 2002) and seaward on the Cocos plate off Nicoya Peninsula (Ticoflux I, 2001; Ticoflux II, 2002) complement older existing data sets by Langseth and Silver (1996). The regional tectonic history with special emphasis on the subduction erosion is discussed by Meschede et al. (1999a, 1999b), Ranero and von Huene (2000), Abratis and Woerner (2001), and Vannucchi et al. (2001). Pore pressures and the accompanying fluid and energy fluxes as well as the presence of gas hydrates in the area of Costa Rica are investigated in numerous papers (McIntosh and Sen, 2000; Kopf et al., 2000; Silver et al., 2000; Vannucchi and Tobin, 2000; Saffer et al., 2000; Ruppel and Kinoshita, 2000; Pecher et al., 2001, and Saffer, in press). This compilation of published results comprise only recently published papers; more references can be found in Kimura, Silver, Blum, et al. (1997) and Silver, Kimura, and Shipley (2001).

Oceanic Plate off Costa Rica

There are significant variations in the origin, morphology, and thermal structure of the incoming plate through the Nicaragua-Costa Rica segment of the Central American convergent margin (Figs. F1, F2). Large-scale tectonic features, such as the Carnegie and Cocos Ridges and the subduction trench, are clearly reflected in the regional bathymetry as shown in Figures F1 and F2. The topography of the incoming plate changes along the length of the margin (Fig. F1) (Ranero et al., 2000b): crust subducting beneath Nicaragua, formed at the East Pacific Rise (EPR), is pervasively faulted with offsets of up to 700 m on back-tilted normal faults (Kelly and Driscoll, 1998; Kelly et al., pers. comm., 2002), possibly associated with extensional tectonics caused by the flexure of the crust as it is subducted. The offsets become smaller as one approaches Nicoya Peninsula, being <200 m. Farther to the southeast, seafloor relief in general is more pronounced (being southeast of the "rough-smooth boundary" after Hey, 1977) and the seafloor is covered by numerous seamounts (Figs. F1, F2). Crustal thickness increases slightly from ~5 km off Nicaragua to ~6 km off Nicoya Peninsula (Ranero and von Huene, 2000). The thickness of the incoming sediments is generally in the range of 400–500 m.

Analysis of marine magnetic measurements (Hey, 1977; Lonsdale and Klitgord, 1978; Barckhausen et al., 2001) shows (Fig. F4) that ~20 km southeast of the Leg 205 transect, a fracture zone trace (FZT) separates lithosphere formed at the EPR from that formed at the CNS. This means that the drill holes of Leg 205 are underlain by crust that formed at the EPR at ~24 Ma. Analysis of magnetic anomaly data (Wilson, 1996) indicates that the crust at this location was formed at a full spreading rate of ~130 mm/yr. Seismic images of the FZT (Barckhausen et al., 2001) confirm the location of the boundary and reveal a jump up in basement depth of ~100–200 m from the EPR to CNS crust. The lithosphere to the southeast of the FZT formed at the CNS, with decreasing age to the southeast. The oldest crust directly at the FZT is 22.7 Ma, which corresponds to the break up age of the Farallon plate. The location for ODP Leg 206 (6°44.19′N, 91°56.06′W) is located on crust generated at the EPR at a full spreading rate of ~200 mm/yr, in the immediate vicinity of the "rough-smooth boundary."

Convergence parameters are broadly similar along the margin. The convergence rate of the Cocos plate vs. the Caribbean plate increases only slightly from 83 mm/yr off Guatemala to 85 mm/yr off Nicaragua and reaches 88 mm/yr off southernmost Costa Rica (De Mets et al., 1990). The convergence direction off Nicoya Peninsula is almost perpendicular to the trench with the subducting plate dipping to the northeast (N25°–30°E). The maximum depth of seismicity gradually becomes shallower from Nicaragua (~200 km) to southern Costa Rica (~45 km). The dip angle of the slab in the upper 100 km is closely similar from Nicaragua to Central Costa Rica (~30°) and becomes steeper at 100 km depth with a value of ~80° (Protti, 1994).

The part of the Cocos plate that is presently being subducted offshore Costa Rica was overprinted by hotspot-related volcanism between 14 and 12 Ma (Barckhausen et al., 2001). This is most evident in the area of the Cocos Ridge off southern Costa Rica, but rock samples dredged from seamounts have proven that the overprinting extended at least as far north as the southern tip of the Nicoya Peninsula (Fisher Seamount). It seems possible that the sills encountered at the base of some of the ODP Leg 170 holes and at Site 1253 of Leg 205 and also observed in nearby seismic reflection profiles may be related to this volcanic event. One other interpretation (U. Barckhausen, pers. comm., 2002) would be that the FZT acted as a "leaky fault" and intruded magma into the bathymetrically lower sediments north of the FZT.

The seismic profile BGR-99-44, shown in Figure F6, reveals the general structure of the seaward side of the trench, the trench itself, and the lowermost seaward part of the prism. All drill sites of Leg 205 are located on this multichannel seismic (MCS) line (C. Reichert and C. Ranero, pers. comm., 2001) shot in

1999. The data were acquired with a 6-km, 1024-channel digital streamer using a 3-m^3 tuned air gun array and differential Global Positioning System navigation. Data shown in Figure F6 are a near-trace (171-m offset) time-migrated section of the complete profile. The incoming pelagic sediments with a thickness of ~400 m show faults with offsets of 50–100 m seaward of the trench. A prominent reflector at 0.25-s two-way traveltime (TWT) below the seafloor marks the base of lithologic Subunit U3A (Fig. F5) (Kimura, Silver, Blum, et al., 1997) of late Miocene age. Beneath the sedimentary sequence, the strong reflector at 0.5 s (TWT below seafloor) images the top of a gabbro sill as revealed by drilling results from Leg 170 at Site 1039. The top of oceanic basement below the sill is very difficult if not impossible to identify based on the seismic records.

Margin

Through extensive work, the structure of the forearc has been imaged. Limited ODP Leg 170 coring, drilling, and seismic data show that the bulk of the Pacific margin is a wedge-shaped high-velocity body probably made of rocks similar to the igneous oceanic rocks (Nicoya Ophiolite Complex) cropping out along the coast (Shipley et al., 1992; Kimura, Silver, Blum, et al., 1997; Ranero and von Huene, 2000), which precludes the existence of any significantly large sediment mass being recently accreted. Only a small sediment prism (<10 km wide) is located at the front of the margin wedge. Initially, MCS images were interpreted in terms of sediment accretion to the Costa Rica margin (Shipley et al., 1992). More recently, however, and in the wake of Leg 170 drilling, seismic images have been interpreted to show that basically the entire sediment cover of the ocean plate is currently underthrust beneath the margin and that the frontal sediment prism can store very little, if any, of the incoming material (Kimura, Silver, Blum, et al., 1997; Christeson et al., 1999, 2000; McIntosh and Sen, 2000; Moritz et al., 2000; Silver et al., 2000; Ranero et al., 2000a; von Huene et al., 2000).

Part of the prism relevant to Leg 205 is imaged in the seismic line shown in Figure F6. Northeast of the deformation front (shotpoint 3210) the décollement is clearly visible up to 5 km arcward as a boundary separating the underthrust sediment sequence from the overlying poorly structured prism sediments. The detailed analysis of a three dimensional seismic data set (Shipley et al., 1992) shows that across the 8.5-km-wide coverage of the lowermost part of the prism the décollement structure is quite diverse. Shipley et al. (1992) were able to identify numerous thrust faults mostly in the lower part of the prism acting as possible fluid conduits, but clear tectonic structures are less evident approaching the deformation front. Only one of these faults is imaged offsetting the underthrust sequence (Fig. F6) (CMP 3155) and appears to continue up into the prism sediments.

Prior to Leg 170, the Nicaragua margin was believed to be a nonaccretionary margin, whereas Costa Rica was believed to be a site of sediment accretion (von Huene and Scholl, 1991; Shipley and Moore, 1986; Shipley et al., 1992). Leg 170 drilling and subsequent research show no current or recent frontal sediment accretion off Costa Rica. The sediment section beneath the décollement at Site 1040 repeats the complete lithology and sequence of the incoming section cored at Site 1039 (Fig. F5), allowing little sediment accretion to the front of the prism at present (Kimura, Silver, Blum, et al., 1997). Cosmogenic ^{10}Be, which decays with a 1.5-m.y. half-life, also shows that there has been little, if any, frontal accretion at this site over the last several million years (Fig. F7) (Morris et al., 2002). The very high ^{10}Be concentrations in the incoming sediment section beneath the décollement are typical of young marine sediments. Were these incoming sediments to be frontally accreted, the prism sediments above the décollement would have measurable ^{10}Be enrichments. The very low concentrations of ^{10}Be in the sediments above the décollement indicate that they are older than several million years and preclude construction of the prism

from accretion of imbricate thrust packets over the last several million years. The prism is thus either a paleoaccretionary prism or is composed largely of slumped slope sediments rather than accreted marine sediments. Sedimentological and chemical data (Kimura, Silver, Blum, et al., 1997) are more consistent with the latter interpretation. The thinning of the underthrust section seen between Sites 1039 and 1040 (Figs. F5, F6) must then reflect compaction and dewatering, rather than sediment offscraping. As noted earlier, the chemical differences in the arc lavas from Nicaragua and Costa Rica suggest that the entire sediment section is subducting to the depths of magma generation beneath Nicaragua, with only the lower part subducting beneath Costa Rica. The seismic and lithologic observations indicate complete sediment subduction past the prism front in both regions. The arc and prism observations can be reconciled if sediments are underplated to the base of the prism beneath Costa Rica or if greatly enhanced subduction erosion occurs beneath the Nicoya segment.

There is evidence for underplating to the base of the prism landward of the Leg 170 and 205 coring area. Christeson et al. (1999) use seismic reflection and refraction data to show stacked velocity duplicates, interpreted as repeated stratigraphic sections because of underplating. The low, but real, ^{10}Be enrichments in the Costa Rican lavas could be explained if the upper 80–100 m of the incoming sediment section was underplated (Valentine et al., 1997).

In addition to evidence for sediment subduction and underplating beneath the Nicoya segment, the seismic stratigraphy of the slope off Nicaragua and the tectonic structure off Costa Rica indicate extension and subsidence of the margin during much of the Miocene (Ranero et al., 2000a; Ranero and von Huene, 2000; Walther et al., 2000). Multibeam bathymetry along the continental slope displays structures that indicate significant mass wasting off Nicaragua and a rugged morphology off Costa Rica (Ranero et al., 2000a; von Huene et al., 2000), which is consistent with tectonic erosion and thinning of the overriding plate. These results are further substantiated by Leg 170 coring and postcruise science. Coring at Site 1042, 7 km landward of the Middle America Trench, encountered a ~30-m-thick sequence of fossiliferous well-lithified calcarenite breccia at a depth of ~4000 meters below sea level (mbsl) (Kimura, Silver, Blum, et al., 1997). Fossil, textural, cement paragenesis, and sedimentological observations document that the calcarenite was formed, brecciated, and cemented in a nearshore setting (Vannucchi et al., 2001). Sr isotope ratios place the depositional age at 16–17 Ma (latest early Miocene) and establish that the breccia section is stratigraphically upright. It is overlain by ~320 m of unconsolidated slope mud showing the complete Pleistocene to Miocene sequence where benthic foraminifers indicate the subsidence of the margin from the upper bathyal to abyssal depths (Meschede, 1999b; Vannucchi et al., 2001). Unfortunately, erosion rates over the last several million years are not well constrained. Speculation is that tectonic erosion has been controlled by the roughness of the subducting plate. The thinning of the overriding plate and the continental margin morphology suggest that subduction erosion increases in intensity from Nicaragua to southern Costa Rica (Ranero and von Huene, 2000).

For the purposes of Leg 205, an important result is that the margin off Nicoya is not currently accreting sediments and has not done so over the last several million years. The conclusion that all sediments fed to the trench over this time frame have been subducted past Site 1040 greatly simplifies estimating the mass and element fluxes. Specifically, changes in underthrust sediment thickness between Site 1039 and 1040 are due to compaction. To calculate the flux of elements out of the compacting sediment section and updip from the deeper décollement, steady-state conditions may be assumed.

Heat Flow off Costa Rica

Heat flow data from the Global Heat Flow Database within the seaward area off Costa Rica and Nicaragua are sparse with a spacing of typically 60 to 100 km. However even with this very limited coverage, a clear trend in the overall picture is very clear. Values north of the FZT heat flow average ~30 mW/m² (about one-third of the expected value from lithospheric cooling after Stein and Stein, 1992) and increase to an average value of ~110 mW/m² south of the FZT. Plates north and south of the FZT have approximately the same age, so one would expect them to show similar average heat flow. This indicates that crust south of the FZT, created at the CNS, is close to the expected value from lithospheric cooling, whereas crust north of the FZT is significantly cooler, which means that a substantial amount of its heat is probably being removed by hydrothermal circulation within the crust. This conceptual model still needs confirmation with more heat flow data and hydrogeological modeling in order to understand the driving forces of the observed heat flow variations.

A detailed heat flow study prior to leg 170, focusing on the trench and the prism offshore Nicoya Peninsula (Langseth and Silver, 1996), confirmed the trend of a cool plate subducting under Costa Rica. Two recent heat flow surveys (Ticoflux I and II) in the Leg 205 area investigated in detail the thermal structure of the incoming plate seaward of the trench by mapping heat flow along seismic lines. Three major conclusions can be drawn: (1) small and isolated areas show either very high or very low heat flow, indicative of active recharge or discharge and (2) profiles across the FZT confirm the increase of heat flow as one steps from the EPR-created crust to the CNS-created crust as suspected from an analysis of the Global Heat Flow Database and (3) a profile seaward of the deepest part of the trench across major extensional faults show no indication that these faults act as major fluid conduits. New heat flow values at the prism from northern Nicaragua to southern Costa Rica (*METEOR* cruise 54-2) clearly support the idea that the FZT is a major thermal boundary, not only seaward of the trench but also underneath the prism. One profile runs along the transect of holes drilled during ODP Legs 170 and 205 and coincides with seismic line BGR99-44. Figure F8A shows the locations of all seafloor and borehole heat flow measurements along the drilling transect, starting at the trench and up to 34 km away from the deformation front. Data from Leg 170, Langseth and Silver (1996), and *METEOR* 54-2 are projected along this profile. All data sets generally show a similar pattern of an increase from a low heat flow of ~7–15 mW/m² to values of ~20–40 mW/m² passing from the trench to the prism (Fig. F8B). Only the extremely low mean value of 6.7 mW/m² at ODP site 1040 is not confirmed by recent measurements during *METEOR* 54-2 that show values twice as high that fit in the general trend of observed heat flow up prism.

Margin Hydrology

At the Costa Rica subduction zone, coring during ODP Leg 170 and subsequent postcruise studies identified three fluid flow systems: active flow of modified seawater within the upper oceanic crust, updip fluid flow within underthrust sediments, and deeply sourced fluid expulsion along the décollement and through faults in the margin wedge (e.g., Silver et al., 2000; Kastner et al., 2000; Saffer et al., 2000; Saffer, in press).

The existence of active fluid flow in the oceanic basement of the incoming plate is evidenced by both the heat flow anomalies discussed earlier and the chemistry of pore fluids sampled during Leg 170. Postcruise studies of pore fluid chemistry (Fig. F9) show chemical characteristics (e.g., $^{87}Sr/^{86}Sr$) typical of modern seawater in the uppermost sediments. Below this, values depart increasingly from seawater at increasing depth as a result of diagenesis, largely ash alteration. The consequence is that measured pore fluid isotope ratios at a particular depth-age interval are lower than those of seawater at the comparable

time, as determined from the paleoseawater Sr isotope curve. The deepest sediments, however, have pore fluid chemistry that trends back toward modern seawater values. This is particularly evident in the Sr isotope profile, where pore fluid values exceed those intrinsic to the Miocene carbonates in a section almost totally lacking terrigenous input other than young volcanic ash. The heat flow anomaly and pore fluid profiles have been modeled in terms of active fluid flow at rates of ~1–5 m/a (Silver et al., 2000). Although certainly model dependent, these results do indicate extensive contemporary flow of seawater to basement and require high permeability horizons thought to be within the uppermost basement based on results from off-axis drilling along the Juan de Fuca and Mid-Atlantic Ridges (Davis and Becker, 1994; Becker et al., 1997, 1998; Fisher, 1998; Davis et al., 2000; Kopf et al., 2000). In addition to cooling the uppermost part of the plate, the flow may further alter the basaltic crust. Any subducted high-permeability horizons may provide conduits for fluids leaving the deeper subduction zone.

The décollement and faults cutting through the margin wedge of the upper plate serve as pathways for updip flow of deeply sourced fluids. Structural observations across the décollement indicate a zoned fault, with heavily fractured fault rocks above a ductile, plastic zone that may act as an aquitard to segregate the flow systems above and below the plate boundary (Vannucchi and Tobin, 2000; Tobin et al., 2001). At Site 1040, the deformation increases gradually downward, and the shipboard structural geologists placed the top of the décollement zone at 333 meters below seafloor (mbsf). The change from brittle to ductile deformation is present at ~355 mbsf, and the base of the décollement is a sharp boundary at 371 mbsf (Fig. F10). Pore fluid chemistry studies during and since Leg 170 at Site 1040 show three distinct intervals. Above ~190 mbsf, Li, propane, and Ca concentrations are relatively uniform, as they are again in the underthrust sediments below the décollement. Generally high Li, propane, and Ca concentrations are observed between ~200 mbsf and the décollement, with peaks typically coincident with fault zones. Similar chemical anomalies are also seen along the décollement zone at Site 1043 (~130–150 mbsf). Extremely high Li concentrations are observed along the thrust and décollement at Site 1040 (Fig. F10). Enrichments in Ca and Sr, changing Sr and Li isotopic compositions, as well as higher concentrations of thermogenic heavy hydrocarbons (propane to hexane) are also observed. Collectively, these data indicate that some fraction of the fluids sampled along these localized horizons are derived from depths great enough that temperatures are at least 150°C. The chemical variations shown in Figure F10 suggest that the zone between 200 and 370 mbsf is heavily infiltrated by deeply sourced fluids; the sharp peaks at ~200 and 350–360 mbsf indicate that the anomalies are supported by relatively recent advective flow. Note that the décollement zone anomaly approximately coincides with the base of the brittle fracture zone, just above the region of ductile deformation. The composition of deeply sourced fluids from the updip limit of the seismogenic zone may be useful in constraining the mineralogy of sediments at depth and the dehydration reactions that are thought to be important in governing the rheological properties of the subduction interface in the region of seismogenesis. Given that most seismogenic zones will be forever beyond the reach of even a riser drill ship, development of chemical proxies for "remote sensing" of processes occurring in the seismogenic zone is an important adjunct of Leg 205.

Structural and chemical studies indicate a third hydrologic system, which drains fluids from the underthrust sediment section. Results from Leg 170 documented the complete underthrusting of the incoming sedimentary section at the trench, with the important implication that observed changes in sediment thickness and porosity directly reflect the evolution of effective stress. Laboratory consolidation tests, combined with LWD data from Leg 170, show that the subducting sediments are effectively undrained at Site 1043 (Fig. F11) (Saffer et al., 2000; Saffer, in press). At Site 1040, the lower carbonate section (Unit III) remains essentially undrained, whereas the upper hemipelagic units (Units I and II) are partially drained, as shown in Figure F11. Pore fluid profiles from sediments immediately below the

décollement at Sites 1040 and 1043 show a distinct chemistry from that of the décollement. A Ba spike immediately below the décollement (Fig. F11) reflects sulfate reduction in the uppermost underthusting section that mobilizes Ba out of barite and into the pore fluids. The very low Ba values in the décollement zone itself indicate that these fluids are not primarily draining into the décollement, indicating little, if any, communication between the hydrologic systems above and below the décollement. Other broad anomalies below and separate from the décollement also imply updip advective flow of locally derived fluids below the décollement (Kastner et al., 2000).

The differences in pore pressure development downsection reflect nonuniform fluid escape (Saffer et al., 2000; Saffer, in press). More rapid drainage of the uppermost ~100 m (Units I and II) than that of Unit III may result from (1) more abundant coarse-grained high-permeability ash layers that focus flow, (2) higher permeability within the hemipelagic sediments, or (3) significant permeability anisotropy within the hemipelagic sediments. The nonuniform dewatering also has important mechanical implications. An inferred minimum in effective stress developed near the top of Unit III between Sites 1043 and 1040 results in a mechanically weak horizon and suggests that detachments may form below the décollement there. This is consistent with the down-stepping of the décollement at 2–3 km from the trench observed in this region (McIntosh and Sen, 2000) and illustrates the role of fluid pressure in mediating structural development. Based on observed changes in porosity, volumetric fluid sources (in $V_{fluid}/V_{sediment}/s$) range from ~10^{-12}/s at the top of the section to ~10^{-13}/s at the base. These values are one to two orders of magnitude larger than those calculated for underthrust sediments at the Nankai and Barbados subduction zones (e.g., Zhao et al., 1998; Screaton et al., in press). This dramatic difference likely reflects higher sediment permeabilities at Costa Rica, resulting in a more active fluid flow system.

Overall, hydrological and geological modeling (e.g., Saffer et al., 2000; Silver et al., 2000) suggests relatively high permeabilities in the oceanic basement, décollement, and underthusting section, with the décollement being locally more permeable than the underthrusting sediments.

SCIENTIFIC OBJECTIVES

During Leg 205, we returned to near the Leg 170 drill sites. The planned Leg 205 sites were 1253, 1254, and 1255. Science objectives for Leg 205 had two primary foci. The first was the igneous and alteration history of the basement at reference Site 1253 on the incoming plate. The second was the three hydrological systems: in basement at Site 1253, along the décollement at Sites 1254 and 1255, and in the uppermost section of the subducting sediment section at Site 1254. In the prism sites, coring in the fault zones provides an opportunity to integrate structure, fluid flow, and fluid chemistry. These goals were accomplished as described in detail below by limited coring of selected intervals, downhole temperature measurements, logging at Site 1253, an extensive shipboard and postcruise analytical plan, the installation of long-term observatories to monitor temperature and pressure, and sampling fluids and gases at key hydrological intervals.

Reference Site 1253 Science Objectives

During Leg 205, coring and sampling began at Site 1253 within the carbonates above the sill encountered during Leg 170 and continued through the sill and the previously undrilled sediments below and ~100 m into the lower igneous unit. The scientific objectives to be addressed through coring, sample analysis, and logging at Site 1253 were as follows:

1. Calculate subduction fluxes to the trench. Leg 170 data provide information for the bulk of the sediment section, whereas Site 1253 coring and shipboard and postcruise analysis will add data for the lowermost sediment section, the sill, and the lower igneous unit. Emphasis will be placed on elements and isotopes of particular interest for evaluating sediment dynamics through the forearc, fluid and element fluxes out of the downgoing plate as it passes through the seismogenic zone, subduction and recycling behavior of carbonate and CO_2 from trench to arc, composition of the subducting igneous basement (fresh and locally altered), and the trench-arc recycling of key tracers for quantifying sediment and oceanic crust contributions to the arc lavas. Leg 205 data will be combined with results from the 600- to 800-m penetration of EPR oceanic crust during Leg 206 to provide a more complete picture of the downgoing oceanic crust.
2. Investigate the extent of sill emplacement, their origin and tectonic implications thereof, and their contribution to the bulk composition of the subducting igneous crust. Leg 170 encountered a gabbro sill, with trace element characteristics consistent with an origin related to Galapagos activity.
3. Determine the igneous and alteration mineralogy, petrology, and geochemistry in the uppermost 140 m of igneous section and characterize the original igneous structure therein, using coring and logging data. Use the geochemical data to calculate subduction fluxes. Attention will be paid to low-temperature alteration features that may result from near-trench fluid flow as well as that deriving from ridge-crest and near-off-axis hydrothermal circulation.
4. Collect microbiological samples within the more fractured and veined parts of the oceanic section for shipboard cell counts and preliminary DNA extractions and postcruise analysis. Contamination testing using perfluorocarbon tracers (PFTs) and microspheres will be carried out.
5. In conjunction with Leg 170, construct an ash stratigraphy that maps Galapagos and Central American ashes as the plate moves from near ridge to near trench.
6. Determine physical properties in the core and borehole that may affect estimations of igneous composition and lithologic variation or that relate to fluid flow and deformation such as porosity, density, fracture distribution and orientation, and strength. Identify regions of higher fracture density as possible sites for osmotic samplers.

A long-term borehole observatory (i.e., a modified CORK-II) (Fig. F12) was installed at Site 1253 to sample fluids and to monitor temperature and pressure within the uppermost permeable basement. Osmotic samplers were installed at two different levels within the section. The science objectives for the CORK-II installation were to

1. Use pressure, temperature, fluid, and gas compositions together with downhole measurements to characterize the fluid and heat fluxes responsible for the abnormally low heat flow in the vicinity of this site caused by seawater incursion inferred to be to basement. Monitoring and sampling will run for 1–2 years, after which pressure data will be downloaded and the temperature loggers and osmotic samplers will be replaced with instruments designed to operate for 4 years before recovery.
2. Evaluate the thermal, hydrological, and chemical implications of this extensive fluid circulation for the thermal structure of the uppermost part of the subducting plate, the hydrological pathways available in the shallow subduction zone and beneath the overlying prism, and global element fluxes.

Prism Holes 1254A, 1254B, and Site 1255 Science Objectives

Limited coring focused on an upper fault zone and the décollement; these two fault zones have pore fluid chemical anomalies indicative of advective flow of deeply sourced fluids. Two penetrations of the décollement and good recovery therein allowed more detailed structural analysis at several sites (in conjunction with Leg 170), higher resolution chemical sampling, and integration of structural characteristics with indicators of fluid flow. Coring results were used to guide installation of a CORK-II to monitor and sample within the area of maximum flow of deeply sourced fluids in the décollement. Together, these approaches plus shipboard and postcruise work will be used to address the following scientific objectives:

1. Make detailed observations of the structural development of the upper fault (one site during Leg 170 and one during Leg 205) and décollement (two sites during Leg 170 and two more during Leg 205) that will contribute to a better understanding of the structural development of the décollement zone as a function of position along and within the plate boundary fault zone, lithologic properties, and fluid flow characteristics.
2. Determine physical properties, including permeabilities, of the décollement horizon from further structural experiments on whole-round samples to constrain hydrological modeling and permit integration of fluid flow and deformation models.
3. Determine heavy hydrocarbon chemistry within the fault and décollement zone sediments and major and minor cation and anion concentrations in pore fluid profiles from fault zone and décollement whole rounds. The advective spikes and diffusive gradients derived therefrom will be evaluated against the structural features in the cores and also compared to profiles measured during Leg 170 to evaluate possible heterogeneity.
4. Collect whole-round samples from the upper fault zone and décollement under appropriate conditions for postcruise microbiological investigations to determine the resident microbial ecology of the zone for comparison to eventual microbial experiments on fluids collected from the décollement. Contamination tests will be carried out using microspheres only to eliminate any possible chemical contamination of pore fluids by the PFT solution.
5. Install a CORK-II at one site into the zone of maximum advective flow to determine pressure, temperature, and composition of fluids and gases along the décollement and evaluate any possible changes through time for hydrologic modeling. OsmoFlow meters will be deployed at these sites in an attempt to constrain fluid flow rates through the sampler screen. This same data set will constrain the flux of elements out of the downgoing sediment section along the décollement to evaluate the role of fluid egress on element fluxes to the ocean and its corollary, changing composition of the residual slab because of fluid loss.
6. Use selected elements, element ratios, and isotopic compositions in the fluids from the décollement, both from whole rounds and ultimately CORK-II osmotic samplers, in an attempt to constrain dehydration reactions at the updip and, perhaps, downdip limits of the seismogenic zone.

SITE SUMMARIES

Site 1253

Site 1253 is located ~200 m seaward of the deformation front, in the deepest part of the Middle America Trench (Figs. F3, F13) Operationally, one primary goal for this site was to recore the sediments immediately above the sill encountered during Leg 170, drill and core for the first time through the sediments below the sill, and core >100 m into the oceanic sections. The other major task was to install a CORK-II observatory in the deep igneous section, where coring and logging were used to identify depths at which to set the packer and osmotic fluid and gas samplers.

There are two primary science objectives for this site. The first goal is to determine the bulk composition and distribution within the incoming plate of key element and isotopic tracers, to provide a baseline in physical, mineralogical, and chemical characteristics against which changes during shallow subduction processes may be measured or inferred. They also provide a starting point from which to examine the recycling from subduction trench to volcanic arc (or deeper mantle) of important components such as CO_2. The second major objective at this site is to investigate the hydrology and thermal structure of the igneous section entering the trench. This objective will be addressed using temperature and pressure data and fluid and gas samples recovered from the observatory 1- to 2-years and 5- to 6-years postcruise. Interstitial water chemistry analyzed shipboard during Leg 205, together with that from Leg 170, provides evidence for contemporary flow of seawater at depth at both reference sites. Although not a primary objective for Leg 205, the ash recovery at the base of the sediment section also tells an interesting story.

The seismic record (Fig. F13) in the vicinity of Hole 1253A (CMP number 3210) images the sedimentary sequence of middle Miocene age with a clear change in resolution at ~6.1 s TWT. This represents the top of the calcareous Unit U3 (Kimura, Silver, Blum, et al., 1997) at ~180 mbsf. Beneath the sedimentary sequence, the strong reflector at 6.34 s TWT images the top of a gabbro sill as revealed by drilling results from Leg 170 at Site 1039. The coherent reflection pattern below the top of the sill is difficult, if not impossible, to interpret below the drilled depth of 600 mbsf.

One hole was drilled at Site 1253, which was partially cored and into which we installed a long-term hydrologic borehole observatory. After setting a reentry cone and 16½-in casing into the seafloor, we reentered this hole with the rotary core barrel (RCB) and drilled without coring to ~370 mbsf. RCB coring below 370 mbsf penetrated 30 m of calcareous and locally clay-rich sediments with intermittent ash layers (average recovery = 75%) before encountering a gabbro sill between 400 and 431 mbsf (average recovery = 74%). Below the sill were ~30 m of partially lithified calcareous sediments with intermittent ash layers (average recovery = 20%). This interval was followed by coring ~140 m into a second igneous unit (average recovery = 75%), with local zones of 55%–50% recovery.

After coring, operations focused on preparing the hole for logging and CORK-II installation. The hole was opened to 14¾ in; 10¾-in casing was installed to a depth of ~413 mbsf and cemented in place to inhibit communication between the borehole and the formation. After drilling out the cement shoe and drilling a rat hole with an RCB bit, we logged the hole. Because we conducted operations at or very near Leg 170 drill sites where LWD was conducted, our logging focused on the igneous section at Site 1253. Here, we ran the triple combination (triple combo) and Formation MicroScanner (FMS)-sonic strings to determine physical properties, fracture distribution, and structure of the basement rocks. After an initial logging run encountered an impassable bridge in the shallow sediment section, casing was run into the uppermost part of the sill to stabilize the hole for subsequent CORKing operations. The subsequent

logging run encountered a bridge at 530 mbsf that limited the triple combo and first FMS-sonic run to the interval between 530 and 413 mbsf; on a second pass, the FMS-sonic tool passed below the bridge and the hole was logged upward from 566 mbsf. A miniaturized temperature logger was run along with the Lamont-Doherty Earth Observatory Temperature/Acceleration/Pressure tool (TAP).

After logging, we assembled the CORK-II components, including a 4½-in casing screen, casing packer, and casing made up to the instrument hanger. The entire assembly was then lowered into the hole and latched in to seal the borehole outside of the 4½-in casing. The OsmoSampler with integral temperature sensors was lowered through the center of, and latched into the bottom of, the 4½-in casing. The final operation was to inflate the packers and shift spool valves that would connect the CORK-II pressure monitoring system to the formation, which would completely seal the zone to be monitored. Problems with the "go-devil" used for this step made it difficult to determine whether the packer had inflated or the valves had turned for pressure monitoring. *Alvin* dives since then have confirmed that the installation is fully operational. Three absolute pressure gauges including a data logger are installed within the instrument hanger head. One sensor monitors pressure within the sealed-off fluid sampling zone at the bottom of the hole; one monitors pressure variations present within the borehole above the sealed-off section; and the third sensor provides seafloor reference pressures. One additional sampling line extends from the CORK-II head all the way down to the screened interval below the packer and is available for future pressure/fluid sampling purposes. The specifics of the CORK-II installation, relative to the structure and petrology of the igneous sections, are discussed in more detail below.

Lithostratigraphy and Sediment Geochemistry

Sediment coring began at Site 1253 at 370 mbsf, where nannofossil chalks with minor clay interlayers were recovered, closely similar to those at Leg 170 Site 1039. Other significant grains identified are siliceous sponge spicules, diatoms, and zeolites derived from the degradation of volcanic glass shards. Volcanic detritus (glass, altered glass, and mineral fragments) is ubiquitous, varying between ~3% and 10% of the total. Tephra layers (<1% of total stratigraphic thickness) are typically thin (<5 cm), with mafic layers accounting for >70% of the layers identified. A thick (8 cm) siliceous white tephra was recovered at 398.8 mbsf (Fig. F14). Diagenesis has resulted in moderate lithification in the section, except immediately above the gabbro sill, where the sediment is much more clay rich, laminated, and lithified. This section (Core 205-1253-4R) is less calcareous (<2% $CaCO_3$), with clays and zeolites forming increasingly large volumes of the sediment in the last 3 m above the gabbro sill. Thin chert layers are also seen at 395.4 mbsf (interval 205-1253A-4R-1, 53–61 cm). Below the first gabbro sill, in Core 205-1253A-10R, less lithified nannofossil chalks were recovered. These are identified as the same lithologic unit as above the sill, but they are dominated by a clastic granular limestone, defined as packstone with clay. Minor amounts of baked sediments, usually inferred to be out of place, were recovered within and below the gabbro sill. Bulk sediment chemistry, by inductively coupled plasma–atomic emission spectroscopy (ICP-AES), largely map the minor variations in lithology, with SiO_2 increasing and CaO and Sr decreasing in the more clay-rich interval immediately above the sill. The TiO_2 and Al_2O_3 in the sediments are largely controlled by the ash contribution; relatively constant Ti/Al ratios through the calcareous and clay sediment sections suggest relatively homogenous amounts of volcanic detritus throughout the section. Baked sediments have chemistry similar to the dominant lithology. No appreciable increases in Fe, Mn, or transition metal concentrations were noted above the sill, in contrast to the increases in Cu, Ni, Zn, and V observed at ~80 m above the sill at Site 1039.

Biostratigraphy

Because of the small amount of new sediment recovery expected during Leg 205, the shipboard science party did not include a micropaleontologist. Samples were taken for a shore-based participant. Results are expected to help constrain the ages of the gabbro sill and the lower igneous unit.

Igneous and Metamorphic Petrology

Coring at this site penetrated two separate igneous subunits (Fig. F15). The upper subunit is a gabbro sill (Fig. F16) and is similar to that encountered at Leg 170 Holes 1039B, 1039C, and 1040C. The sill (Subunit 4A) has been subdivided tentatively into 2 subunits, based on the distribution of voids, veins, grain size variation with depth, and the proportions of plagioclase to pyroxene. The lower igneous subunit (Subunit 4B) has been tentatively subdivided into seven subunits using the same criteria. Both the upper and lower igneous sections contain plagioclase and clinopyroxene phenocrysts, with rare olivine, orthopyroxene, and ilmenite and magnetite (Fig. F17). Subunit 4B, particularly below 513 mbsf, is more glass rich and more altered. Phenocrysts are set in a groundmass that typically varies between microcrystalline and fine grained, with occasional medium-grained material. A 1.3-m-thick interval of cryptocrystalline material is present at 513 mbsf (Fig. F18), where larger amounts of glass and a greater degree of alteration are observed. The petrologic data suggest that Subunit 4B is either a sill complex with multiple intrusions or a series of thick and slowly cooled lava flows. Its possible that changes in petrology and physical properties at ~513 mbsf mark the change from a sill complex to basement; postcruise dating and detailed analysis will be necessary to evaluate the two possible origins of Subunit 4B.

Discrete alteration is highest at the tops of the subunits, is generally higher in the lowermost cores, but is generally low (1%–5%) overall. Veins sampled below 485 mbsf in Subunit 4B contain up to ~11 wt% carbonate, although quantification is difficult because vein material is mixed with various amounts of igneous rock. Diffuse alteration of the bulk rock, in the form of zeolite formation and clay replacement of minerals and glass, ranges from ~10%–50%, with higher levels of alteration seen below 513 mbsf. Chemically, all rocks from both subunits are of basaltic composition (46–49 wt% SiO_2 and 6–9 wt% MgO), with compositional variation in part due to olivine, clinopyroxene, and plagioclase fractionation. Variations in elements such as Ti, V, Ba, and Zr indicate that Subunits 4A and 4B are not comagmatic and possibly could have been derived from different mantle sources. Chemical and isotopic analyses beyond those available shipboard will be necessary to determine whether these mantle sources are associated with the Galapagos hot spot, the EPR, or both.

Structural Geology

The most evident feature of the sediments above the magmatic intrusion (in cores firm enough to preserve original structures) is the tilted bedding with 30° average dip; paleomagnetically reoriented dip azimuths show a westward orientation with a cluster toward 221°, similar to the geometry observed at Sites 1039 and 1040. Small normal faults perpendicular to bedding, with millimeter-scale offsets are common throughout, as are pressure solution structures 3–10 cm long. A conjugate system of reverse faults is observed in interval 205-1253A-2R-3,128–135 cm, in which the principal stress orientation reconstruction gives a north–south oriented (183°), horizontal one. This stress field is oriented at ~30° to the convergence direction (De Mets et al., 1990). The close association of reworked pelagic sediment in the lower part of Subunit U3C, westward-tilted bedding, and the magmatic intrusion suggest that the lowermost part of the sedimentary section was deformed during the gabbro emplacement. At Site 1253,

the sediments do not show a clear signal that the subhorizontal shortening observed in the cores is related to the incipient stage of subduction, despite the presence of the deformation front only several hundred meters to the east.

The magmatic intrusions were carefully analyzed with respect to the CORK-II experiment and to provide data for comparison to the FMS data (Fig. F19). A sediment/gabbro contact was recovered in interval 205-1253A-27R-1, 1–6 cm, and it dips 72°, although this piece sits at the top of the core above possible dropstones. The intrusions are commonly cut by magmatic veins. Dilational joints are also frequent, usually filled with a film of green minerals (clay and zeolite?), and rarely are present as open fractures (Fig. F20). The paleomagnetic reorientation of the fractures to the real geographical coordinates has been done with particular care; most joints share preferred orientations with magmatic veins, but two populations do not. Overall fracture density increases with depth (Fig. F19). Common in the lower part of the deeper magnetic intrusion (Core 205-1253A-36R and below) are brittle shear zones, represented by enechelon Riedel shears, usually showing a reverse sense of movement.

Physical Properties

Variations in physical properties correlate with major lithologic changes between sediments and igneous units (Fig. F15). A limited number of measurements indicate decreased porosity and increased grain density and *P*-wave velocity within sediments immediately above and between the igneous units; these differences may reflect alteration (recrystallization) and porosity reduction caused by emplacement of the igneous units.

Clear trends in the physical property data are: (1) the small but systematic increase in velocity, bulk density, and grain density and decrease in porosity within the lower igneous unit and (2) the higher natural gamma ray (NGR) in the upper igneous unit and the clear shift in NGR emissions at 512 mbsf within the lower igneous unit. The cause of these trends in porosity, density, grain density, and velocity with depth in the lower igneous unit is unclear. The differences in NGR emissions suggest chemical differences between and within the igneous units, which may reflect primary compositional differences or varying degrees of alteration within igneous units that were initially chemically similar. The fact that the trends in porosity, density, and velocity are not correlated with the NGR trend suggests that the processes that control porosity, density, and *P*-wave velocity are separate from the chemical or lithologic processes that affect the NGR.

Paleomagnetism

Shipboard magnetic studies on the archive-half sections and discrete samples (Fig. F15) established a reliable set of magnetic polarity reversals and investigated rock magnetism, especially the domain state of magnetic minerals in the sediments and igneous rocks. The small amount of coring above the sill yielded a reversal stratigraphy consistent with that seen in Holes 1039B, 1039C, and 1040C during Leg 170. Sediments below the sill generally showed negative polarity, but low recovery and high drilling disturbance preclude identification of a magnetic chron or subchron. Good recovery in the upper gabbro sill allows identification of several intervals of normal and reversed magnetic polarity. In the lower igneous unit, the upper part (between 450 and 513 mbsf) is primarily within an interval of reversed polarity. Two brief intervals of possibly normal polarity are identified, but discrepancies between archive-half and discrete sample results preclude firm identification. Below this depth, multiple intervals of normal and reversed polarity are observed. Postcruise age dating will be necessary to provide an absolute framework for this chronostratigraphy. Saturation remanent magnetization and Lowrie's test of the

sediments show three separate unblocking temperatures, interpreted to reflect the presence of goethite, pyrrhotite (or griegite), and magnetite. In the igneous section, magnetization is often unstable and appears to reflect largely multidomain (>100 m) magnetic minerals, presumed to be magnetite. Intervals of more stable magnetization and high magnetic intensity are observed at 400 mbsf in the upper unit and at 462–474, 513–523, and 572–593 mbsf in the lower unit.

Inorganic Geochemistry

Interstitial water chemistry was used to investigate in situ diagenetic reactions and the possibility of fluid flow in basement (Fig. F21). Several features in the pore water chemistry suggest a role for enhanced ash alteration and associated authigenic mineral formation just above and below the sill. Higher Na and much lower K and Si are observed just above the sill, and the Ca and Sr gradients stop decreasing at this depth. Cl concentrations are very slightly freshened (1.5%) relative to seawater, which may reflect opal-A or clay dehydration reactions immediately above the sill. The implied liberation of Na, Ca, and Sr to the fluids suggests ash alteration. The sharp decrease in K and Si are consistent with the uptake of these liberated elements via the authigenic formation of zeolites and quartz, also observed lithologically. Just below the sill, the Mg concentration in the fluid is quite low, consistent with the authigenic formation of more Mg-rich clays associated with ash alteration. Clear overall gradients with depth are noted for calcium, strontium, sulfate, silica, and lithium. The gradients parallel those measured during and after Leg 170 (Kimura, Silver, Blum, et al., 1997) but are shifted deeper by ~40 m, thus maintaining the same depth relationship to the top of the sill. The gradients trend toward values typical of modern seawater in the intervals just above and below the sill.

Organic Geochemistry

Organic geochemistry at this site reflects the low heat flow of the incoming plate, with all hydrocarbon concentrations measured for shipboard safety requirements being below the detection limit of the gas chromatographs. Calcium carbonate concentrations in the sediments above and below the sill range from 32 to 65 wt% and overlap those of Site 1039, except in the laminated, clay-rich sediments just above the sill, where values drop to <2 wt%. $CaCO_3$ in the igneous rock is low, (<0.4 wt%, except in veins) even in the top and bottom of Subunit 4A and the top of Subunit 4B, immediately adjacent to the sediment section. Veins below 485 mbsf typically contain carbonate (<11 wt%), where some of the differences may be due to variable dilution with igneous material. Total organic carbon is low, and frequently below detection limit, throughout. Sulfur concentrations are <2 wt% in the sediment sections and near zero in the igneous section, except for one vein sampled at 546.1 mbsf.

Microbiology

Sediment whole rounds (5 cm) were taken for contamination testing (microspheres and PFTs) and postcruise microbiological measurements (adenosine 5′-triphosphate [ATP] assay, cell counts, and DNA extractions and analysis). As expected with RCB coring in partially lithified sediments, contamination was significant and variable. In the igneous section, veined intervals were taken as whole rounds (up to 40 cm) and split under sterile conditions. Aliquots will be used for DNA extraction and analysis, culturing experiments and cell counts, fluorescent in situ hybridization studies, and for studies of mineral alteration and chemical change associated with microbial activity. Contamination tests, although difficult to use

quantitatively, indicate that the tracers were delivered to all but one cored interval. Interior tracer concentrations are variable, but microsphere concentrations are lower to very low in the interiors.

Downhole Measurements

At Site 1253, the Davis-Villinger Temperature-Pressure Probe (DVTPP) was deployed twice in an attempt to determine the in situ temperature and pressure of the formation. The first measurement was performed directly beneath the casing of the reentry cone at a depth of 60 mbsf; the second was at a depth of 150 mbsf. Prior to these measurements, the bottom water temperature was determined using a high-resolution and calibrated miniaturized temperature data logger (MTL) (Pfender and Villinger, 2002) attached to the video system during reentry, giving a bottom water temperature of 1.989°C at Site 1253. At Site 1039, the bottom water temperature was 1.81°C, as measured by two different tools (water-sampling temperature probe and Adara). The cause of this difference is not clear. The MTL was also affixed to the triple combo logging tool near the TAP and run during logging. Unfortunately, thermal changes attributed to the curing of the cement used to tag the casing to the formation created a large signal visible in the temperature record in the upper logged interval, and temperature differences recorded between the two runs indicate that equilibrium formation temperatures had not been attained. The two DVTPP runs encountered difficulties with electronic noise and excessive tool motion, precluding their use to provide high-quality temperature or pressure measurements at this site.

Logging

The hole was logged upward with one pass of the triple combo and one pass of the FMS from 530 mbsf to the bottom of the casing shoe at 413 mbsf (Figs. F15, F19). On the second pass, the FMS slid past the obstruction at 530 mbsf and the hole was logged upward from 564 mbsf, where a second bridge was encountered. Measured inclination of the hole was very small (0.5°–1.6°). The caliper data indicate that the hole diameter in the logged portions of the upper and lower igneous units (423–431 and 461–561 mbsf) was relatively uniform, ranging mostly between 10 and 12 in. Thin intervals of increased hole diameter are present at 482, 485, 487–489, and 502–504 mbsf. The caliper reached maximum extension between 435 and 461 mbsf, corresponding to the sedimentary section between the igneous units.

The logs can be clearly separated into three intervals on the basis of obvious changes in hole diameter, velocity, resistivity, bulk density, and porosity, corresponding to the upper igneous subunit (Subunit 4A: gabbro sill), the sediments below, and the lower igneous subunit (Subunit 4B) (Fig. F15). In the logged part of sill (413–431 mbsf, with a 14¾-in hole above 423 mbsf and a $9^{3}/_{8}$-in hole below), porosities are low and densities, resistivities, and *P*-wave velocities are high. In the sedimentary section of enlarged borehole (431–461 mbsf) high porosities and low bulk densities, resistivities, and *P*-wave velocities identify sediments. A return to high bulk densities, resistivities, and *P*-wave velocities at 461 mbsf indicates the top of the lower igneous subunit. The logs better identify the exact depth of the lower igneous subunit than do core depths, because of partial recovery and the standard curatorial practices of moving any recovered material to the top of the core. The NGR intensity is distinctly higher in Subunit 4A than in the sediments and Subunit 4B. Natural gamma logs are not available below 513 mbsf, where NGR measured on cores using the multisensor track (MST) suggest a small increase in K, U, or Th concentrations in the lower part of the lower igneous subunit.

The logging data identify a change in the character of the resistivity and *P*-wave velocity logs in Subunit 4B at ~491–493 mbsf. Above this depth in the lower subunit, values are relatively homogenous; below, the logs have similar average values but a more spiky character. FMS images indicate a change in character at a

depth of ~508 mbsf. Above that depth, conductive features are generally discontinuous. Below, more closely spaced, thin, near-horizontal to slightly dipping conductive features are present in several intervals that are separated by intervals of poor images and irregular borehole size that could be fractured material or sediment interlayers. Intervals of decreased bulk density but no corresponding velocity decrease may indicate a fractured interval rather than sediment interlayers, which should cause a velocity decrease. Based on the bulk density and sonic logs, potential fractured intervals are inferred at 466–468, 484–486, 490–493, and 506–508 mbsf. Sediment interlayers thinner than the vertical resolution of the sonic tool (107 cm), would not be clearly distinguishable in this log, but the general high density and low porosity in areas of smaller borehole diameter preclude the presence of any significant sediment layers.

FMS images can be used to characterize structure and fabric in the igneous units. The gabbro sill (Subunit 4A) between 419 and 426 mbsf exhibits a blocky texture with an ~0.5-m size to the blocks. Between 426 and 432 mbsf, the formation appears more massive with thin conductive features at a 0.5- to 2-m spacing, although it is difficult to trace the conductive features across the four FMS pads. At the very top of Subunit 4B (463–467 mbsf), curved conductive features (fractures or irregularities in the borehole wall) are common. Between 467 and 493 mbsf, the formation appears more massive to blocky, with 0.5- to 1-m spacing between thin conductive features. These conductive features can be clearly traced across the four pads only between ~472 and 478 mbsf. Between 487 and 493 mbsf, irregular to curved vertical conductive features are present, representing possible fractures or irregularities in the borehole wall. From 493 to 498 mbsf, conductive features are rare, becoming more common again between 498 and 508 mbsf. At 508 mbsf, the character of the FMS image changes to more closely spaced conductive features (<0.5-m spacing). In rare cases, such as at 513–514 mbsf, these conductive features can be traced across the four pads and suggest a low dip angle. Image quality between 514.5 and 518 mbsf is poor because of an enlarged borehole. Relatively low (3800–4000 m/s) *P*-wave velocities and low (5–15 Ωm) spherically focused resistivities occur at similar depths. Below 518 mbsf, the layered character returns, but the absolute value of resistivity increases. Imaging is poor from 525–527, 534–539, and 542–555 mbsf. From 539 to 541 and 555 to 563 mbsf, the image is characterized by more closely spaced (<0.5 m) thin, nearly horizontal conductive features. These conductive features appear to dip to the southwest. The static FMS images indicate that both intervals have high resistivity. Therefore, it appears unlikely that these are sediment layers.

Synthesis Topics

Central American Ash Eruption

Leg 205 coring recovered an exceptionally thick Central American ash layer (Fig. F14) deep in the section, deposited in sediments of ~17 Ma, when the plate was more than ~1650 km distant from the Middle America Trench. A thick (~8 cm), white siliceous (>62 wt% SiO_2) ash was recovered at 398.8 mbsf at Site 1253, in the lithified and laminated clay-rich sediments just above the gabbro sill. This tephra contrasts with the majority of the ash layers recovered at Site 1253, which are thin (<2 cm), dark gray in color, and typically have 40–50 wt% SiO_2. These tephras appear to be the product of primary air fall events rather than forming through redeposition as volcaniclastic turbidites or hyaloclastites. The white ash is altered, containing fine sand– and silt-sized particles of cloudy, partially palagonitized glass. Shipboard chemical analysis allowed ash data to be evaluated in terms of Nb/Y and Zr/Y ratios. These tracers are regarded as being little affected by alteration because they are immobile in aqueous solutions. They also distinguish effectively between lavas generated from a hot spot source such as the Galapagos and volcanic arc sources such as Central America. The white tephra has a distinct chemical signature from those in the

dark ash layers; the white ash is interpreted as being from a volcanic arc source, presumably Central America, whereas the dark ashes appear to derive from a Galapagos source.

Using the thickness of the tephra (8 cm) and the maximum grain size of the glass shards (200 µm) together with the inferred distance from the site of eruption in Central America (presumed to be Costa Rica), it is possible to compare this deposit to those from other major eruptions. The white tephra is similar, in both thickness and grain size as a function of inferred distance, to the late Pleistocene Toba eruption of Sumatra (Ninkovich et al., 1978). It is far greater in size than the large, well-documented Quaternary events in the Campanian Province of Italy, or on Santorini in the Aegean Sea. The presence of a second white ash at interval 205-1253A-4R-3, 44–46 cm, raises the possibility that the 8-cm-thick white tephra is simply the largest in a series of powerful events. Both occurred during a period of strong explosive volcanic activity in the eastern Circum-Pacific region (Kennett et al., 1977), which has been linked to rapid spreading rates and plate reorganization in the Pacific. Both siliceous white tephras lie within an atypical 4-m-thick section of laminated claystone, almost carbonate free (<2 wt% $CaCO_3$), which is over and underlain by bioturbated nannofossil chalks. This interval may represent a period when the biological productivity of the eastern Pacific was in a state of temporary collapse precipitated by a period of powerful explosive volcanism.

Fluid Flow in the Incoming Plate

As at Site 1039, 1.4 km to the west, interstitial water chemistry determined at Site 1253 is also indicative of fluid flow in or below Subunit 4B, where the chemical composition of the fluid is inferred to approach values typical of modern seawater. Figure F21 shows depth profiles for major, minor, and biogeochemical components determined shipboard in the sediment interval above and below the sill. In the limited sediment interval cored, Site 1253 profiles for Ca and Sr mimic those at Site 1039 (Fig. F21). Highest Ca values (~18.5 mM) seen at ~300 mbsf at Site 1039 likely reflect the effects of mafic ash alteration, which liberates Ca. Mg-calcite and dolomite production are also suggested by Mg and Mg/Ca profiles at Site 1039 (Kimura, Silver, Blum, et al., 1997). In the pore waters from the deeper sediments at Site 1253, Ca and Sr decrease by ~20%–30%, toward, but not to, values typical of seawater. A similar magnitude change is seen in the Si content of the pore fluids above and below the sill, excluding the exceptionally low values seen at the immediate boundary with the sill (where quartz precipitation was noted). Li contents increase by ~60% over the lowermost 30 m of the section above the sill. Sulfate concentrations in the pore waters from Site 1253 are relatively uniform (27.2–28.6 mM, with no clear depth variation) and nearly of seawater composition. This contrasts with values of 12–20 mM measured higher in the section at Site 1039. These gradients are in directions opposite to those expected for most biogeochemical and fluid/rock reactions in deep siliceous and calcareous sediments at low and elevated temperatures, which would be expected to reduce sulfate and to release Si, Ca, and Sr while consuming Mg and Li. The gradients observed at Site 1253, like those at Site 1039, suggest communication with a fluid of nearly seawater composition at depths below those from which interstitial waters have been recovered. At Site 1039, residence time calculations based on Sr and Li isotopes and concentrations (Silver et al., 2000) indicate that the gradients toward seawater are supported by flow within the last 15–20 ka. The gradients at Site 1253 are closely similar to those at Site 1039, supporting an argument for recent flow here also, which may have extracted heat from the plate to produce the unusually low heat flow in this region. The nature of this large regional-scale flow system, presumed responsible for the large heat flow anomalies as well as the chemical gradients, remains enigmatic; the CORK-II was installed at this site in hopes of providing necessary new information for better understanding the flow system.

Igneous Stratigraphy

The petrology of the igneous units can be combined with paleomagnetic and rock magnetism studies and logging results to better understand the nature of the two units and the internal structure of Subunit 4B (Fig. F15). Paleomagnetic results show that the sill (Subunit 4A) spans several polarity reversals, implying multiple pulses of magma intrusion, although the elapsed time cannot be evaluated until age dating is completed postcruise. Magnetic intensity is highest at the top of the sill, indicating more stable magnetization, probably because of the presence there of finer-grained magnetite than at deeper levels in the sill. The petrologic boundary between the two subunits approximately corresponds with a polarity reversal boundary. Subunit 4A-2 is composed entirely of microcrystalline gabbro. Logging results show a large hole diameter at the top of Subunit 4A-2, which corresponds to the 14¾-in hole drilled to provide a rathole for the casing installation. Seismic velocity and shallow resistivity (considered more reliable in the igneous units; see "Downhole Logging") are relatively high and uniform, and the cores recovered are massive in appearance, breaking into large pieces. At the base of the sill, recovery drops, the hole size increases, and velocity and resistivity decrease in general and exhibit a more spiky character, suggesting that fractured rock is present or possibly thin (<1 m) sediment interlayers.

The lower igneous subunit (Subunit 4B) begins at a depth of 450 mbsf in the core reference frame, which was used for petrologic and paleomagnetic work, and at ~460 mbsf in the logging data. A depth of 460 mbsf for the top of Subunit 4B is considered more reliable, given the very low recovery at the top of the subunit and the standard curatorial practice of moving all recovered material to the top of the core. Subunit 4B was subdivided into seven subunits, using the same criteria used for Subunit 4A. Within each subunit, multiple alternations between microcrystalline and fine-grained material may indicate the presence of multiple cooling units. Subunits 4B-1 through -3 all formed during what may be a single reversed polarity interval, although dating is required. Magnetic intensity is again high at the top of Subunit 4B, and decreases with depth. The logging data show that Subunits 4B-1 through 4B-3 are characterized by high, and relatively uniform, resistivity and *P*-wave velocity. There is a marked increase in resistivity at the top of Subunit 4B-4, which corresponds to a short massive interval that was drilled very slowly (0.75 m/hr) with high recovery. In this interval, conductive features are rare in the FMS data (see "Downhole Logging"). There is a hint of increased *P*-wave velocity at and below this interval, seen in the logging data and as measured in the cores. From ~490 mbsf to the base of the logged section, the borehole character become more heterogeneous, with intermittent highs and lows in resistivity and seismic velocity. At 508 mbsf, FMS images change to more closely spaced conductive features, which are continuous across all four pads at rare intervals, such as 513–514 mbsf. This is an interesting depth, as it corresponds to a thin layer of rock with true basaltic texture and a return to high magnetic susceptibility, similar to that seen at the top of the sill and the top of Subunit 4B, and interpreted as indicating single domain (<100 µm) magnetite. Below this depth, several clear sets of polarity reversals are seen, indicating multiple periods of magmatic activity. The MST natural gamma measurements on the core suggest increased K, U, or Th concentrations in this lower part of Subunit 4B. Glass is more abundant below this depth, discrete and diffuse alteration is more extensive, and carbonate-bearing veins are present. Despite these differences, the generally microcystalline and fine-grained material below this depth share many textural, mineralogical, and chemical similarities to the overlying sections.

CORK-II Installation

Details of the CORK-II installation in Hole 1253A are shown in Figure F22 with the petrological and structural character of key depths as shown in Figures F15 and F19. The center of the packer was set at ~473 mbsf, with the inflatable element being between 471.5 and 475.5 mbsf. The cores indicate that this

is an interval of high recovery of massive rock with relatively few fractures. The logging results (see "Downhole Logging") show this to be in an area of relatively uniform physical properties (high resistivity, bulk density, and *P*-wave velocity). Interpretation of FMS images indicates a massive-blocky formation, with 0.5- to 1-m spacing between thin conductive features, which can be traced across the four pads. The upper OsmoSampler, located inside a 7.35-m-long screen in the 4½-in casing, is set between 496.7 and 504 mbsf (Fig. F19). A 2-m pressure screen is located within the casing screen, and a fluid sampling line runs from this screen to the CORK-II wellhead. Figure F19 shows this to be an interval of modest recovery of moderately fractured rock composed of alternating microcrystalline and fine-grained material (see "Igneous Petrology"). Logging data in Figure F15 show this to be an interval of generally uniform hole diameter, with minor variations in bulk density and *P*-wave velocity. FMS images show closely spaced conductive features. The lower sampler is dangled in the open hole between 512.1 and 519.5 mbsf. This is again a zone of moderate recovery and fracture density in a cryptocrystalline (basaltic) to microcrystalline part of the section, with relatively high concentration of voids and 10% to locally 50% secondary mineral formation. The logging data (Fig. F15) show this to be an interval of decreased resistivity and sonic velocity and variable hole diameter. In the upper part of this interval, FMS images show closely spaced (<0.5 m) shallowly dipping conductive features that are continuous and can be traced across the four FMS pads. The intervals for the osmotic samplers were chosen using a combination of scientific and operational constraints. Originally, the intervals between 513–521 (now OsmoSampler 2) and 560–568 mbsf were targeted, where the latter is a zone of high fracture density and maximum alteration in largely microcrystalline rock. However, the bridge encountered by the logging tools at 530 mbsf restricted the OsmoSampler deployment to shallower levels. The upper pressure screen, located above the packer, was set into the sediments between the two igneous subunits, where sediments collapsing around the screen are expected to make an effective seal. The final installed configuration for this modified CORK-II geochemical and hydrologic borehole observatory is shown in Figure F22.

Site 1254

Site 1254 is located ~1.5 km arcward from the deformation front at a water depth of 4183 m, close to the holes drilled at Site 1040 during Leg 170 (Kimura, Silver, Blum, et al., 1997). Hole 1254A is positioned ~15 m west of Hole 1040C, and Hole 1054B is ~50 m northeast of Hole 1040C (Figs. F3, F23, F24). Therefore, all comparisons to Leg 170 results are to Hole 1040C at Site 1040, as it was the only one which penetrated the décollement and underthrust.

The primary objective of Site 1254 was to investigate a fault zone in the prism, investigate the décollement, and install a long-term observatory for monitoring of fluid flow, pressure, and temperature in the décollement. Results from Site 1040 (Kimura, Silver, Blum, et al., 1997) and seismic data (Fig. F24) provided the framework for drilling the sedimentary sequence and the interpretation of pore fluid geochemistry and structure. Site 1040 geochemical anomalies suggest that deeply sourced fluids, perhaps from seismogenic depths, are migrating along the décollement and prism fault. Site 1254 was intended to investigate in detail the structure and geochemistry of these zones and install an observatory in the décollement. Although perturbed by drilling disturbance, high recovery at Site 1254 enabled detailed structure observations where they were considered reliable and higher-resolution chemical sampling than was possible during Leg 170. It is also possible to better correlate intervals of maximum fluid flow to specific structural horizons.

The seismic record (Fig. F24) in the vicinity of Site 1254 (CMP number 3130) shows no coherent reflections above the décollement. This reflects the general chaotic sedimentary pattern observed in cores

from Hole 1254A. The first prominent reflector relevant for drilling objectives is at 6 s TWT which marks the boundary between margin sediments and the underthrust sequence, which was cored at 361 mbsf. The prism fault zone is not imaged in the seismic data.

After setting the reentry cone at Hole 1254A, we cored the prism fault zone (150 to 230 mbsf) and the décollement (300 to 367.5 mbsf) with the RCB. Recovery averaged at ~88% throughout the cored interval. With generally good hole conditions we planned to case the hole with 10¾-in casing. However, after running the casing to 232 mbsf, the casing could no longer advance and had to be pulled up. Soon it became clear that the reentry cone had hung up on the casing; when the sections that were jammed into the cone were pulled up into the moonpool, it became obvious that the casing had collapsed in the throat of the reentry cone for unknown reasons. Hole 1254B, the second attempt for a CORK-II installation, was offset 50 m to the northeast. However, drilling conditions there prevented us from deepening the hole to >278 mbsf, when the drill string got stuck during several attempts to deepen the hole. Therefore, we decided to install the osmotic fluid sampler in the upper fault zone with the screen located at 225 mbsf; this interval cored and analyzed at Hole 1254A was not recored because of time constraints. The depth for the screen was determined by inference from the geochemical results of Hole 1254A, which indicate that deeply sourced fluids containing thermogenic hydrocarbons are present in the target zone. After a successful installation of the 10¾-in casing, the installation of the CORK-II failed as it got stuck ~20 m above the final depth. Attempts to penetrate further probably caused the 4½-in casing to break right below the CORK-II head. Thus, we had to abandon Hole 1254B with ~20 m of casing sticking out of the reentry cone.

In total, we drilled 367.5 m at Site 1254, with 140.5 m cored and 227 m drilled and washed. Because of the nature of the tectonic structures encountered, part of the core was heavily disturbed by RCB drilling, which makes structural and paleomagnetic studies especially difficult. However, the generally good recovery with an average of 89% allowed extensive whole-round sampling of the cored sections for pore water and organic geochemistry in addition to shipboard sampling for physical property and paleomagnetic studies as well as personal samples for postcruise studies.

The sedimentary sequence recovered at Site 1254, Subunit P1B after Leg 170, is dominated by structureless and typically unsorted dark greenish gray claystones with variable, subsidiary quantities of silt and rare interbedded volcanic ashes, sandstone, and clasts, spanning a badly dated sequence of presumed Pliocene–Pleistocene age (Fig. F25). Recovered cores often show moderate to extreme degrees of drilling disturbance, nonetheless, coherent fragments of more lithified sedimentary rocks do indicate that much of the section is either massive or slightly mottled, which is suggestive of moderate bioturbation.

The dominance of clay minerals within the sequence is readily apparent from smear slides, as is the downcore decrease in volcanic ash. Fresh volcanic glass is present at low (<10%) and moderate levels (<30%) above 230 mbsf, becoming heavily altered deeper (>300 mbsf) in the section. The continental provenance of the sediments cored in Hole 1254A is clear from the abundance of quartz and feldspar grains and also from the bright, brownish red biotite mica flakes that are found at all stratigraphic levels. The terrigenous nature of the sediments is confirmed by the very low biogenic component (<5%) of the sediment, restricted to occasional nannofossils above 200 mbsf and below 360 mbsf. Below Section 205-1254A-15R-2 (360.62 mbsf), the proportion of diatoms increases sharply (>10%). The appearance of diatoms is considered important for understanding the structure of the forearc prism because the uppermost sedimentary subunit in the subducting Pacific stratigraphy (Subunit U1A) recorded high percentages of diatom abundance (Kimura, Silver, Blum, et al., 1997).

Redeposited blocks of shallow water peloid limestones, lithified prior to incorporation within mudstones, are found throughout the section, which is consistent with fluidized gravity and debris flows

being the dominant mode of sedimentation. The cobbles show evidence for a shallow-water depositional environment, identified by shallow-water bivalve shell fragments and small gastropods.

Compared to the sequence of well-preserved tephra found at ODP Sites 1039 and 1253 on the subducting Cocos plate, there is little well-preserved tephra stratigraphy found at Site 1254. Although occasional, thin altered ash layers are recognized, they are rare, typically <2 cm thick and often completely altered to claystone. Volumetrically the tephra represent <1% of the total section. Two thicker coherent ash layers are recorded at Site 1254 (205-1254A-5R-8, 14–20 cm, at 193.49 mbsf and 8R-8, 22–65 cm, at 222.37–222.80 mbsf). Both the thicker ashes preserve relatively fresh glass shards and are interpreted to be the product of primary airfall deposition followed by settling through the water column. The base of the tephra recovered in Section 205-1254A-8R-8 was not recovered, resulting in a minimum thickness estimate of 43 cm. Because Site 1254 is ~150 km from the nearest arc volcano in Central America, this thickness at this range indicates that this must have been a very large eruption, comparable to the Minoan Ash from Santorini as the closest analogue (Watkins et al., 1978). Major and trace element analyses of this tephra (interval 205-1254A-8R-8, 22–65 cm) characterize its source as being the volcanic arc of Central America.

Coring at Site 1254 targeted two different structural domains based on Site 1040 results: (1) a fault zone from 150 to 223 mbsf containing fractured sediment and locally steep bedding dips called the prism fault zone and (2) the décollement zone from 300 to 368 mbsf (Fig. F25). A variety of deformation structures is present at Site 1254, and description of deformation was based on breccia size, foliation, hardness of breccia clasts, and polished surfaces. Because structural observations in poorly lithified material require good quality cores and the recovered cores are sometimes severely disturbed by drilling, it is difficult to distinguish natural from drilling-induced features.

Cores from 150 to 223 mbsf show various degrees of deformation, with the intensity of deformation, particularly breccciation and brittle shearing increasing downward, reaching a peak at ~219 mbsf. Deformation is discontinuous, being focused along sheared horizons, 20 cm to 2 m thick. These horizons are characterized by stratal disruption, foliated breccia with fragments as small as a few millimeters in length, brittle shear zones, deformation bands, and distinctly inclined bedding. Concentration of deformation structures at ~210 and 219 mbsf documents that this is indeed a fault zone that has a distinct geochemical anomaly as discussed below. A well-preserved foliated breccia (interval 205-1254A-R8-1, 0–24 cm; 213 mbsf) indicates reverse movement, based on Riedel shears, which may imply that the fault system is reverse. Paleomagnetic reorientation of this shear zone suggests that the fault is a northeast- or southwest-dipping feature, implying that it is a thrust fault (Fig. F25) that strikes parallel to the deformation front.

The second interval cored started at 300 mbsf, and well-preserved structures are observed starting at Core 205-1254-11R (319.30 mbsf) (Fig. F25). Cores typically show pervasive drilling disturbance, previously described during Leg 170 as “spiraliferous” (Kimura, Silver, Blum, et al., 1997), consisting of a spiral rotation of clay-rich sections. Despite the drilling disturbance, some bedding plane orientations were observed. Bedding and fissility show various dips, indicating heterogeneity of deformation, but the paleomagnetic reorientation shows that they consistently dip northeast or southwest, parallel to the deformation front. The recovered section from 319.30 to 367.50 mbsf is characterized by intense deformation. The deformation is heterogeneous, and brecciation, usually associated with a strong foliation, is the basis for dividing the deformed interval in two zones.

The upper zone from 319.30 to 328.90 mbsf is characterized by generally increasing brecciation with depth, producing fragments of <0.3 cm. Foliation is common throughout Core 205-1254-11R resulting in a clear alignment of clasts, which are equidimensional, but internally strongly foliated. Below 324.15

mbsf (Core 205-1254A-12R) deformation sharply decreases, and consolidated and coarsely brecciated sand layers become common. These sandstone layers have steeply dipping laminations and a few web structures. We interpret this well-defined change in deformation intensity to mark the top of a relatively less-deformed rock volume that may be the footwall of the fault identified between 319. and 328.9 mbsf and may be related to the décollement zone. This indicates a more articulate structural geometry than that observed at Site 1040 (Kimura, Silver, Blum, et al., 1997; Tobin et al., 2001).

The upper boundary of the décollement zone at 338.5 mbsf is defined by the increasing amount of deformation in Core 205-1254A-R13. The definition of the décollement upper boundary is always difficult to place because the deformation gradually increases in its intensity toward the zone of concentrated shear; a sharp increase in deformation is not observed between Cores 205-1254A-12R and 13R. The décollement zone itself is heterogeneous, with a general downward increase of brecciation intensity, fragment aspect ratio, and hardening of the sediments. Despite the good recovery, "spiraliferous" drilling disturbance affects the cores, even though less extensive than at Site 1040. Unlike Site 1040, "spiraliferous" disturbance is not concentrated in the lowermost part of the décollement zone. Brecciation can be pervasive and severe with fragments characterized by polished surfaces; the development of scaly fabric is precluded by the abundant silt and sand in the sediments. From 354.8 to 355.9 mbsf sandstone layers are brecciated and foliated. At 360.60 mbsf the appearance of diatoms in the sediments marks the lithologic boundary with the hemipelagic Subunit U1A of the underthrust (Figs. F25, F26). The lithologic boundary is present below 50 cm of finely brecciated sand and 10 cm of highly sheared clay indicating a surface of ductility contrast which appears as a major structural discontinuity. The hemipelagic sediments below the lithologic boundary are still intensely deformed and brecciated with aligned clasts showing a strong internal foliation (Fig. F27). The base of the décollement is placed at 364.2 mbsf and is below the lithologic boundary. Deformation starts to decrease and becomes discrete below 364.2 mbsf, where intact sediments are separated by 3- to 8-cm-thick brittle shear zones producing gouge or Riedel shears (Fig. F28). These brittle shear zones show exceptionally consistent normal movement and landward dips when reoriented to the geographical coordinates. The hemipelagic sediments above 364.2 mbsf are also deformed by normal faults, a few of them are present as conjugate features. At Site 1254 the décollement zone has a thickness of 25.7 m. In this analysis the décollement has cut down into the uppermost underthrust section incorporating a small amount (4.2 m) of Subunit U1A into its base. The complex geometry of the décollement system at Site 1254 contrasts with that described at Site 1040 and 1043, where the top of the décollement was placed at an increase in brecciation, even though somewhat arbitrarily, and the lithologic boundary between the prism and the hemipelagic subunit coincides with the base of the décollement.

Paleomagnetic measurement on archive-half sections and discrete samples are severely degraded by pervasive drilling disturbance and drill string overprints. Natural remanent magnetization inclinations are highly variable after alternating-field demagnetization and make the identification of magnetic polarity and the construction of a magnetostratigraphy impossible. However, the data were useful in carefully selected intervals to reorient core segments for structural interpretation. Demagnetization curves of discrete samples from the prism sediments (Subunit P1B) are often poorly behaved, indicating that they have a very unstable magnetization. Two significant high magnetic intensity and susceptibility zones were observed in the intervals from 184 to 202 mbsf and from 310 to ~350 mbsf. The interval of the first anomaly is close to the prism fault zone at ~210 to 220 mbsf, and the second anomaly is within the décollement zone. These variations suggest changes in concentration, grain size, and chemical components of magnetic minerals related to lithology and/or chemical alteration perhaps related to fluid flow.

A total of twenty 35- to 45-cm whole rounds were sampled at Site 1254 for pore fluid geochemistry. Pore waters were analyzed for Ca, Mg, K, Na, B, Ba, Fe, Mn, Sr, H_4SiO_4, NH_4^+, and SO_4^{2-} concentrations (Fig. F25). Li, Ca, K, Mg, and Na were analyzed in "real time" on the shipboard ICP-AES between 305 and 366 mbsf to identify the horizons of maximum fluid flow within the décollement zone based on correlation to nearby Site 1040. The "real-time" chemical analyses were available 2 hours after core recovery and, together with careful observations of hydrocarbon gas concentrations and penetration rate, helped to identify the top of the underthrust section.

The pore fluid salinity in the prism sediments (Subunit P1B) is lower than that of seawater by 20% and focused excursions of higher dilutions up to a maximum of 29% are present at 218 and ~351 mbsf (13 m from base of the décollement zone). The two main focused salinity minima also show propane, lithium, and calcium concentration maxima, as well as Mg/Ca, potassium, and magnesium minima. The geochemical excursions between 210 and 218 mbsf are present within a highly fractured interval interpreted as a fault zone, whereas the excursions at ~351 mbsf coincide with a brecciated sandy interval that is moderately indurated. A small peak in calcium, lithium, and propane concentrations is present at 330 mbsf, and it is associated with another sandy, brecciated interval in the décollement. These data suggest, together with results from the entire interval cored during Leg 170, that fluid has migrated along conduits and permeated the lower half of the deformed wedge. Assuming that the geothermal gradient is ~20°–30°C/km, the source region must be present at >4 km depth because the minimum temperature required for thermogenic gas formation is 90°–100°C. The minimum in potassium concentrations at 218 and 351 mbsf further suggests that the deformed sediments have been permeated by a fluid from an elevated temperature source of 80°C to 120°C where the illitization reaction is effective, which consumes potassium. Also, the K depletion signature of this fluid provides an approximate upper limit to the temperature at the source of ~<150°C. Above this temperature, fluid-rock reactions leach potassium from the rocks. Lithium, like potassium, is partitioned into solids at low to moderate temperatures. At higher temperatures, >100°C but <250°C, lithium is released into the fluid phase (Chan and Kastner, 2000). The precise threshold temperatures for the partitioning of Li and K into the solid or fluid phases are as yet unknown. Clays and other silicate dissolution or alteration releases boron into the fluid phase; however, clay, especially illite, formation consumes boron and may be responsible for the low boron concentrations within the deformed sediments. The deeply sourced fluid, however, is not enriched in dissolved silica.

Geochemical excursions in calcium, lithium, propane, potassium, and magnesium are present at ~218 mbsf within the prism fault zone at Site 1254. Similar increases in calcium, lithium, and propane concentrations, as well as marked decreases in magnesium and potassium concentrations, were observed at an observed prism fault zone at Site 1040; however, it was present between ~180 and 200 mbsf. Therefore, the upper geochemical boundary at Hole 1254A is ~20 m below the same boundary observed during Leg 170.

The geochemical boundary at ~218 mbsf separates intervals with pore fluid chemistry typical of clay-rich sediments from those permeated by a fluid from an elevated temperature source, and it seems to be independent of any lithology. Bulk sediment chemistry is also relatively homogenous throughout the entire prism. Changes in pore water chemistry in a lithologically and chemically homogenous sediment section likely result from fluid advection into the lower half of the deformed sediment section. The chemical changes observed at the base of the fault zone (conduit) at ~218 mbsf are similar to those observed near the bottom of the décollement zone associated with the fluid anomaly in a sandy interval. Except for the biogeochemical components, the pore fluid concentration depth profiles of the underthrust section are similar to those at the reference Site 1039. The concentrations themselves are slightly different in magnitude than at Site 1039, presumably reflecting the changes in solubilities and

dissolution rates of the major sediment components under the new pressure regime as they are underthrust. In contrast to Site 1039, the higher ammonium concentrations and the absence of sulfate at the interface between décollement and the underthrust sediments reflect the fact that all the sulfate is reduced at Site 1254 by microbiological activity. Sulfate reduction thus reaches completion in the uppermost few meters of the underthrust hemipelagic section, resulting in somewhat elevated methane concentrations within the zero-sulfate depth interval. These geochemical patterns are similar to those observed at Hole 1040C.

Volatile hydrocarbon gases were sampled by headspace and vacutainer techniques at a higher frequency than pore water samples to assist in determining the exact depths of the inferred fluid conduits associated with fault zones discovered at Site 1040. Analyses of the vacutainer samples (Fig. F25) show that the gas mainly consists of methane but also contains considerable amounts of higher alkanes up to pentane. Methane concentrations were very high (7–9 × 10^5 ppmv) throughout the cored interval but dropped to ~4 × 10^4 ppmv directly below the décollement zone at 364 mbsf. Propane, which is a strong indicator of deeply sourced fluids because of its thermogenic origin (>90°–100°C required), shows one peak at 216 mbsf and another in the basal part of the décollement zone at 355 mbsf, with maximum levels of 326 and 370 ppmv, respectively. These high propane concentrations correlate with structurally identified fault zones. Similar patterns, at much lower concentrations, were also observed in the headspace gas samples.

Samples for microbiological investigations were taken and either frozen or fixed for postcruise ATP quantification, DNA assessment, or cell counts. Samples of drilling water were frozen to evaluate contamination of cores. The chemical tracer for quantifying microbiological contamination was not deployed during coring at Site 1254 because of concern that the trace element chemistry of the PFT may affect postcruise pore fluid geochemical analyses. Particulate tracer tests yield fluorescent microsphere counts suggesting very low to no particulate contamination in the interior of the microbiology whole rounds.

Porosities and bulk densities at Site 1254 (Fig. F25) exhibit trends similar to those seen at Hole 1040C. Variations in porosity and density within the structurally defined décollement zone correlate with core descriptions: in general, zones of lower porosity (40%–45%) correspond to zones characterized by "spiral" deformation interpreted as drilling disturbance; zones of higher porosity (50%–55%) correspond to zones characterized by brecciation. Porosity is also low (42%–44%) between 358 and 361 mbsf, within and adjacent to a zone of localized shear. Porosity increases and bulk density decreases sharply below 361 mbsf across the lithologic boundary between prism sediments and Pleistocene diatomaceous claystone.

We attempted three downhole measurements of formation temperature and pressure, two with the DVTPP at 50 and 200 mbsf and one at 150 mbsf with the Davis-Villinger Temperature Probe (DVTP). The temperature measurement at 200 mbsf was the only deployment with an interpretable decay curve and indicated a temperature of 3.59°C. This is in good agreement with measurements from Site 1040C. All pressure measurements were unsuccessful as a result of tool movement when in formation. However, pressures measured at the mudline and bottom of the hole are in very good agreement with expected hydrostatic pressures expected at that depth which clearly demonstrates that the pressure measurements are reliable.

In summary, the analyses of structural fabric and geochemical anomalies allowed us to identify a geochemical boundary at ~218 mbsf that separates pore fluids typical of clay-rich sediments above from those permeated by a fluid from a source at elevated temperature below within a lithologically homogenous section. At ~338.5 mbsf a fault marks the upper boundary of the décollement zone, which extends into the upper meters of the underthrust sequence at 364.2 mbsf. Maximum pore fluid chemical

anomalies, indicative of active fluid flow, appear to preferentially follow zones characterized by brittle fabric. Analysis of cores from the two intervals allowed us to select the optimal depth interval for the long-term borehole fluid sampler experiment. However, because of unstable hole conditions, two attempts to install a CORK-II failed and Site 1254 had to be abandoned because of time constraints.

Site 1255

Site 1255 is located ~0.4 km arcward from the deformation front at a water depth of 4311.6 m and in close vicinity to the holes of Site 1043 drilled during Leg 170 (Kimura, Silver, Blum, et al., 1997). Hole 1255A is ~20 m east of Hole 1043A and ~30 m northwest of Hole 1043B (Figs. F3, F29, F30). At Hole 1043A the complete section was cored to 282 mbsf in the underthrust sequence (Unit U3), whereas Hole 1043B was logged using LWD to 482 mbsf, to the top of the igneous basement. As both holes penetrated the décollement, their results were used to plan the drilling strategy and the installation of the CORK-II observatory.

The objective of Site 1255 was to identify the décollement with "real-time" geochemical analyses and penetration rate and to install a long-term observatory for monitoring of fluid flow, pressure, and temperature in the décollement. Because of time constraints, only four cores were taken from 123 to 157 mbsf. We recovered 7.2 m (21%) from the 34 m of cored section. Because of the limited recovery and whole-round sections taken for pore water analyses for locating the décollement, other studies on the cores were limited.

The seismic record (Fig. F30) in the vicinity of Hole 1255A (CMP number 3174) shows no coherent reflections above the décollement. This reflects the general chaotic sedimentary pattern observed already in cores from Site 1254 and in Leg 170 results. The confused seafloor reflection pattern, masking a clear seafloor identification, is probably due to side echoes, generated by local bathymetric relief (Fig. F3). The first prominent reflector relevant for drilling is at 5.96 s TWT that marks the boundary between margin sediments and the underthrust sequence, which was cored at 144 mbsf at Hole 1255A. The current seismic data do not show any evidence for fault zones above the décollement.

After setting the reentry cone at Hole 1255A, we drilled to a depth of 123 mbsf with a 14¾-in bit. We then installed 10¾-in casing to a depth of 117 mbsf and cemented it in. Coring started at 123 mbsf, after drilling out the cement shoe, and stopped at 157 mbsf when a sudden increase in penetration rate during cutting of the fourth core indicated that the underthrust sediments were reached. The installation of the CORK-II was successful and completed with the deployment of the remotely operated vehicle (ROV) platform. A postcruise *Alvin* dive showed the installation to be fully operational, and pressure data showed a return to hydrostatic conditions within the borehole.

The section recovered from Hole 1255A can be separated into lithostratigraphic Unit T1 (equivalent to Subunit P1B at Site 1254) and Subunit U1A just beneath the level of the décollement at 144.08 mbsf. The division marks a sharp junction between a series of structureless greenish gray claystones with silts and few or no diatoms above an underlying series of diatom-rich claystones with interbedded silts, sands, and occasional fine-grained conglomerates. The clastic sediments in the underthrust section (Subunit U1A), interpreted as near-trench turbidites during Leg 170, differ from the purely hemipelagic diatom ooze recovered at Site 1043 (Kimura, Silver, Blum, et al., 1997). The fact that these turbidites were not recovered at Site 1043 may indicate that this section is very thin and simply not recovered or not present at all because of lateral facies changes over short distances. Blocks of reworked carbonate in Unit T1 indicate that these sediments are mostly debris flows, in part derived originally from shallow, nearshore environments. The presence of a pelagic nannofossil chalk interval and the larger proportion of diatoms

at Site 1255 suggests that this site experienced a larger amount of pelagic sedimentation than did Site 1254. The underthrust section represents a trench depositional setting, with turbidite silts and sand interbedded with hemipelagic mudstones. Unlike other sites of Leg 205, sediments at Site 1255 contain no primary ash layers in the short section recovered; however, fresh and altered volcanic glass shards do comprise a significant proportion (10%–15%) of the prism sediments.

At Site 1255, structural deformation, with brecciation and polished clast surfaces as an indication of incipient scaly fabric, increases within the recovered section from 132.7 mbsf to the base of the décollement at 144.08 mbsf. The top of the décollement zone could not be defined as a result of limited coring and recovery. The base of the décollement is sharp and well defined and coincides with the division between Unit T1 and Subunit U1A. Only one measurement of bedding dip was possible in the décollement zone, giving a dip of 44°. The hemipelagic layers in the underthrust section below 144.08 mbsf show some medium-scale brecciation (1- to 3-cm fragments) with unpolished surfaces, whereas the sandy layers are undeformed.

Volatile hydrocarbon gases were sampled using the vacutainer and headspace technique. As no gas voids were apparent at Site 1255 in contrast to Site 1254, vacutainer samples show large air contamination. Headspace methane concentrations drop rapidly from >3000 ppmv in Core 205-1255A-2R to 5 ppmv below the décollement (145 mbsf). Propane as an indicator for deeply sourced fluids is low in the prism section (~1 ppmv) and absent below the décollement.

Only three whole rounds (one per core) could be taken for geochemical analyses of pore waters because of low recovery, and all conclusions are therefore somewhat speculative. As observed at Site 1254, the chemical composition of the pore fluids at Site 1255 also is distinctly different in the wedge and underthrust section, with a less sharp transition at the base of the décollement zone at ~144 mbsf. Fluid flow is indicated by salinity, sodium and calcium concentration minima, and lithium concentration maxima within the décollement sample at 134.2 mbsf. These concentration minima were observed at Site 1043 along with a magnesium concentration maxima within the same interval. Across the décollement, changes in Ca and Mg concentrations are in the opposite direction to those seen at Site 1254. In general, the pore fluids within the upper fault zone and in the décollement at Sites 1254 and 1040 are characterized by having a significantly stronger signature of a deeply sourced fluid than the pore fluids from Sites 1255 and 1043. At Sites 1255 and 1043, the pore fluid chemistry in the wedge and the uppermost underthrust sediments appears to reflect some mixing between the lower wedge and uppermost hemipelagic pore fluids, thereby partially obscuring the deeply sourced fluid signature observed at Site 1254. This pore water mixing could be achieved by advection of fluid from the underthrust section across the décollement and into the lower wedge. Furthermore, leakage of a portion of the deeply sourced fluid sampled at Site 1254 may have occurred through faults, fractures, and more permeable conduits between Site 1254 and Sites 1255 and 1043.

Two samples for microbiological investigations were taken and either frozen or fixed for postcruise ATP quantification, DNA assessment, or cell counts. Samples of drilling water were frozen as well to evaluate contamination of cores. The chemical tracer for quantifying microbiological contamination was not deployed during coring at Hole 1255A because of concern that the trace element chemistry of the PFT may affect postcruise pore fluid geochemical analyses. Particulate tracer tests yield fluorescent microsphere counts suggesting very low to no particulate contamination in the interior of the microbiology whole rounds.

Paleomagnetic declination and inclination, measured on discrete samples and archive halves, disagree in the upper part (132.76 to 134.84 mbsf) of the cored interval, making any magnetostratigraphic interpretation questionable. Across the décollement, a clear polarity change can be seen in both archive

halves and discrete samples. However, the polarity changes cannot be assigned to a particular chron and are not usable for dating purposes. Magnetic intensities are generally low in the upper part of the section but increase substantially in the sandy layers of the underthrust sequence.

Sample porosities and LWD porosities from Leg 170 show a clear increase of porosities at the base of the décollement from values of ~55% in the prism section to values of ~70% in the underthrust. Sample porosities from Hole 1255A clearly confirm the values in the prism, but the few data points below the décollement are not representative for the porosity of the underthrust sequence but show rather the influence of sampling clayey or sandy material. Only the magnetic susceptibility shows a marked increase below the décollement, which reflects a presumably higher magnetite content in the turbidites of the underthrust.

A CORK-II observatory was successfully installed as shown in Figure F31. The center of the packer is at 129 mbsf and the center of the screen at 140 mbsf, in the middle of the geochemical anomaly as determined from Site 1255 data and Site 1043 results. The second pressure port inside a small screen was installed just above the upper packer.

OPERATIONS

Leg 205 was originally scheduled to begin in San Diego, California, on 6 September 2002. Because of the threat of a dock workers strike in the western United States, the port call was changed to Victoria, Canada. As a result, the start of the Victoria port call changed to 2 September.

Victoria, Canada, Port Call

Leg 205 officially began with the first line ashore at 0900 hr 2 September. A number of changes resulted from the short time between the decision to change the port call and the start of the port call: (1) the ODP technical staff crossover occurred on 4 September; (2) the Transocean staff crossover took place on 6 September; and (3) the Leg 205 science party boarded the ship on 17 September in Acapulco, Mexico, during the transit from Victoria, Canada, to proposed Site 1039R-A.

Prior to loading the Leg 205 supplies, a substantial amount of equipment used to support the Leg 204 gas hydrate objectives had to be taken off the ship. Pressurized gas hydrate samples, gas hydrate samples immersed in liquid nitrogen, and 340 boxes of core samples were off-loaded. A 20-ft refrigerated van used for processing and storing the gas hydrate samples on board was also removed from the ship. A number of special coring tools (HYACINTH [Deployment of HYACE Tools in New Tests on Hydrates]) and special laboratory equipment for gas hydrate research also were off-loaded.

Immediately upon arrival in Victoria, 1095 metric tons of marine gas oil was taken on board and we started to load 60 metric tons of barite and 80 metric tons of sepiolite. After the food for Leg 205 was loaded, the following equipment was loaded: (1) seven joints of 16-in casing, (2) 30 joints of 10¾-in casing, (3) 139 joints of 4½-in casing, (4) a new spool of core winch wire, (5) four standard reentry cones, (6) four CORK-II wellheads and associated instruments, (7) four 16-in casing hangers, (8) two 10¾-in casing hangers, (9) a new bicentered hole opener, and (10) other miscellaneous hardware.

An essential element of the long-term geochemical observatories to be installed during the leg was the downhole water, gas, pressure, and temperature sampling/monitoring equipment. During the port call, six downhole OsmoSamplers were assembled and stored in a water bath in the downhole measurements laboratory so that they would be completely prepared for deployment later in the leg. During assembly,

temperature sensors were placed inside of them. The pressure meters and data logger units were checked out and programmed in preparation for deployment.

At the request of the port authority, starting on 4 September, loading operations had to be suspended at 1700 hr each day for noise abatement. The ship left Victoria at 0754 hr on 7 September and began the transit to Acapulco, Mexico, to pick up the Leg 205 science party.

Transit from Victoria, Canada, to Acapulco, Mexico

Because of Leg 204 operations continuing up to the last possible minute and a very short (39 hr) transit to Victoria, Leg 204 personnel had only minimal time for the routine end-of-leg maintenance of the drilling equipment; much of this activity took place during the transit. In addition, the new core winch wireline was installed and some minor plumbing runs associated with the CORK-II wellheads were made during the transit.

Calm seas were encountered during the initial portion of the transit. On 15 September, however, the vessel began passing through the edge of a tropical depression (36- to 42-nmi/hr winds and 20-ft seas) which reduced the ship's speed. The weather moderated during the day of 16 September, and moderate seas were encountered for the rest of the transit to Acapulco, Mexico.

The transit ended with the first line ashore at 1030 hr on 17 September in Acapulco, Mexico. The total transit was 2636 nmi and took 239.4 hr at an average speed of 11.0 nmi/hr.

Acapulco, Mexico, Port Call

The primary objective of the brief Acapulco port call was to board the Leg 205 scientists and load a few pieces of equipment that were essential for Leg 205 operations but did not make the Victoria port call. This included two 10¾-in casing hangers and the 32-in vibration isolated television (VIT) camera guide sleeve.

Because the weather forecast for the transit to Site 1039R-A did not look favorable for using the cranes while under way, we decided to assemble the Site 1039R-A reentry cone while in port. Work on the reentry cone began at 1200 hr. By 1700 hr the reentry cone had been bolted together and tack welded enough to make it secure for the transit, and a pilot was requested for departure. During this time, a required safety briefing on the vessel's survival gear was given to the science party. In addition, we also took advantage of the fact that the vessel was moored with starboard side to the dock and lowered lifeboats 2 and 4 to the water and started their engines. With all tasks completed in Acapulco, the last line was released at 1738 hr on 17 September and we began the transit to proposed Site 1039R-A.

Transit from Acapulco, Mexico, to Proposed Site 1039R-A

The final welding of the reentry cone was completed (0600 hr on 18 September) during the transit to proposed Site 1039R-A. We also held additional safety meetings, introduced key Transocean personnel and the ODP operations manger to the science party, and gave science party members tours of the ship to familiarize them with the vessel.

At 1053 hr on 19 September, we changed course toward shore to disembark one of the ship's steward because of a family emergency. At 1830 hr on 19 September, the vessel was positioned just off the south breakwater at Puerto Madero, Mexico. A small fishing boat arrived from Puerto Madero and took the steward to shore. At 1845 hr the vessel resumed the transit to proposed Site 1039R-A.

At 1400 hr on 21 September, the vessel arrived at proposed Site 1039R-A.

Site 1253 (Proposed Site 1039R-A)

The thrusters were lowered and the vessel was placed in dynamic positioning mode at 1431 hr on September 21, and we deployed a seafloor positioning beacon at 1620 hr. The upper guide horn was then laid out and the reentry cone moved to the center of the moonpool doors. Drill collars were picked up for the bottom-hole assembly (BHA), assembled, and stored in the derrick. Three joints of 16-in casing (42.5 m) were assembled, and a 16-in casing hanger was made up to the casing string. The casing running tool was then attached to the casing string, and the casing string was lowered into the reentry cone until the casing hanger latched into the reentry cone. The weight of the reentry cone was picked up to verify it had latched properly. We then released the casing running tool and pulled out of the reentry cone. A visual inspection confirmed that the casing hanger latch ring was properly seated in the reentry cone landing ring latch ring groove.

The next step was to attach a 14¾-in tricone bit to the stinger below the casing running tool. The rest of the BHA was then made up and lowered into the reentry cone until the running tool landed. The running tool was latched into the 16-in casing hanger, and the entire assembly (16-in casing, reentry cone, BHA) was picked up off the moonpool doors. The moonpool doors were opened, and at 2100 hr on 21 September, the reentry cone was lowered below the keel. The moonpool doors were then closed and the pipe trip to the seafloor began.

At 0745 hr on 22 September, with the 16-in casing shoe and bit near the seafloor, the jetting-in process began, initiating Hole 1253A. At 0945 hr, the reentry cone mud skirt landed on the seafloor and the running tool was released. This was verified using the VIT camera system. The seafloor depth was determined to be 4387.1 meters below rig floor (mbrf) (4376.3 mbsl), and the bottom of the 16-in casing shoe was at 43.82 mbsf. We then retrieved the drill string in preparation to assemble an RCB BHA.

After installing the reentry cone and 16-in casing, we assembled an RCB BHA with a $9^{7}/_{8}$-in bit and bit release. The bit was lowered to the seafloor, and Hole 1253A was reentered at 0555 hr 23 September. We then drilled ahead without coring from 4431.0 to 4444.0 mbrf (43.8 to 56.8 mbsf) where a DVTPP measurement was taken. The temperature and pressure data appeared to indicate that the tool moved while in the formation.

When the DVTPP was recovered, the colletted delivery system (CDS) was jammed with rust and sediment. This created a seal inside the upper barrel above the collets, trapping pressure inside the barrel. A vent hole was drilled in the upper barrel to prevent this from recurring, and the CDS was cleaned up and redressed with a new set of collets. After stroking the tool to verify performance, the CDS was set aside for use at a later time.

We continued to drill ahead without coring from 4444.0 to 4537.2 mbrf (56.8 to 150 mbsf) when the DVTPP was deployed a second time. Unfortunately, this run of the DVTPP also experienced tool movement while in the formation resulting in poor data. A review of the tool and deployment procedures is under way.

We then drilled ahead without coring to 4757.1 mbrf (369.9 mbsf), where we started RCB coring. Cores 205-1253A-1R through 4R, consisting of nannofossil chalk and claystone, were taken from 4757.1 to 4787.6 mbrf (369.9 to 400.5 mbsf). The rate of penetration (ROP) in the sediments was 23 m/hr, and we had a core recovery of 73%.

Cores 205-1253A-5R through 9R were cut from 4787.6 to 4817.0 mbrf (400.5 to 429.9 mbsf) in a very dense and hard gabbro sill. The ROP in the gabbro was 1.7 m/hr, and core recovery was 70.3%. Another change in the drilling occurred when we encountered sediments in Cores 205-1253A-10R through 13R. The ROP was 18.2 m/hr, and core recovery dropped to 17%.

We encountered more gabbro in Cores 205-1253A-14R through 28R from 4817.0 to 4916.0 mbrf (429.9 to 528.9 mbsf). A few thin sediment layers were present in the gabbro, but these were only minimally recovered. The ROP dropped to 1.4 m/hr, and core recovery rate was 50%.

At the end of cutting Core 205-1253A-25R, a small amount of erratic torque in the drill string was observed. With 53.2 total rotating hours on the bit, 45.2 hr of which were in hard rock, the decision was made to trip the drill string for a bit change. The bit cleared the seafloor at 1950 hr on 27 September. During the trip out of the hole, tight spots were noted at 4816, 4734, and 4647 mbrf. The bit cleared the rig floor at 0245 hr on 28 September. The used drill bit was in good condition but was slightly reduced in gage.

A new $9^{7}/_{8}$-in RCB bit was made up to the BHA. Because of the length of time drilling in hard rock, the mechanical bit released was also replaced. The BHA was spaced out for the RCB and lowered to the seafloor.

Hole 1253A was reentered at 1108 hr on 28 September. The bit was lowered into the hole to 4816 mbrf (429 mbsf), where excessive drag was encountered. We picked up the top drive and washed/reamed from there to the bottom of the hole at 4903.1 mbrf (516 mbsf). Once the 32 m of fill in the bottom of the hole was cleaned out, we resumed RCB coring.

After the bit change, we continued RCB coring from 4903.1 to a total depth of 4987.1 mbrf (515.9 to 600.0 mbsf) and recovered 59.6 m (71%). The penetration rate through this hard gabbro section was a painstakingly slow 1 m/hr. The lowermost 6 m of the hole appeared to have numerous ledges and may be deviated. Because of the slow penetration rate and no clear indication that we were close to the bottom of the gabbro, we decided to stop coring.

Next, we circulated 30 barrels of sepiolite to clean out the hole and made a wiper trip in preparation for logging. While lowering the pipe back to bottom during the wiper trip, an obstruction was encountered at 4920 mbsf (533 mbsf). The top drive was picked back up and used to rotate and wash to the bottom of the hole. Several ledges were reamed on the way back to total depth. Torque in the bottom 6 m of the hole led us to speculate that this section may be deviated. As this section is so close to the bottom of the hole, there was no way to confirm this with a survey.

After the 2 m of fill in the hole was washed out, 30 barrels of sepiolite was circulated to ensure all the debris was washed out of the hole. Then, in preparation for logging, the entire borehole volume hole was displaced with 185 barrels of sepiolite. The bit was pulled out of the hole, and the was ship offset 50 m north to drop the bit on the seafloor. At 2308 hr on 2 October, the pipe reentered Hole 1253A and the end of the pipe was positioned at the 16-in casing shoe at 4431 mbrf (44 mbsf).

The logging equipment was rigged up, and the triple combo tool string was lowered into the hole. The tools would not penetrate past a bridge at 4537 mbrf (150 mbsf). Because the upper sediment section had been logged previously during Leg 170 and our primary logging objective was the deeper part of the section, we decided to postpone logging until after we set the 10¾-in casing into the top of the first sill.

We retrieved the drill string, and the bottom of the BHA was back on the rig floor at 1615 hr on 3 October. To prepare for the installation of the 10¾-in casing, we needed to widen the $9^{7}/_{8}$-in hole to 14¾ in. We attached a 14¾-in reaming bit to the BHA, lowered it to the seafloor, and reentered Hole 1253A at 0044 hr on 4 October. We then drilled (without coring) from the 16-in casing shoe (4431 mbrf; 44 mbsf) to 23 m into the top of the upper gabbro (4810 mbrf; 422.8 mbsf). To make sure the hole was in the best condition possible to install the 10¾-in casing, the entire borehole volume was circulated two times, a wiper trip was made (without any significant hole problems), the borehole volume was circulated again, and then the hole was filled with sepiolite. The 14¾-in reaming bit was then pulled out of the hole; it reached the rig floor at 1345 hr on 5 October.

After assembling 30 joints of 10¾-in casing (411 m) and a cementing shoe, we lowered it to the seafloor and reentered Hole 1253A at 0210 hr on 6 October. We picked up the top drive with a cementing manifold and landed the 10¾-in casing hanger in the reentry cone at 0445 hr on 6 October. The casing was cemented in place with 40 barrels of cement (15.8 lb/gal). The cementing was completed at 0650 hr, the casing running tool was released, the cementing manifold was laid out, the top drive was racked back, and the drill string was pulled out of the hole. The camera system was recovered while the pipe was pulled out of the hole, and the drill string was back on the rig floor at 1530 hr on 6 October.

Our next step was to drill out the cement plug at the bottom of the casing as well as clean out the hole to total depth (600 mbsf) in preparation for logging and installing the CORK. We assembled the BHA with a tricone bit (Reed HP21 $9^{7}/_{8}$-in mill tooth), ran it down to the seafloor, and reentered the hole at 0011 hr on 7 October. The top of the cement was encountered at 4795 mbrf (407.8 mbsf), which is ~5 m above the bottom of the 10¾-in casing shoe.

The cementing plug and cement inside the casing were drilled out in 45 min, and then the hole was cleaned to 4987.1 mbrf (600.0 mbsf). The hole was swept clean with 30 barrels of sepiolite, and we started a wiper trip by raising the bit up to the 10¾-in shoe. On the way back down to 600 mbsf, 20,000 lb of weight was taken at 4976 mbrf (588.8 mbsf), so we rotated and washed the hole from there to total depth. We found 7 m of fill in the bottom of the hole. The hole was swept again with 50 barrels of sepiolite and then displaced with 60 barrels of sepiolite in preparation for logging.

Before we could log, we had to drop the bit on the seafloor. The bit was pulled clear of the reentry cone at 1630 hr on 7 October, and the vessel was offset 50 m north. The rotary shifting tool (RST) was deployed on wireline to release the bit. The mechanical bit release (MBR) shifted smoothly; however, the bit did not drop off. The RST was picked up and then dropped on top of the MBR support bearing, knocking the bit free at 1840 hr.

We reentered Hole 1253 (at 2027 hr), positioned the bottom of the pipe near the 10¾-in casing shoe at 4798 mbrf (410.8 mbsf), racked back the top drive, and started to rig up for logging. After assembling the triple combo tool string and lowering it into the hole to 4917 mbrf (530 mbsf), we lost communications with the tool and it had to be pulled out of the hole. The Hostile Environment Litho-Density Sonde was leaking oil; it was replaced with the Hostile Environment Litho-Density Tool. The reconfigured triple combo was lowered down the drill string until it landed on a bridge at 4917 mbrf (530 mbsf). The tools could not be worked past the bridge, so the hole was logged from that point up to the seafloor and then pulled out of the hole.

The FMS-sonic velocity tool string was assembled and lowered into the hole until it landed on a bridge at 4917 mbrf (530 mbsf). The tools would not pass the bridge, and we logged from there up to the 10¾-in casing shoe (4798 mbrf; 411 mbsf). The FMS was lowered for a second pass, and this time it passed through the bridge at 4917 mbrf, coming to rest on another bridge at 4951 mbrf (564 mbsf). We logged from that point up to the 10¾-in casing shoe and then pulled the tools out of the hole. Once we had disassembled the logging tools, we pulled the drill string out of the hole, clearing the reentry cone at 2215 hr on 8 October. After the bottom of the pipe was back on the rig floor (0515 hr on 9 October), the drill line was slipped and cut.

The next operational step at Hole 1253A was to deploy the CORK-II. After preparing the rig floor and all the tools required, the 4½-in casing screen was picked up and hung off at the rotary table. A latch nipple for landing/latching the OsmoSampler inside the casing was attached to the screen. To the top of the screen, we attached one full joint of 4½-in casing, one 2-m-long piece of 4½-in casing, and one 3-m-long piece of 4½-in casing. The screen was lowered into the moonpool, where the flat umbilical was connected

to the two ¼-in pressure monitoring hydraulic lines extending from the top of the screen. The screen was then lowered through the moonpool as the umbilical was strapped to the 4½-in casing.

A CORK-II inflatable packer was picked up next and attached to the top of the 4½-in casing. The packer was lowered into the moonpool, where the umbilical was severed and connected to the two ¼-in pressure monitoring hydraulic pass through lines extending from the bottom of the packer. The packer was then lowered through the moonpool, and the umbilical was connected to the two ¼-in pressure monitoring hydraulic pass through lines extending from the top of the packer.

We then attached 33 joints of 4½-in casing, one 2-m-long piece of 4½-in casing, and one 3-m-long piece of 4½-in casing (467.44 m total length) to the top of the packer. The umbilical was strapped to the 4½-in casing and centralizers attached to the casing as the screen/packer subassembly was lowered through the moonpool.

During deployment of the 4½-in casing string and umbilical, at ~16 m above the packer, one of the three umbilical ¼-in hydraulic lines was severed and split out of the umbilical. A ¼-in pressure monitoring line termination screen was connected to the split-out umbilical hydraulic line. The termination screen will be used to monitor the pressure above the packer and below the 10¾-in casing shoe. The termination screen was banded to the 4½-in casing, and centralizers were positioned at the top and bottom of the termination screen to protect it.

The CORK-II running tool was latched onto the CORK-II wellhead. The wellhead was then picked up and made up to the top of the 4½-in casing string. The wellhead was lowered into the moonpool where the umbilical was severed and connected to the bottom of the wellhead. The packer setting hose was made up between the CORK-II running tool and the top of the wellhead, completing the assembly.

All of the sampling valves and bleed valves on the wellhead were opened, and the wellhead was lowered into the water to purge the hydraulic lines of air. The $^{1}/_{16}$-in hydraulic lines connecting the pressure meter control valves to the pressure meters were filled with water prior before the wellhead was picked up. The wellhead was raised back to the moonpool level, where all valves were closed. Large rubber bands were then attached to the individual valve handles such that they would hold the valves in the closed position during the deployment. This was done to prevent the valves from partially opening during the deployment as happened with the ACORK valves deployed during Leg 196. With all hydraulic lines purged, all valves closed, and a last-minute inspection of the wellhead completed, the CORK-II assembly was lowered to the seafloor.

Hole 1253A was reentered at 0320 hr on 10 October. The 4½-in casing screen shoe was lowered to 4874 mbrf (487 mbsf), where we picked up the top drive and lowered the wireline sinker bar assembly into the hole for a sounding run. The wireline sinker bar assembly reached 4915 mbrf (527.8 mbsf), which was 7 m below the OsmoSampler sinker bar's final position.

The lower weak link (900 lb) was made up to the top of the OsmoSampler sinker bar. This subassembly was then picked up and landed in the top of the drill string. The upper OsmoSampler was attached to the latch/running tool subassembly with 4.88 m of $^{3}/_{8}$-in braided nylon rope. The upper weak link (1500 lb) was attached to the bottom of the upper OsmoSampler followed by 13.4 m of $^{3}/_{8}$-in braided nylon rope. The lower OsmoSampler was then attached to the rope.

The Hole 1253A OsmoSampler subassembly (23.61 m over all length) was picked up, and the bottom of the lower OsmoSampler was connected to the lower weak link on top of the sinker bar that hung off in the drill pipe. The entire assembly (27.31 m overall length) was then lowered down the drill string until the latch/running tool subassembly landed on the drill string. The wireline sinker bar assembly was made up to the latch/running tool subassembly, and then the entire assembly was slowly lowered down the drill string in steps to prevent differential pressure from damaging the osmotic pumps.

The OsmoSampler assembly was lowered until the latch/running tool subassembly landed in the latch nipple on top of the 4½-in casing screen. The latch/running tool was jarred down on to set and lock the latch (lock mandrel) in the latch nipple. A 3,000 lb overpull with the wireline confirmed that the latch was locked in place. The latch/running tool was then jarred up on, shearing the running tool release pin and releasing the running tool from the latch at 1110 hr on 10 October. The running tool and wireline were then pulled out of the hole.

The packer setting go-devil was then dropped down the inside of the drill string. The CORK-II wellhead was then lowered into the hole until it landed and latched into the reentry cone. A 5,000 lb overpull with the drill string confirmed that the wellhead was latched into the reentry cone.

The drill string was pressured up to 800 psi and held for 30 min to set the packer. While the drill string was being pressurized, the pressure gauge fluctuated once as if there was a sudden small change in volume. Also, occasionally while holding the 800-psi pressure, the pump had to be engaged at 2–3 strokes per minute to maintain the pressure. After 30 min, the drill string pressure was increased to 1,800 psi and held for 10 min to activate the spool valves (to connect the pressure sensors in the wellhead to the downhole screens). Finally, all of the drill string pressure was bled off through the rig floor standpipe manifold relief valve.

The final step was to install the ROV platform around the wellhead on top of the reentry cone. The landing platform and deployment bridle were assembled in the moonpool and then lowered down the drill string to the reentry cone on the logging line. After landing the platform on top of the reentry cone the deployment bridle acoustic releases were activated at 2245 hr on 10 October. The logging line was raised and the weight indicator showed a reduction in weight of 800 lb, confirming that the platform had been released. The logging line and platform deployment bridle were then pulled out of the hole.

We then deployed the camera system to visually inspect the installation. No problems were observed during the visual inspection, so the CORK-II running tool was released from the wellhead at 0050 hr on 11 October.

The wireline sinker bar assembly was deployed to recover the packer setting go-devil to prevent having to retrieve the drill string when it was full of water. However, the go-devil was encountered at 400 mbrf instead of at the CORK-II running tool, where it should have been. It took 1.5 hr and jarring with 8,000 lb of overpull to recover the go-devil. When it was recovered, the go-devil seals were missing. The top drive was racked back, and the drill string and camera system were pulled out of the hole. The CORK-II running tool cleared the rig floor at 0945 hr on 11 October.

While the drill string was being retrieved, the ship moved in dynamic positioning mode to Site 1254 (1.1 nmi). The beacon from Site 1253 was recovered at 0430 hr on 11 October and redeployed at 0945 hr on 11 October at Site 1254A.

Transit from Site 1253 to Site 1254 (Proposed Site 1040R-B)

After the drill string was pulled out of Hole 1253A, the ship moved in dynamic positioning mode to Site 1254 (1.1 nmi) while the drill string was being retrieved. The beacon from Site 1253 was recovered at 0430 hr on 11 October and redeployed at 0945 hr on 11 October at Site 1254A.

Site 1254 (Proposed Site 1040R-B)

Hole 1254A

The first operation at Site 1254 was to install a reentry cone and 16-in surface casing. Two joints (29.37 m) of 16-in casing were made up to a casing hanger and latched into a standard reentry cone. The reentry cone was lowered to the seafloor and Hole 1254A was initiated at 2225 hr on 11 October. The water depth was determined to be 4194 mbrf.

The sediments proved to be quite consolidated near the seafloor, and 10 hr was required to jet in the 16-in casing. The casing running tool was released at 0850 hr on 12 October, and the drill string was pulled out of the hole clearing the reentry cone at 0900 hr. The camera system was recovered, and the casing running tool cleared the rotary table at 1645 hr 12 October.

After installing the reentry cone and 16-in casing, we assembled a RCB BHA and lowered it to the seafloor. Hole 1254A was reentered at 0110 hr on 13 October, and we drilled without coring from the 16-in casing shoe at 4223 mbrf (29 mbsf) to 4244 mbrf (50 mbsf). A DVTPP measurement was made at 50 mbsf, but the data were not usable. Hole 1254A was then drilled from 4244 to 4344 mbrf (50 to 150 mbsf), where a second DVTP deployment was made; the data were once again not usable. Hole conditions through this part of Hole 1254A were stable, and the ROP was 9.3 m/hr.

RCB Cores 205-1254A-1R through 6R were cut from 4344 to 4397.8 mbrf (150 to 203.8 mbsf). A third DVTPP measurement was made at 203.8 mbsf, and for the first time this leg, good temperature data were recorded. The pressure data, however, were not good. RCB Cores 205-1254A-7R and 8R were taken from 4397.8 to 4417 mbrf (203.8 to 223.0 mbsf). Cores 205-1224A-1R through 8R penetrated 73 m, and we recovered 66.59 m (91%); the overall penetration rate was 10.8 m/hr. No hole problems were encountered, and the hole remained stable while coring this interval.

Hole 1254A was then drilled without coring from 4417 to 4494 mbrf (223 to 300 mbsf) in 8.5 hr (9 m/hr). The hole remained stable through this drilled interval requiring only periodic circulation of sepiolite mud to keep the hole clean.

To determine the upper and lower boundaries of the décollement, Hole 1254A was cored from 4494 to 4561.7 mbrf (300 to 367.5 mbsf). Cores 205-1254A-9R through 16R recovered 58.41 m (87%), and the penetration rate through this interval was 10 m/hr.

Sepiolite mud was circulated periodically over this cored interval to maintain hole stability; however, none of the anticipated hole problems associated with drilling through a décollement occurred. The hole was displaced with 111 barrels of sepiolite, and the RCB bit was pulled out of the hole. The RCB bit cleared the reentry cone at 0530 hr on 16 October and reached the rig floor at 1230 hr.

A BHA was assembled with a 14¾-in bit for opening the hole in preparation for installing the 10¾-in casing string. We reentered Hole 1254A at 2135 hr on 16 October and rotated and washed from the 16-in casing shoe at 4223 mbrf (29 mbsf) to 4527 mbrf (333 mbsf). Fifty barrels of sepiolite mud were then circulated to clean out the hole, and then we circulated twice the borehole volume. We then conducted a wiper trip that encountered a tight spot at 4395 mbrf (201 mbsf). The bit was washed and reamed through the tight spot and lowered back down to the total depth of the 14¾-in hole at 4527 mbrf (333 mbsf); 2 m of fill at the bottom of the 14¾-in section of hole had to be washed out.

We circulated another 50 barrels of sepiolite and twice the hole volume with seawater. A second wiper trip was undertaken back to the 16-in casing shoe and encountered tight spots at 4482, 4420, and 4386 mbrf (288, 226, and 192 mbsf). During the wiper trip back down, the bit encountered a bridge at 4386

mbrf (192 mbsf); it could support ~20,000 lb of drill string weight. We washed and reamed through this tight spot and back down to 4527 mbrf (333 mbsf).

Once again, we swept the hole with 60 barrels of sepiolite and twice the hole volume with seawater. The hole was then displaced with 255 barrels of sepiolite to help stabilize the hole while we prepared to assemble and install the 10¾-in casing string. The drill string encountered no significant drag while pulling out of the hole. The bit cleared the reentry cone at 2215 hr on 17 October, and the bit reached the rig floor at 0500 hr on 18 October.

Twenty-eight joints (324 m) of 10¾-in casing were made up and attached to a 10¾-in casing hanger. The cementing tools were assembled and attached to the casing running tool which in turn was made up to the 10¾-in casing string. The 10¾-in casing string was then lowered to the seafloor, and Hole 1254A was reentered at 1738 hr on 18 October.

The 10¾-in casing shoe was lowered to 4426 mbrf (232 mbsf) when it suddenly appeared to hang up as identified by reduction in string weight of 20,000 lb. The drill string was immediately picked up to the hanging weight of the string. The casing was lowered again and took weight at the same depth.

A stand of drill pipe had just been picked up, and there was not much traveling space in the rig available to work the casing up and down. The casing was worked within these traveling limits without being able to pass the tight spot.

The space-out was such that the drill string could not be picked up without activating the Crown-O-Matic (the stand of drill pipe was too close to the top of the derrick) and could not be lowered and secured on the rig floor without putting the casing in compression. Thus the ship was offset far enough to allow the drill string to be landed on the drilling elevator stool without putting the casing in compression. A stand of drill pipe was laid out, and the ship was moved back over the hole. When we raised the drill string so that we could remove a single joint of drill and attach the top drive, the reentry cone was pulled up off the seafloor along with the 10¾-in casing string.

The 10¾-in casing string and reentry cone were worked in an unsuccessful attempt to free the reentry cone from the casing string. The VIT camera system was lowered to the reentry cone for a visual inspection. It appeared that a joint of 10¾-in casing had collapsed inside the reentry cone. With all options for freeing the reentry cone from the 10¾-in casing string exhausted, the 10¾-in casing string, with the reentry cone and 16-in casing attached, was pulled out of the hole.

Once the casing string with the stuck reentry cone was clear of the seafloor, we offset the ship 0.5 nmi perpendicular to the seismic line on which Site 1254 is located. If the reentry cone or other hardware fell off during recovery, we didn't want it to fall in the area where the scientists wanted to attempt another CORK-II installation. The reentry cone was pulled into the moonpool at 0845 hr on 19 October. While laying out the 10¾-in casing string, we found four joints that were bent. This bending likely occurred during attempts to break off the casing inside the reentry cone at the seafloor. Approximately 3 m of a collapsed joint of 10¾-in casing was found protruding out of the top of the reentry cone.

It was deemed unsafe, and too costly in time, to attempt to salvage the reentry cone and casing. Thus preparations were made for jettisoning the reentry cone. The connection between joints 7 and 8 was partially loosened. The reentry cone was then lowered below the keel of the ship and hung off near the top of joint 9 in slips at the rotary table. Although the casing was hung off in the slips, the elevator was left attached to the casing and positioned just beneath the collar. A padeye was then welded to the casing just below the elevator to prevent the joint from jumping upward when the reentry cone was released. With all personnel cleared from the rig floor and the moonpool area, the rotary table was engaged to finish unscrewing the loosened connection, and at 0920 hr on 19 October the reentry cone was jettisoned, ending Hole 1254A.

Hole 1254B

The scientists decided to make a second attempt at installing a CORK-II at Site 1254. The ship was then moved to ~48 m at N36°E from Hole 1254A. After the 10¾-in casing handling equipment was rigged down, the 16-in casing handling equipment was rigged up. A reentry cone, which had been previously assembled for our next site, was moved into the well center on top of the moonpool doors. Two joints of 16-in casing (20 m) plus a 16-in casing cementing shoe were then made up to a 16-in casing hanger, and the assembly was latched into the reentry cone. The jetting BHA was then made up and latched into the 16-in casing hanger. The reentry cone was then picked up off the moonpool doors, and the reentry cone was then lowered to the seafloor. We started washing in the 16-in casing at 2550 hr 19 October, beginning with Hole 1254B. After it was washed into the seafloor to 20.42 mbsf in 6.5 hr, the casing running tool was released and the drill string was retrieved. Our next step was to drill a 14¾-in hole into which we could install the 10¾-in casing. We assembled a drilling BHA with a 14¾-in bit, lowered it to the seafloor, and reentered Hole 1254B at 2134 hr 20 October.

The 14¾-in hole was advanced to 4418 mbrf (231 mbsf) when the upper fault zone was penetrated. As we advanced through the fault, increased fill and torque were encountered. The fault had to be reamed and swept clean by circulating sepiolite before the bit could penetrate deeper.

When the bit reached 4452 mbrf (265 mbsf), the hole began to pack off around the drill string. The bit was raised 20 m and then washed and reamed back down to 265 mbsf. We drilled to 4465 mbrf (278 mbsf) when the pipe became stuck. After three hours of working the pipe with overpull up to 200,000 lb, the pipe could be raised again.

Because of the poor drilling conditions, we decided to conduct a wiper trip. The bit was pulled up to 4289 mbrf (102 mbsf), encountering 80,000 lb drag from 4453 to 4415 mbrf (266 to 228 mbsf). It took 6.75 hr to wash and ream back to the bottom of the hole at 4465 mbrf (278 mbsf); 40 m of fill in the bottom of the hole had to be drilled/washed out. With hole conditions deteriorating and no hope of setting casing to the décollement, we decided to install a CORK-II to monitor the upper fault zone.

The bit was pulled up to the 16-in casing shoe at 4210 mbrf (23 mbsf), and then the pipe was lowered back down. The bit encountered resistance (took weight) at 4397 mbrf (210 mbsf) and was washed and reamed from there to 4424 mbrf (237 mbsf). With the bit at the bottom of the hole, we circulated bottoms up in preparation for setting 10¾-in casing. Because the 14¾-in hole extended through the zone of interest, the hole was left full of seawater and no sepiolite mud was used. The bit was pulled out of the hole and was back on the rig floor at 0830 hr on 23 October.

Seventeen joints (197 m) of 10¾-in casing were then assembled, and a casing hanger was attached to the top. The cementing and casing running tools were latched into the casing hanger, and the entire assembly was lowered to the seafloor. At 1822 hr on 23 October, Hole 1254B was reentered with the 10¾-in casing string. It appeared that the hole was producing fluid as we observed, as evidenced by a billowing cloud within the reentry cone and water flowing out of the drill pipe at the rig floor between connections.

The casing was lowered to 4360 mbrf (173 mbsf) when it encountered some resistance and began to take weight. At this point, we picked up the top drive to wash the casing in. The cementing manifold was picked up, and the casing was landed at 2045 hr on 23 October. We confirmed that it was latched in and cemented it in place with 20 barrels of 15.8 lb/gal cement. The 10¾-in casing shoe was at 198.88 mbsf. The casing running tool was released and was back on the rig floor at 0915 hr on 24 October.

Our next operation was to drill out the cement plug and clean out a rathole for the CORK. We assembled a drilling BHA with a $9^{7}/_{8}$-in tricone bit, lowered it to the seafloor, and reentered Hole 1254B at 1716 hr on 24 October. After lowering the bit to the casing shoe, it took 1.5 hr to drill through the shoe.

The hole was then cleaned to 4424 mbrf (237 mbsf) in preparation for deploying the CORK-II. The hole was then circulated bottoms up and left with only seawater in it. The drill bit was pulled out of the hole and was back on the rig floor at 0445 hr on 25 October.

After some routine preventative maintenance (slipping and cutting the drill line), then we started assembling the CORK-II. A screen, packer, 15 joints of 4½-in casing (230 m), umbilical, centralizers, and the wellhead made up the complete CORK-II. The wellhead was lowered to the moonpool doors, where the pressure data logger was tested; it was then lowered into the water to purge the hydraulic lines. At 1445 hr on 25 October, the CORK-II assembly was lowered to the seafloor and Hole 1254B was reentered with the CORK-II at 2050 hr. The 4½-in casing was lowered to 4366 mbrf (179 mbsf) when it encountered some resistance and began to take weight. The top drive was picked up so that we could jet the 4½-in casing in. The jetting process was hampered as a result of having to maintain the drill string pressure below 400 psi to prevent inflation of the packer.

After ~8 hr of attempting to jet the 4½-in casing in with the active heave compensator on at 0745 hr on 26 October, the top joint pin of the 4½-in casing failed through the last engaged thread. With the CORK-II wellhead still attached to the running tool, the vessel was offset to observe the reentry cone. At the time of the failure the end of the pipe was ~10 m above the reentry cone. The broken end of the 4½-in casing was extending out of the reentry cone, but otherwise the reentry cone did not appear to have any observable problems. The CORK-II wellhead was retrieved and was back on the rig floor at 1645 hr on 26 October, ending Hole 1254B. The scientists decided to abandon efforts to deploy a borehole installation at this site and decided to move to Site 1255 (proposed Site 1043R).

The Site 1254 beacon was released at 1106 hr and was back on deck at 1221 hr on 26 October. The ship moved the ~1.1 nmi to Site 1255 in dynamic positioning mode while the CORK-II wellhead was being recovered.

Site 1255 (Proposed Site 1043R)

The beacon at Site 1254 was released at 1106 hr and was on deck at 1221 hr on 26 October. The ship moved the ~1.1 nmi to Site 1255 in dynamic positioning mode while the CORK-II wellhead was being recovered. We deployed a seafloor position beacon at Site 1255 at 2116 hr on 26 October.

A reentry cone was then moved onto the moonpool doors and two joints (20 m) of 16-in casing were assembled to a 16-in casing hanger and latched into the reentry cone. A jetting BHA was assembled and latched into the 16-in casing hanger. At 2000 hr on 26 October, the reentry cone was lowered to the seafloor. Because of complex seafloor topography in the vicinity of the drill site, the 3.5-kHz precision depth recorder returned six different echoes. The most conservative shallowest depth indicated (4234 mbrf) was used. The casing was lowered to 4325 mbrf before the seafloor was detected by a reduction in drill string weight. Hole 1255A was started at 0550 hr on 27 October when jetting-in of the 16-in casing began.

The 16-in casing was jetted in to 4343.49 mbrf (20.49 mbsf) in 5 hr. The casing running tool was released, pulled out of the hole, and was back on the rig floor at 2045 hr on 27 October.

The next step was to prepare the hole for installing 10¾-in casing. A BHA with a 14¾-in drilling bit was assembled, lowered to the seafloor, and Hole 1255A was reentered at 0430 hr on 28 October. We drilled from 4343.49 to 4446 mbrf (20.49 to 123 mbsf). The hole was swept with 50 barrels of sepiolite, and then we circulated the complete borehole volume with seawater. We then conducted a wiper trip by raising the bit to the 16-in casing shoe at 4343.49 mbrf (20.49 mbsf) and then lowering it back down to 4429 mbrf (106 mbsf), where slight weight was taken. The hole was washed and reamed from 4429 mbrf (106 mbsf)

back to total depth (4446 mbrf; 123 mbsf). The hole was again swept with 50 barrels of sepiolite, circulated twice the hole volume with seawater, and 85 barrels of sepiolite pumped into the hole in preparation for deploying 10¾-in casing. The bit was then pulled out of the hole and was back on the rig floor at 0526 hr on 30 October.

Ten joints of 10¾-in casing (115.5 m) were made up with a 10¾-in Dril-Quip casing hanger. A casing cementing plug was then made up to the Dril-Quip casing running tool that, in turn, was latched into the casing hanger. The 10¾-in casing string was then lowered to the seafloor. Hole 1255A was reentered with the casing at 1629 hr on 29 October. The casing was lowered to 4425 mbrf (102 mbsf) when slight resistance was encountered. The top drive was picked up and the casing was washed in to a total depth of 117.42 mbsf. After it was confirmed that the casing hanger had latched into the reentry cone (10,000 lb overpull), the casing was cemented in place with 20 barrels of 15.8-lb/gal cement.

The casing running tool was released at 1940 hr on 29 October and pulled clear of the reentry cone. Before the drill string was tripped back to the ship, the drill line had to be slipped and cut. The casing running tool was back on deck at 0405 hr on 30 October.

An RCB BHA was assembled and lowered to the seafloor, and Hole 1255A was reentered at 1207 hr on 30 October. It took 4.5 hr to drill out the 10¾-in casing shoe with the RCB bit before coring began.

We then cut four RCB cores (Cores 205-1255A-1R through 4R) from 4446.0 to 4480.0 mbrf (132.7 to 157.0 mbsf) and recovered 7.22 m (21%). Once the base of the décollement was identified (based on a substantial change in penetration rate), we began preparing the hole for installing the CORK-II and OsmoSampler.

We swept the hole with 50 barrels of sepiolite, and the borehole volume was circulated with seawater. The bit was raised up to the 10¾-in casing shoe and then lowered back down to 4467 mbrf (144 mbsf), where the bit took weight; the hole was reamed and washed from there to 4476.0 mbrf (153.0 mbsf). Once again, we swept the hole clean with 50 barrels of sepiolite and then circulated the borehole volume with seawater. The bit was again raised up to the 10¾-in casing shoe and then lowered back down to total depth with only slight drag near the bottom of the hole. To keep the hole open without exposing the décollement to barite-weighted mud, 20 barrels of sepiolite was placed in the bottom of the hole. The bit was pulled up to 4416 mbrf (93 mbsf) inside the 10¾-in casing, and the hole was displaced with 32 barrels of heavy mud. The bit was pulled out of the hole and was back on the rig floor at 2015 hr on 31 October.

A CORK-II assembly was assembled consisting of a screen, packer, 123.4 m of 4½-in casing, and a CORK-II wellhead. The CORK-II assembly was lowered to the seafloor to just above the reentry cone. The top drive was picked up so we could pump seawater through the end of the 4½-in casing as it was lowered in the hole to displace the heavy mud and keep the screen clean. Hole 1255A was reentered at 1000 hr on 1 November and the 4½-in casing was lowered to 4465 mbrf (142 mbsf) while seawater was circulated.

The OsmoSampler seat was attached to the coring wireline and lowered down the drill string. The seat landed and was jarred on to latch/lock the lock mandrel in place. When the wireline was recovered the seat was still attached and the running tool was partially sheared and the seat seals were missing. The running tool was redressed, new seals were installed on the seat, and the seat was lowered back down the drill string. The seat landed in what appeared to be the upper latch nipple at top of the packer. The mud pump was engaged, the drill string was pressured to 300 psi, and the seat passed through the upper latch nipple. The seat was then lowered until it landed in the middle latch nipple at top of the screen. Once again the pump was engaged, and the seat passed through the middle latch nipple. The seat was then lowered until it landed in the latch nipple inside the screen. The pump was engaged to fully latch the seat. The seat was jarred down on to latch the lock mandrel in place. An overpull of 3000 lb was applied and

held, indicating that the lock mandrel was latched in place. The running tool was then jarred up on and released. The running tool was then pulled out of the hole and redressed.

When the OsmoSampler was attached to the running tool on the rig floor, the screws holding the OsmoSampler top connection in place were sheared. The running tool was removed, and the broken OsmoSampler was replaced with another one. The OsmoSampler fill port pipe plug (inside the top connection of the OsmoSampler) was protruding above the bottom of the blind box, preventing the double pin crossover sub to be properly attached. Bakerlok was applied to the double pin sub, and the sub was made up to the OsmoSampler top connection. Bakerlok was also applied to the collet housing, and the housing was made up to the OsmoSampler probe tip.

The OsmoSampler assembly picked up with a tugger and landed in the top of the drill pipe. The coring wireline was attached to the assembly, and it was lowered down the drill string in stages to allow pressure equalization of the osmotic pumps. Because the OsmoSampler lock mandrel had no seals, it easily passed through the upper latch nipple and was landed on top of the seat.

With the OsmoSampler probe tip stung through the seat, all of the OsmoSampler sampling ports were sealed off from the 4½-in casing above. The pump was engaged to fully seat the OsmoSampler and help hold the assembly down during jarring. The running tool was jarred down on to latch the lock mandrel in place. When the wireline was raised, no overpull was observed and the weight of the OsmoSampler was lost, indicating that the running tool had released.

The OsmoSampler seat allows the pressure below and above the ported seal bore and plug to equalize. Thus, when the OsmoSampler probe tip is stung into the seat, the OsmoSampler is pressure balanced, so confirmation of latch-in (requiring pulling the OsmoSampler and deploying it again) was not critical to the installation. Once we verified that the OsmoSampler was at the correct depth (by tagging it with the wireline), we pulled the running tool out of the hole.

The modified packer setting go-devil was then dropped down the drill string and chased with the coring wireline without latch. The go-devil was tagged inside the CORK-II running tool, and the wireline was pulled out of the hole.

The CORK-II wellhead was then landed and latched into the reentry cone at 2000 hr on 1 November. The drill string was pressurized to 1,200 psi for 30 min to inflate the packer. The drill string pressure was then increased to 1,800 psi for 10 min to shift the spool valves. While the packer was set, the VIT camera system was pulled out of the hole in preparation for deploying the ROV platform.

The ROV platform was assembled around the drill string in the moonpool. The deployment bridle and the logging line were then attached. The platform was lowered down the drill string on the logging line and landed on the reentry cone.

At 0155 hr on 2 November, the acoustic releases were activated. When the logging line was picked up, overpull was observed, suggesting that the ROV platform was not completely free. The logging line was lowered and the acoustic releases were activated again. When the logging line was picked up, overpull was observed again. The overpull was increased above the weight of the platform, indicating the deployment bridle was hung up on something. The logging line was worked for 30 min without freeing the bridle when a straight pull was applied. The bridle came free with ~4500 lb overpull (9100 lb total wire load) and was pulled out of the hole.

When the bridle was recovered, one of the nylon strap termination eyes was found to have failed. The acoustic release yoke may have hung up in the nylon strap eye and had been pulled down to the platform strap bail. When overpull was applied, the platform was pulled up on one side only until the strap failed. If this scenario is correct, there should be no damage to the wellhead. After recovering the platform deployment bridle, the camera was lowered to inspect the installation and no problems with the

installation were observed. The CORK-II running tool was released at 0615 hr on 2 November. The running tool and VIT were then recovered; the running tool was back on the rig floor at 1600 hr on 2 November.

Once the seafloor positioning beacon was released (0759 hr) and back on deck (0929 hr on 2 November), we moved back to Hole 1254B in dynamic positioning mode to attempt to fish the screen, packer, and 4½-in casing that was left in the hole.

Return to Hole 1254B

After finishing operations at Site 1255, we moved back to Hole 1254B in dynamic positioning mode to attempt to fish the screen, packer, and 4½-in casing that was left in Hole 1254B.

The vessel was positioned over Hole 1254B at 1721 hr on 2 November. A fishing BHA was assembled, consisting of a choker loop formed from wire rope slings, a rig-fabricated jet sub, five 8¼-in drill collars, one tapered drill collar, and the usual two stands of 5½-in drill pipe and a crossover sub.

The fishing tool was lowered to 4157 mbrf, and at 2343 hr 2 November the 4½-in casing was snared. We applied 20,000 lb of overpull to the fish (4½-in casing), and it suddenly dropped off. When the snare was set, the end of the wire rope slings was too far below the end of the BHA for us to visually confirm if the fish was still there. Also, the total weight of the casing string being fished was too small to be distinguished on the weight indicator. The vessel was offset 0.5 nmi as the BHA was pulled out of the hole so that if the fish dropped off, it would not land back on the reentry cone. When the fishing BHA was back on the rig floor, the snare was empty and the casing was not recovered. When the ship was positioned back over the hole so that we could inspect the reentry cone with the VIT camera, we observed that the casing was still sticking out of the reentry cone. After the camera was back on deck and all equipment secured we began the transit to Balboa, Panama, at 1600 hr on 3 November. Leg 205 ended with the last line ashore at 1030 hr on 6 November.

REFERENCES

Abratis, M.W., and Woerner, G., 2001. Ridge collision, slab-window formation, and the flux of Pacific astenosphere into the Caribbean realm. *Geology*, 29:127–130.

Barckhausen, U., Ranero, C.R., von Huene, R., Cande, S.C., and Roeser, H.A., 2001. Revised tectonic boundaries in the Cocos plate off Costa Rica: implications for the segmentation of the convergent margin and for plate tectonic models. *J. Geophys. Res.*, 106:19207–19220.

Barckhausen, U., Roeser, H.A., and von Huene, R., 1998. Magnetic signature of upper plate structures and subducting seamounts at the convergent margin off Costa Rica. *J. Geophys. Res.,* 103:7079–7093.

Becker, K., Fisher, A.T., and Davis, E.E., 1997. The CORK experiment in Hole 949C: long-term observations of pressure and temperature in the Barbados accretionary prism. *In* Shipley, T.H., Ogawa, Y., Blum, P., and Bahr, J.M. (Eds.), *Proc. ODP, Sci. Results,* 156: College Station, TX (Ocean Drilling Program), 247–252.

Becker, K., the Leg 174B Scientific Party, and Davis, E.E., 1998. Leg 174B revisits Hole 395A: logging and long-term monitoring of off-axis hydrothermal processes in young oceanic crust. *JOIDES J.*, 24:1–3, 13.

Carr, M.J., Feigenson, M.D., and Bennett, E.A., 1990. Incompatible element and isotopic evidence for tectonic control of source mixing and melt extraction along the Central American arc. *Contrib. Mineral. Petrol.,* 105:369–380.

Chan, L.-H., and Kastner, M., 2000. Lithium isotopic compositions of pore fluids and sediments in the Costa Rica subduction zone: implications for fluid processes and sediment contribution to the arc volcanoes. *Earth Planet. Sci. Lett.*, 183:275–290.

Christeson, G.L., McIntosh, K.D., and Shipley, T.H., 2000. Seismic attenuation in the Costa Rica margin wedge: amplitude modeling of ocean bottom hydrophone data. *Earth Planet. Sci. Lett.,* 179:391–405.

Christeson, G.L., McIntosh, K.D., Shipley, T.H., Flueh, E., and Goedde, H., 1999. Structure of the Costa Rica convergent margin, offshore Nicoya Peninsula. *J. Geophys. Res.,* 104:25443–25468.

Davis, E.E., and Becker, K., 1994. Formation temperatures and pressures in a sedimented rift hydrothermal system: ten months of CORK observations, Holes 857D and 858G. *In* Mottl, M.J., Davis, E.E., Fisher, A.T., and Slack, J.F. (Eds.), *Proc. ODP, Sci. Results,* 139: College Station, TX (Ocean Drilling Program), 649–666.

Davis, E.E., Wang, K., Becker, K., and Thomson, R.E., 2000. Formation-scale hydraulic and mechanical properties of oceanic crust inferred from pore pressure response to periodic seafloor loading. *J. Geophys. Res.,* 105:13423–13435.

De Mets, C., Gordon, R.G., Argus, D.F., and Stein, S., 1990. Current plate motions. *Geophys. J. Internat.,* 101:425–478.

Fisher, A.T., 1998. Permeability within basaltic oceanic crust. *Rev. Geophys.,* 36:143–182.

Guendel, F., 1986. Seismotectonics of Costa Rica: an analytical view of the southern terminus of the Middle America Trench [Ph.D. thesis]. Univ. of California, Santa Cruz.

Hey, R.N., 1977. Tectonic evolution of the Cocos-Nazca spreading center. *Geol. Soc. Am. Bull.*, 88:1404–1420.

Hyndman, R.D., and Wang, K., 1993. Thermal constraints on the zone of major thrust earthquake failure: the Cascadia subduction zone. *J. Geophys. Res.,* 98:2039–2060.

Hyndman, R.D., Yamano, M., and Oleskevich, D.A., 1997. The seismogenic zone of subduction thrust faults. *Isl. Arc,* 6:244–260.

JOIDES Planning Committee, 1996. *Understanding our Dynamic Earth through Ocean Drilling: Ocean Drilling Program Long Range Plan into the 21st Century:* Washington, D.C. (JOI).

Kastner, M., Morris, J., Chan, L.H., Saether, O., and Luckge, A., 2000. Three distinct fluid systems at the Costa Rica Subduction Zone: chemistry, hydrology, and fluxes. *Goldschmidt 2000, J. Conf. Abstr.*, 5:572. (Abstract).

Kelly, R.K., and Driscoll, N.W., 1998. Structural controls on ^{10}Be occurrences in arc lavas. *Eos*, 79:45.

Kennett, J.P., McBirney, A.R., and Thunnell, R.C., 1977. Episodes of Cenozoic volcanism in the Circum-Pacific region. *J. Volcanol. Geotherm. Res.,* 2:145–163.

Kimura, G., Silver, E.A., Blum, P., et al., 1997. *Proc. ODP, Init. Repts.,* 170: College Station, TX (Ocean Drilling Program).

Kopf, A., Deyhle, A., Zuleger, E., 2000. Evidence for deep fluid circulation and gas hydrate dissociation using boron isotopes of pore fluids in forearc sediments from Costa Rica (ODP Leg 170). *Mar. Geol.,* 167:1–28.

Langseth, M.G., and Silver, E.A., 1996. The Nicoya convergent margin: a region of exceptionally low heat flow. *Geophys. Res. Lett.,* 23:891–894.

Lonsdale, P., and Klitgord, K.D., 1978. Structure and tectonic history of the eastern Panama Basin. *Geol. Soc. Am. Bull.,* 89:981–999.

McIntosh, K.D., and Sen, M.K., 2000. Geophysical evidence for dewatering and deformation processes in the ODP Leg 170 area offshore Costa Rica. *Earth Planet. Sci. Lett.,* 178:125–138.

McIntosh, K.D., Silver, E.A., and Shipley, T., 1993. Evidence and mechanisms for forearc extension at the accretionary Costa Rica convergent margin. *Tectonics,* 12:1380–1392.

Meschede, M., Zweigel, P., Frisch, W., and Völker, D., 1999a. Mélange formation by subduction erosion: the case of the Osa mélange, southern Costa Rica. *Terra Nova,* 11:141–148.

Meschede, M., Zweigel, P., and Kiefer, E., 1999b. Subsidence and extension at a convergent plate margin: evidence for subduction erosion off Costa Rica. *Terra Nova,* 11:112–117.

Moore, J.C., and Saffer, D.M., 2001. Updip limit of the seismogenic zone beneath the accretionary prism of southwest Japan: an effect of diagenetic to low-grade metamorphic processes and increasing effective stress. *Geology,* 29:183–186.

Moritz, E., Bornholdt, S., Westphal, H., and Meschede, M., 2000. Neural network interpretation of LWD data (ODP Leg 170) confirms complete sediment subduction at the Costa Rica convergent margin. *Earth Planet. Sci. Lett.,* 174:301–312.

Morris, J.D., Valentine, R., and Harrison, T., 2002. ^{10}Be imaging of sediment accretion, subduction along the northeast Japan and Costa Rica convergent margins. *Geology*, 30:59–62.

Newman, A.V., Schwartz, S.Y., Gonzalez, V., DeShon, H.R., Protti, J.M., Dorman, L.M., 2002. Along-strike variability in the seismogenic zone below Nicoya Peninsula, Costa Rica. *Geophys. Res. Lett.,* 10.10292002GL015409.

Ninkovich, D., Sparks, R.S.J., and Ledbetter, M.T., 1978. The exceptional magnitude and intensity of the Toba eruption, Sumatra: an example of the use of deep-sea tephra layers as a geological tool. *Bull. Volcanol.,* 41:286–297.

Patino, L.C., Carr, M.J., and Feigenson, M.D., 2000. Local and regional variations in Central American arc lavas controlled by variations in subducted sediment input. *Contrib. Mineral. Petrol.,* 138:265–283.

Pecher, I.A., Kukowski, N., Ranero, C.R., and von Huene, R., 2001. Gas hydrates along the Peru and Middle America Trench system. *In* Paull, C.K., Dillon, W.P. (Eds.), *Natural Gas Hydrates: Occurrence, Distribution, and Detection*. Am. Geophys. Union, Geophys. Monogr., 124:257–271.

Pfender, M., and Villinger, H., 2002. Miniaturized data loggers for deep sea sediment temperature gradient measurements. *Mar. Geol.*, 186:557–570.

Protti, M., Guendel, F., and McNally, K., 1994. The geometry of the Wadati-Benioff zone under southern Central America and its tectonic significance: results from a high-resolution local seismographic network. *Phys. Earth Planet. Internat.*, 84:271–287.

Ranero, C.R., and von Huene, R., 2000. Subduction erosion along the Middle America convergent margin. *Nature*, 404:748–752.

Ranero, C.R., von Huene, R., Flueh, E., Duarte, M., Baca, D., and McIntosh, K.D., 2000a. A cross section of the convergent Pacific margin of Nicaragua. *Tectonics*, 19:335–357.

Ranero, C.R., von Huene, R., Weinrebe, W., McIntosh, K.D., and Reichert, C., 2000b. Mass transfer and fluid flow paths related to subduction erosion at the Middle America convergent margin. *Eos, Am. Geophys. Union,* 81:F81.

Reagan, M., Morris, J., Herrstrom, E., and Murrell, M., 1994. Uranium series and beryllium isotopic evidence for an extended history of subduction modification of the mantle below Nicaragua. *Geochim. Cosmochim. Acta,* 58:4199–4212.

Ruppel, C.K., and Kinoshita, M., 2000. Fluid, methane, and energy flux in an active margin gas hydrate province, offshore Costa Rica. *Earth Planet. Sci., Lett.,* 179:153–165.

Saffer, D.M., in press. Pore pressure development and progressive dewatering in underthrust sediments at the Costa Rica subduction margin: comparison with Northern Barbados and Nankai. *J. Geophys. Res.*

Saffer, D.M., Silver, E.A., Fisher, A.T., Tobin, H., and Moran, K., 2000. Inferred pore pressures at the Costa Rica subduction zone: implications for dewatering processes. *Earth Planet. Sci. Lett.,* 177:193–207.

Scholz, C.H., 1998. Earthquakes and friction laws. *Nature*, 391:37–42.

Screaton, E.J., Saffer, D.M., Henry, P., Hunze, S., and the Leg 190 Shipboard Scientific Party, in press. Porosity loss within underthrust sediments of the Nankai accretionary complex: implications for overpressures. *Geology*.

Shipley, T.H., McIntosh, K.D., Silver, E.A., and Stoffa, P.L., 1992. Three-dimensional seismic imaging of the Costa Rica accretionary prism: structural diversity in a small volume of the lower slope. *J. Geophys. Res.,* 97:4439–4459.

Shipley, T.H., and Moore, G.F., 1986. Sediment accretion, subduction, and dewatering at the base of the trench slope off Costa Rica: a seismic reflection view of the décollement. *J. Geophys. Res.,* 91:2019–2028.

Silver, E.A., Kastner, M., Fisher, A.T., Morris, J.D., McIntosh, K.D., and Saffer, D.M., 2000. Fluid flow paths in the Middle America Trench and Costa Rica margin. *Geology,* 28:679–682.

Silver, E.A, Kimura, G., Shipley, T.H. (Eds.), 2001. *Proc. ODP, Sci. Results,* 170 [CD-ROM]. Available from: Ocean Drilling Program, Texas A&M University, College Station TX 77845-9547, USA.

Stein, C.A., and Stein, S., 1992. A model for the global variation in oceanic depth and heat flow with lithospheric age. *Nature,* 359:123–129.

Tera, F., Brown, L., Morris, J., Sacks, I.S., Klein, J., and Middleton, R., 1986. Sediment incorporation in island-arc magmas: inferences from ^{10}Be. *Geochim. Cosmochim. Acta,* 50:535–550.

Tobin, H., Vannucchi, P., and Meschede, M., 2001. Structure, inferred mechanics, and implications for fluid transport in the décollement zone, Costa Rica convergent margin. *Geology,* 29:907–910.

Valentine, R., Morris, J.D., and Duncan, D., 1997. Sediment subduction, accretion, underplating and arc volcanism along the margin of Costa Rica: constraints from Ba, Zn, Ni, and ^{10}Be concentrations. *Eos,* 78:F673.

Vannucchi, P., Ranero, C.R., Galeotti, S., Straub, S.M., Scholl, D.W., McDougall-Ried, K., in press. Rates of subduction erosion along the Costa Rica Pacific margin: implications for non-steady rates of Austral recycling at subduction zone. *J. Geophys. Res*.

Vannucchi, P., Scholl, D.W., Meschede, M., and McDougall-Reid, K., 2001. Tectonic erosion and consequent collapse of the Pacific margin of Costa Rica: combined implications from ODP Leg 170, seismic offshore data, and regional geology of the Nicoya Peninsula. *Tectonics*, 20:649–668.

Vannucchi, P., and Tobin, H., 2000. Deformation structures and implications for fluid flow at the Costa Rica convergent margin, Ocean Drilling Program Sites 1040 and 1043, Leg 170. *J. Struct. Geol.,* 22:1087–1103.

von Huene, R., Ranero, C.R., Weinrebe, W., and Hinz, K., 2000. Quaternary convergent margin tectonics of Costa Rica, segmentation of the Cocos plate, and Central American volcanism. *Tectonics*, 19:314–334.

von Huene, R., and Scholl, D.W., 1991. Observations at convergent margins concerning sediment subduction, subduction erosion, and the growth of the continental crust. *Rev. Geophys.,* 29:279–316.

Watkins, N.D., Sparks, R.S.J., Sigurdsson, H., Huang, T.C., Federman, A., Carey, S., and Ninkovich, D., 1978. Volume and extent of the Minoan tephra layer from

Santorini volcano: new evidence from deep-sea sediment cores. *Nature,* 271:122–126.

Walther, C.H., Flueh, E., Ranero, C.R., von Huene, R., and Strauch, W., 2000. An unusual crustal structure across the Pacific margin of Nicaragua. *Geophys. J. Internat.,* 14:759–777.

Wilson, D.S., 1996. Fastest known spreading on the Miocene Cocos-pacific plate boundary. *Geophys. Res. Lett.,* 23:3003–3006.

Zhao, Z., Moore, G.F., and Shipley, T.H., 1998. Deformation and dewatering of the subducting plate beneath the lower slope of the northern Barbados accretionary prism. *J. Geophys. Res.,* 103:30432–30449.

TABLE CAPTION

Table T1. Leg 205 operations summary.

FIGURE CAPTIONS

Figure F1. Bathymetric map of the eastern central Pacific showing the location of the Leg 205 drilling area (white box) in the Middle America Trench off Costa Rica. The white box shows the location of the map in Figure F2. The white circle denotes the location of the Leg 206 site. The map is modified after Vannucchi et al., (in press) based on a data compilation of C. Ranero.

Figure F2. Bathymetric map of the Middle America Trench off the Nicoya Peninsula, Costa Rica. The white box shows the location of the Leg 205 drilling area shown in Figure F3. Bathymetry is from Hydrosweep (Ranero and von Huene, 2000) and Simrad (E. Flueh, pers. comm. 2002) swath-mapping data combined with ETOPO5.

Figure F3. Bathymetric map of the Leg 205 drilling area showing Leg 205 (yellow dots) and 170 (white dots) drill sites. Seismic profiles are shown by the red (Fig. F25) (BGR-99-44; C. Reichert and C. Ranero, pers. comm., 2001) and yellow (CR-20; Shipley et al., 1992) lines. Leg 170 drill sites were based on seismic profile CR-20 (yellow line). Numbers along the BGR 99-44 seismic line are shotpoints. The white arrow gives the convergence direction (N30°E) and rate (88 mm/yr) (De Mets et al., 1990). The location of the map is shown in Figure F2; bathymetric contours are in meters. The bathymetric map is an integration of the compilation by Ranero and von Huene (2000) and Simrad data from E. Flueh (pers. comm., 2000).

Figure F4. Leg 205 Costa Rica drilling area (red box) (Fig. F3) and isochrons derived from seafloor magnetic anomalies (Barckhausen et al., 2001). Numbers indicate crustal age in million years. Tectonic boundaries, convergence direction and rate (arrow) (De Mets et al., 1990), and arc volcanoes (triangles) are shown. *FS* = Fisher Seamount, QSC = Quesada Sharp Contortion.

Figure F5. Summary of recovered lithology at drill sites on the incoming plate off Guatemala (DSDP Site 495) and Costa Rica (Site 1039) as well as on the Costa Rica margin (Sites 1040 and 1043). Note the similarity of incoming sediment sections at Sites 1039 and 495, as well as the repetition of the Site 1039 section below the décollement at Sites 1040 and 1043. Lithologic columns are modified from Kimura, Silver, Blum, et al. (1997).

Figure F6. Migrated multichannel seismic profile BGR-99-44 (C. Ranero and C. Reichert, pers. comm., 2001) across the Middle America Trench. Red lines = Leg 205 Sites 1253, 1254, and 1255. Thin black lines = Site 1039, 1040, and 1043 (Leg 170) locations (Kimura, Silver, Blum., et al., 1997). CMP = common midpoint.

Figure F7. Plot of cosmogenic ^{10}Be vs. depth below seafloor at Site 1040. Produced by cosmic rays in the atmosphere and decaying with a 1.5-m.y. half-life, measurable ^{10}Be enrichments are seen in sediments younger than 7–10 Ma. The underthrust sediments beneath the décollement (blue and purple) have high values typical of the incoming sediment section. Throughout the prism sediments of the upper plate, ^{10}Be concentrations are very low, typical of sediments that are older than 3–5 Ma. Biostratigraphic (triangles) and magnetostratigraphic (x's) ages as well as sedimentation rates from Leg 170 cores (Kimura, Silver, Blum, et al., 1997) are shown on the right.

Figure F8. A. Heat flow measurements in the Leg 205 study area. Red box shows data projected onto a line (blue) across the Leg 205 and 170 drill sites which are shown below. The *METEOR* and Langseth and Silver (1996) data are from shallow penetration probes, and the Leg 170 data are from deeper penetration boreholes at Sites 1039, 1040, and 1043. **B.** Heat flow projected onto a line across the Legs 205 and 170 drill sites. The x-axis shows the distance from the deformation front.

Figure F9. Strontium isotope ratios from pore water samples from Site 1039 are indicated by data points and the solid line, with the dashed line showing the strontium seawater curve appropriate to the sediment age. Note the basal pore water trend toward modern seawater composition, with values greater than Miocene seawater, indicating a strong seawater component in basement fluids. Similar variations are seen in calcium and strontium concentration data.

Figure F10. Structures and geochemical anomalies at Site 1040A.

Figure F11. Pore pressures determined from consolidation tests for Site 1040 (Leg 170) and compaction ratios after Saffer (in press). The very sharp gradient in barium concentrations across the base of the décollement indicates limited vertical diffusion or advection (after Kastner, pers. comm., 2002).

Figure F12. Schematic of a CORK-II installation for monitoring fluid flow, flow rates, pressure, and temperature. ROV = remotely operated vehicle, RCB = rotary core barrel.

Figure F13. Portion of multichannel seismic profile BGR 99-44 across Sites 1253 and 1039. Figure F25 shows the BGR 99-44 seismic profile across all drill sites. Vertical exaggeration is ~1.6.

Figure F14. Bathymetric map of the Leg 205 drilling area (Ranero et al., 2000b) showing the location of ODP Site 1253 and its projected position at 17 Ma, the approximate age of the white tephra recovered at 398.8 mbsf. The inset shows the 8-cm-thick altered ash over and underlain by laminated clay-rich sediments.

Figure F15. Composite diagram showing selected logging data annotated with physical property measurements on the cores, petrologic observations, and paleomagnetic and rock magnetism results. Petrologic and magnetic results are reported in the core reference frame, wherein Subunit 4B was curated at a depth of 450 mbsf. Logging data show that Subunit 4B begins at a depth of ~460 mbsf. Correlations between core and logging intervals are shown as solid lines to indicate major boundaries (bottom of Subunit 4A and top of Subunit 4B) or as dashed lines to indicate subunit boundaries identified petrologically. Labeled zones at the base of the petrologic section indicate the following observations: (1) location of the cryptocrystalline horizon of basaltic texture; (2) greater number of magmatic contacts; (3) more veins or voids filled with holo- and cryptocrystalline groundmass/altered glass, clay and zeolites; (4) up to 5% degree of alteration within 1 m of Section 205-1253A-37R-1 and higher abundance of voids filled with clays and zeolites ending in an homogeneous microcrystalline gabbro; (5) increasing number of centimeter scale fractures and veins; and (6) very homogeneous microcrystalline to fine-grained gabbro with very weak magmatic contacts. Also indicated are the positions of the two OsmoSamplers (OS).

Figure F16. Core photograph and thin section photomicrographs from Subunit 4A. **A.** Close-up photograph of microcrystalline to fine-grained homogeneous holocrystalline gabbro (interval 205-1253A-8R-2 [Piece 2, 45–60 cm]). **B.** Microcrystalline gabbro observed within Subunit 4A. **C.** Completely altered primary mineral, replaced by clay (thin section 10-A; Sample 205-1253A-7R-1, 130–133 cm; 414.6 mbsf). **D.** Olivine, completely altered to clay (thin section 13-C; Sample 205-1253A-8R-1, 24–27 cm; 416.24 mbsf). **E.** Olivine, mostly replaced by clay (thin section 13-D; Sample 205-1253A-8R-1, 24–27cm; 416.24 mbsf). **F.** Altered plagioclase, replaced by a mixture of clay and isotropic secondary products (thin section 13-E; Sample 205-1253A-8R-1, 24–27 cm; 416.24 mbsf). Mag = magnetite, Pl = plagioclase, Ilm = ilmenite, Ol = olivine.

Figure F17. Core photograph and thin section photomicrographs from Core 205-1253A-17R, in the upper part of Subunit 4B. **A.** 4-mm-wide vein with glassy margin and zeolite filling (Sample 205-1253A-17R-2, 100–117 cm). **B.** Photomicrograph in cross-polarized light (XPL) taken with a blue filter at 5× magnification, showing microcrystalline gabbro (Sample 205-1253A-17R-2, 108–111 cm). **C.** Photomicrograph showing zeolites, probably mesolite or thomsonite (thin section 27-E; Sample 205-1253A-17R-2, 108–111 cm; 478.18 mbsf). Cpx = clinopyroxene, Pl = plagioclase.

Figure F18. Core photograph and photomicrograph from Sample 205-1253A-25R-1 (Piece 9, 57.5–63.5 cm; 513 mbsf). **A.** Chilled margin of cryptocrystalline basalt including voids filled with zeolites and clay (interval 205-1253A-25R-1, 58–63 cm). **B.** Photomicrograph in cross-polarized light (XPL) taken with a blue filter at 5× magnification showing cryptocrystalline groundmass (Sample 205-1253A-25R-1, 57.5–63.5cm). Cpx = clinopyroxene.

Figure F19. Composite diagram showing fracture distribution within the igneous units, core recovery and a summary of petrologic observations, and detailed FMS images for the depths at which OsmoSamplers (OS) 1 and 2 were installed.

Figure F20. A. Photomicrograph showing the zeolite stilbite as a cavity filling in Section 205-1253A-33R-1, in lower part of Subunit 4B. **B.** Vein up to 0.5 cm wide filled with pale green clay in interval 205-1253A-42R-2, 72–101 cm. The interior of the vein shows a lighter color, which could be zeolites. The sample in B was taken for microbiological studies at the interval immediately adjacent to the bottom of part B. pl = plagioclase.

Figure F21. Composite diagram of pore fluid chemical data from Legs 205 and 170, measured just above and below the gabbro sill (Subunit 4A). Dashed horizontal line = depth of the sill at Hole 1039C for comparison.

Figure F22. Hole 1253A borehole installation showing subseafloor depths for OsmoSamplers, screens, packers, and casing strings. This figure is not to scale.

Figure F23. Location of Site 1254. Open circles = drill sites occupied during Leg 205, closed circles = drill sites occupied during Leg 170. Bathymetric map is an integration of the compilation by Ranero and von Huene (2000) and Simrad data from E. Flueh (pers. comm., 2000). LWD = logging while drilling.

Figure F24. Portion of multichannel seismic profile BGR 99-44 across Sites 1254 and 1040. Figure F3 shows the BGR 99-44 seismic profile across all drill sites. Vertical exaggeration is 1.7. CMP = common midpoint.

Figure F25. Summary of results at Hole 1254A. Composite view of structural and geochemical results from Hole 1254A with identification of major structural elements.

Figure F26. Photograph of the lithologic boundary between forearc prism sediments (Subunit P1B), represented here as darker claystone (interval 205-1254A-15R-2, 128–145 cm) and the underthrust sediment (Subunit U1A), which is shown here as a lighter, more silt-rich claystone.

Figure F27. Photograph of deformed hemipelagic sediments (Subunit U1A) within the lowermost décollement zone (interval 205-1254A-16R-1, 96–100 cm), demonstrating that the lithologic boundary does not coincide with the base of the décollement.

Figure F28. Photograph of a fault gouge (Riedel shear) developed by brittle shearing in a zone in the hemipelagic sediments of Subunit U1A (interval 205-1254A-16R-2, 23–32 cm) of discrete deformation.

Figure F29. Location of Site 1255. Red circle = the drill site occupied during Leg 205, black circles = the drill sites occupied during Leg 170. The bathymetric map is an integration of the compilation by Ranero and von Huene (2000) and Simrad data from E. Flueh (pers. comm., 2000).

Figure F30. Portion of multichannel seismic profile BGR 99-44 across Sites 1255 and 1043. Figure F24 shows the BGR 99-44 seismic profile across all drill sites. Vertical exaggeration is 1.7. CMP = common midpoint.

Figure F31. Hole 1253A borehole installation showing subseafloor depths for OsmoSamplers, screens, packers, and casing strings. This figure is not to scale.

Table T1. Leg 205 operations summary.

Hole	Latitude	Longitude	Water depth (mbsl)	Number of cores	Cored interval (m)	Core recovered (m)	Core recovery (%)	Drilled interval (m)	Total penetration (m)	Time on hole (day)	Comments
1253A	9°38.8583′N	86°11.4337′E	4376.3	43	230.0	148.38	65.0	370.0	600.0	19.72	Cored; installed CORK-II
1254A	9°39.6989′N	86°10.7435′W	4182.8	16	140.5	125.00	89.0	227.0	367.5	7.98	Cored fault zone and décollement; attempted CORK-II installation; 10¾-in casing collapsed; hole abandoned.
1254B	9°39.7187′N	86°10.7274′W	4175.6	0	0.0	0.00	0.0	278.0	278.0	7.31	Attempted CORK-II installation; 4½-in casing parted; attempted but failed to remove casing stuck in hole; hole abandoned. Note: Time on hole does not include time fishing at end of leg.
1255A	9°39.2716′N	86°11.1492′W	4311.6	4	34.0	7.22	21.0	123.0	157.0	6.97	Cored décollement; installed CORK-II.
		Leg 205 totals:		63	404.5	280.60	69.0	998.0	1402.5	41.98	

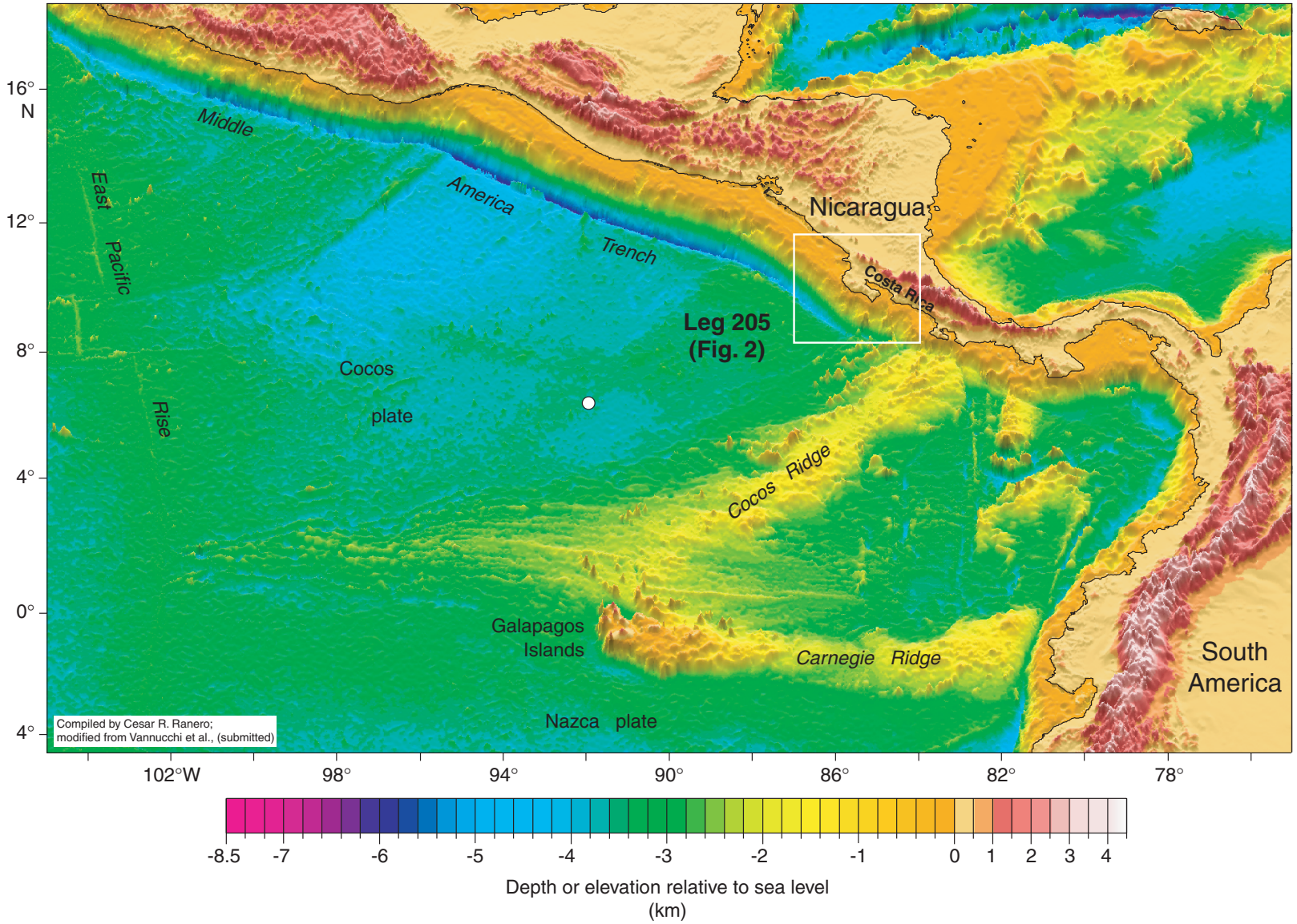
16° N
12°
8°
4°
0°
4°
102°W
98°
94°
90°
86°
82°
78°
Middle
America
Trench
East
Pacific
Rise
Cocos
plate
Nicaragua
Costa Rica
Leg 205
(Fig. 2)
Cocos Ridge
Galapagos
Islands
Carnegie Ridge
Nazca plate
South
America
Compiled by Cesar R. Ranero;
modified from Vannucchi et al., (submitted)
-8.5
-7
-6
-5
-4
-3
-2
-1
0
1
2
3
4
Depth or elevation relative to sea level
(km)

Figure F1

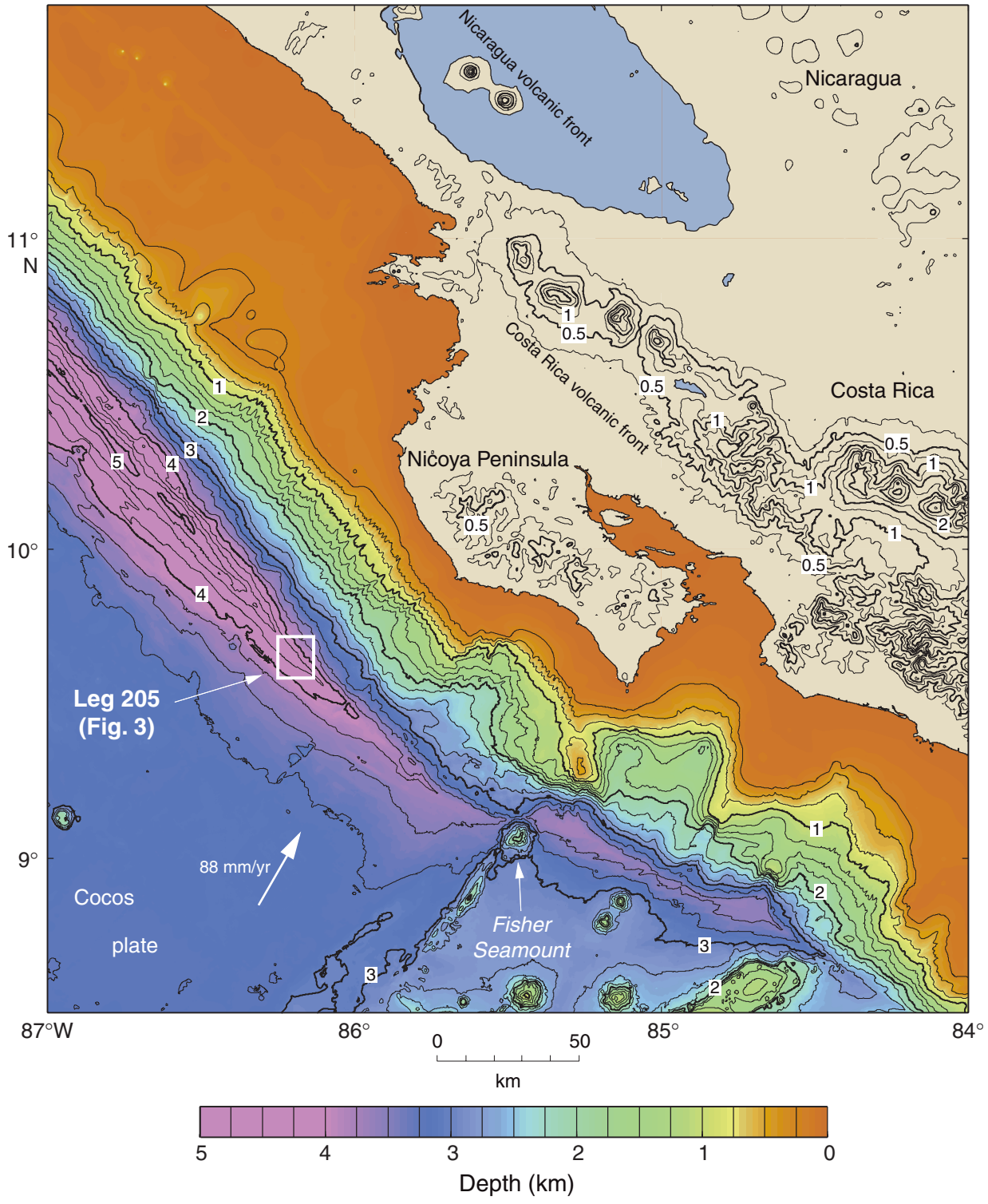
Nicaragua volcanic front
Nicaragua
Costa Rica volcanic front
Costa Rica
Nicoya Peninsula
11° N
10°
9°
87°W
86°
85°
84°
0
50
km
Leg 205
(Fig. 3)
88 mm/yr
Cocos
plate
Fisher
Seamount
5
4
3
2
1
0
Depth (km)

Figure F2

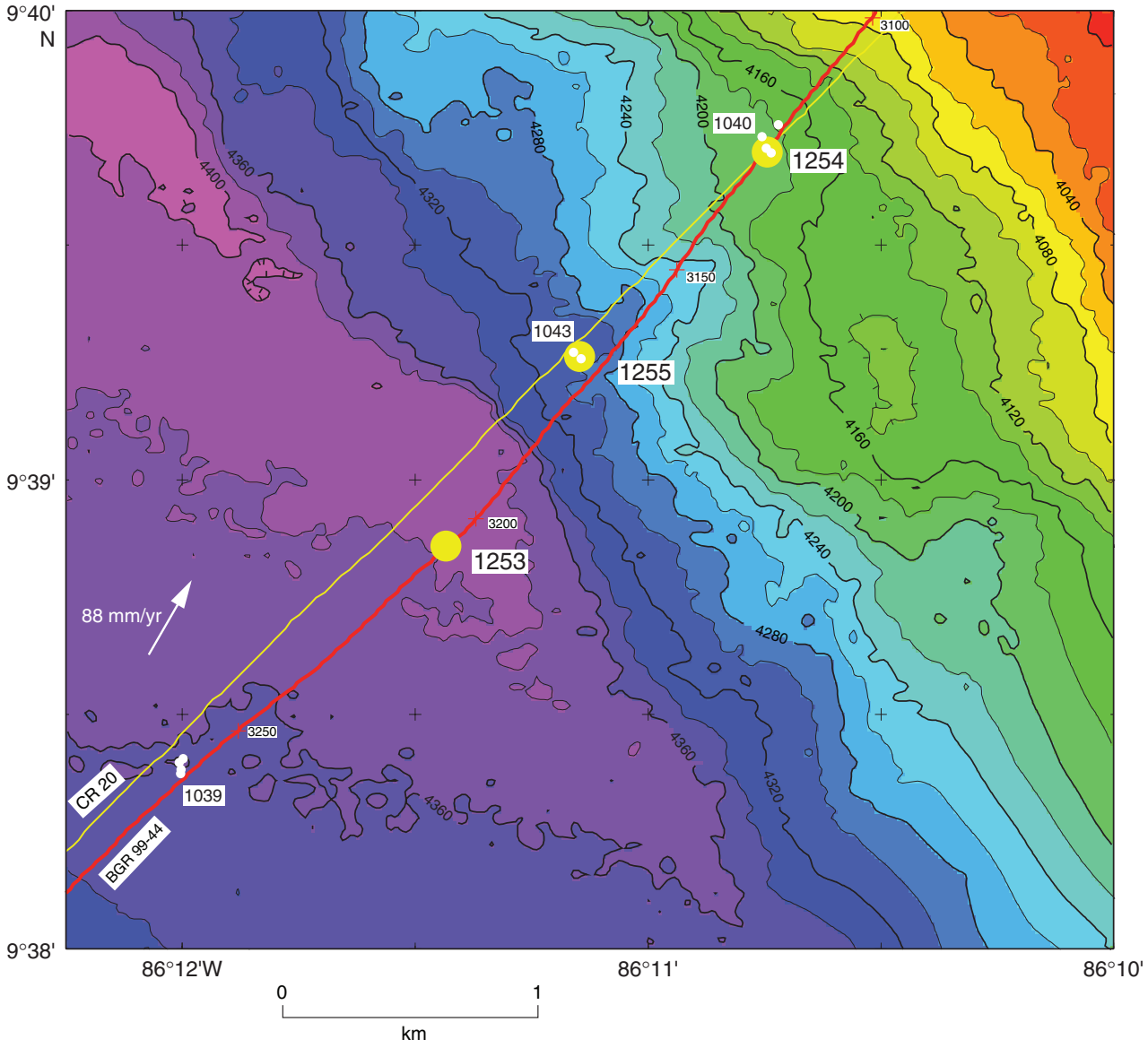
9°40'
N
9°39'
9°38'
86°12'W
86°11'
86°10'
0
1
km
3100
4160
4200
4240
4280
4040
4080
4120
4360
4400
4320
3150
1040
1254
1043
1255
3200
1253
88 mm/yr
3250
1039
CR 20
BGR 99-44

Figure F3

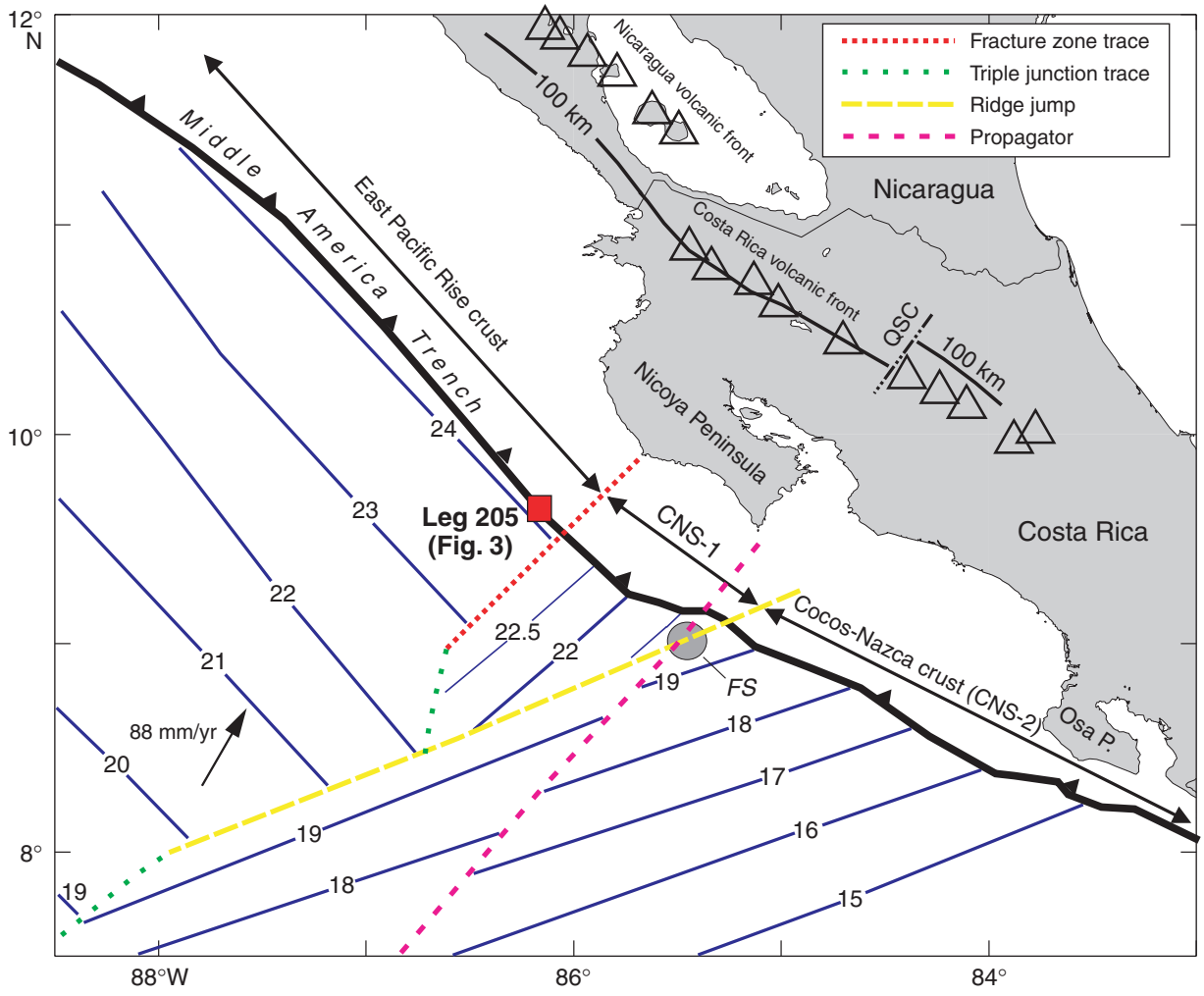
Fracture zone trace
Triple junction trace
Ridge jump
Propagator
Nicaragua volcanic front
100 km
Nicaragua
Costa Rica volcanic front
CRR
100 km
Nicoya Peninsula
Costa Rica
Middle America Trench
East Pacific Rise crust
Leg 205
(Fig. 3)
CNS-1
Cocos-Nazca crust (CNS-2)
Osa P.
FS
88 mm/yr
24
23
22
22.5
22
21
20
19
19
18
18
17
16
15
12° N
10°
8°
88°W
86°
84°

Figure F4

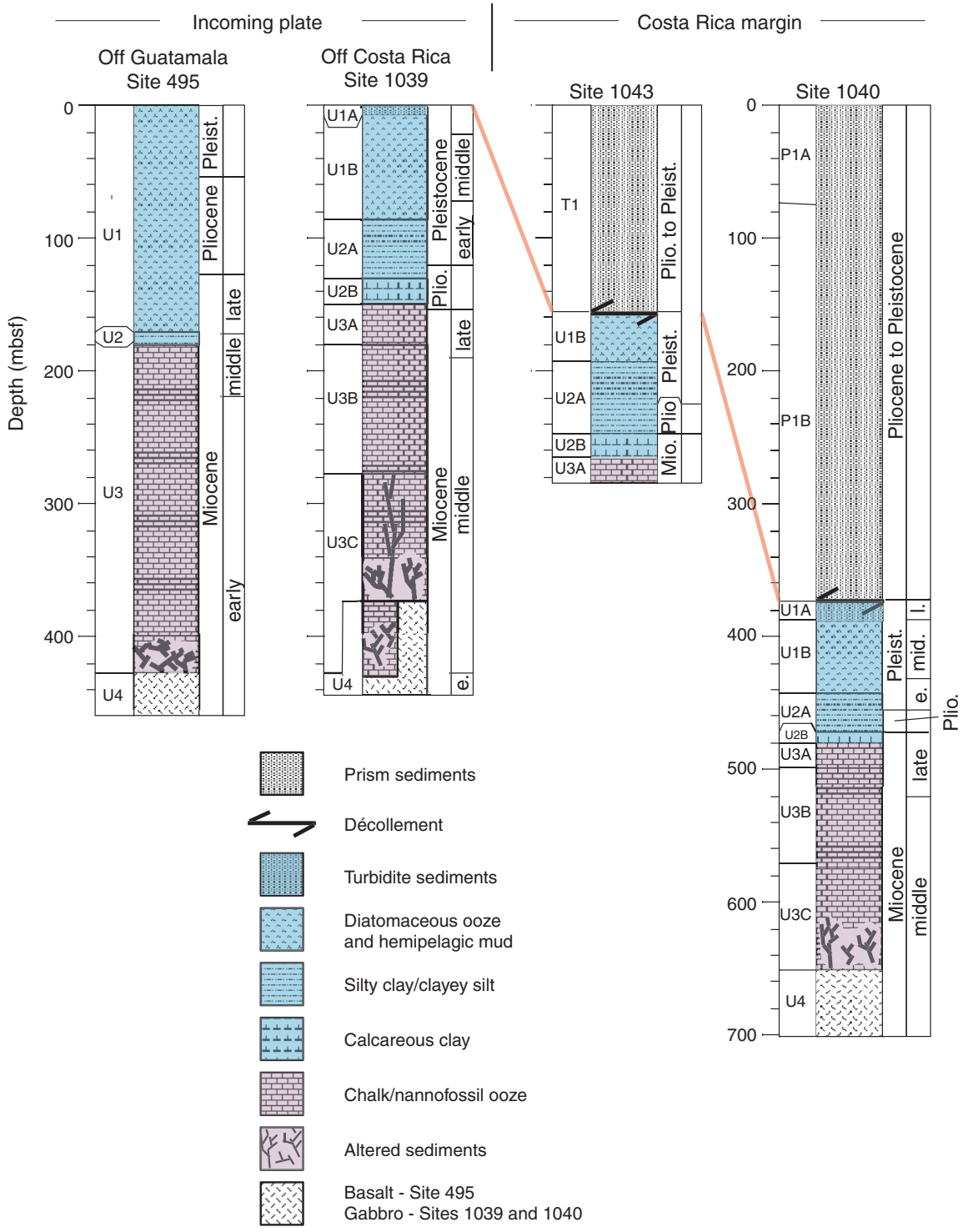
Incoming plate
Costa Rica margin
Off Guatamala
Site 495
Off Costa Rica
Site 1039
Site 1043
Site 1040
Depth (mbsf)
0
100
200
300
400
500
600
700
U1
U2
U3
U4
U1A
U1B
U2A
U2B
U3A
U3B
U3C
T1
P1A
P1B
Pleist.
Pliocene
Miocene
Pleistocene
Plio.
Mio.
Plio. to Pleist.
Pliocene to Pleistocene
early
middle
late
e.
mid.
l.
Prism sediments
Décollement
Turbidite sediments
Diatomaceous ooze
and hemipelagic mud
Silty clay/clayey silt
Calcareous clay
Chalk/nannofossil ooze
Altered sediments
Basalt - Site 495
Gabbro - Sites 1039 and 1040

Figure F5

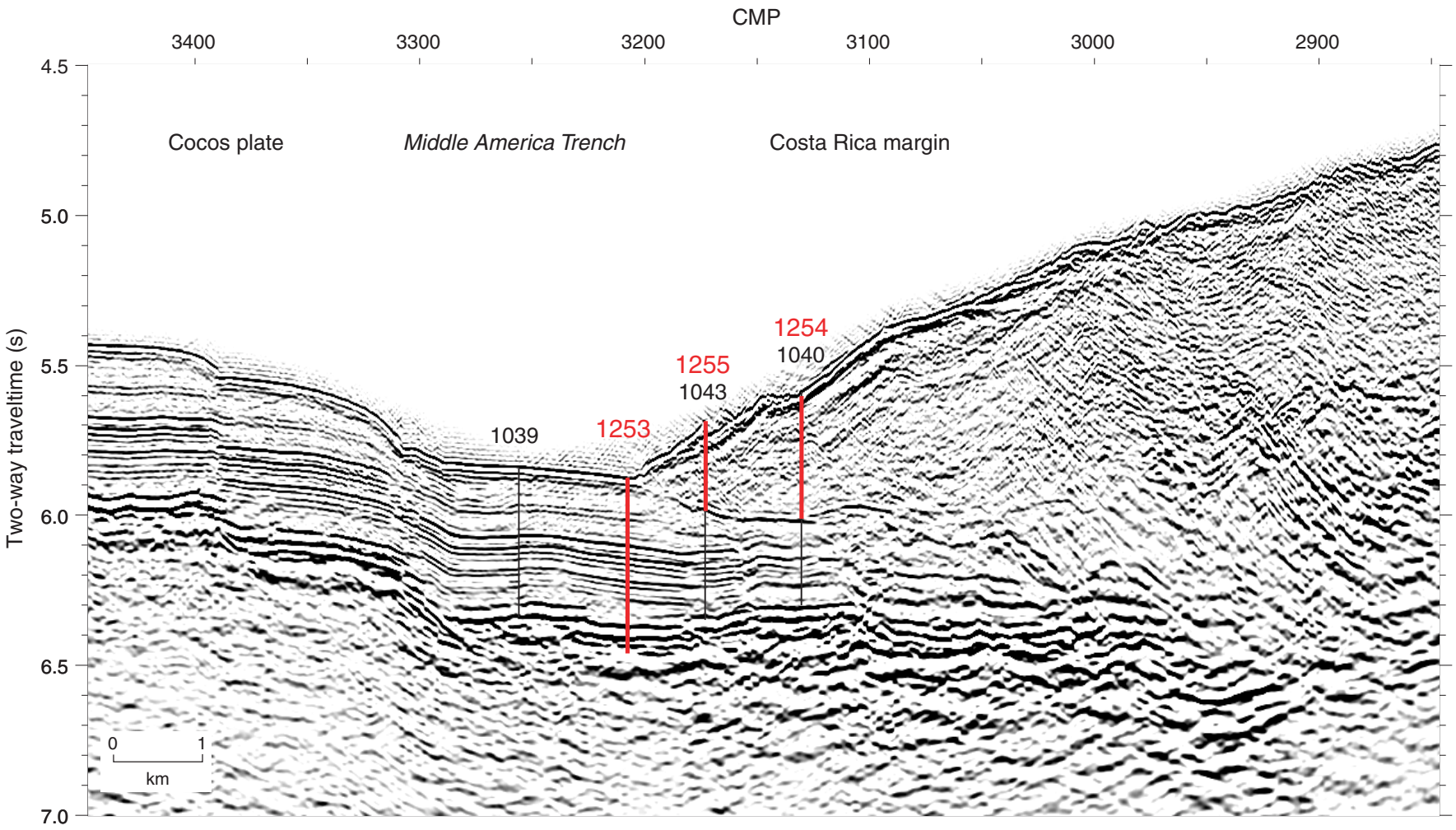
CMP
3400
3300
3200
3100
3000
2900
4.5
5.0
5.5
6.0
6.5
7.0
Two-way traveltime (s)
Cocos plate
Middle America Trench
Costa Rica margin
1039
1253
1255
1043
1254
1040
0
1
km

Figure F6

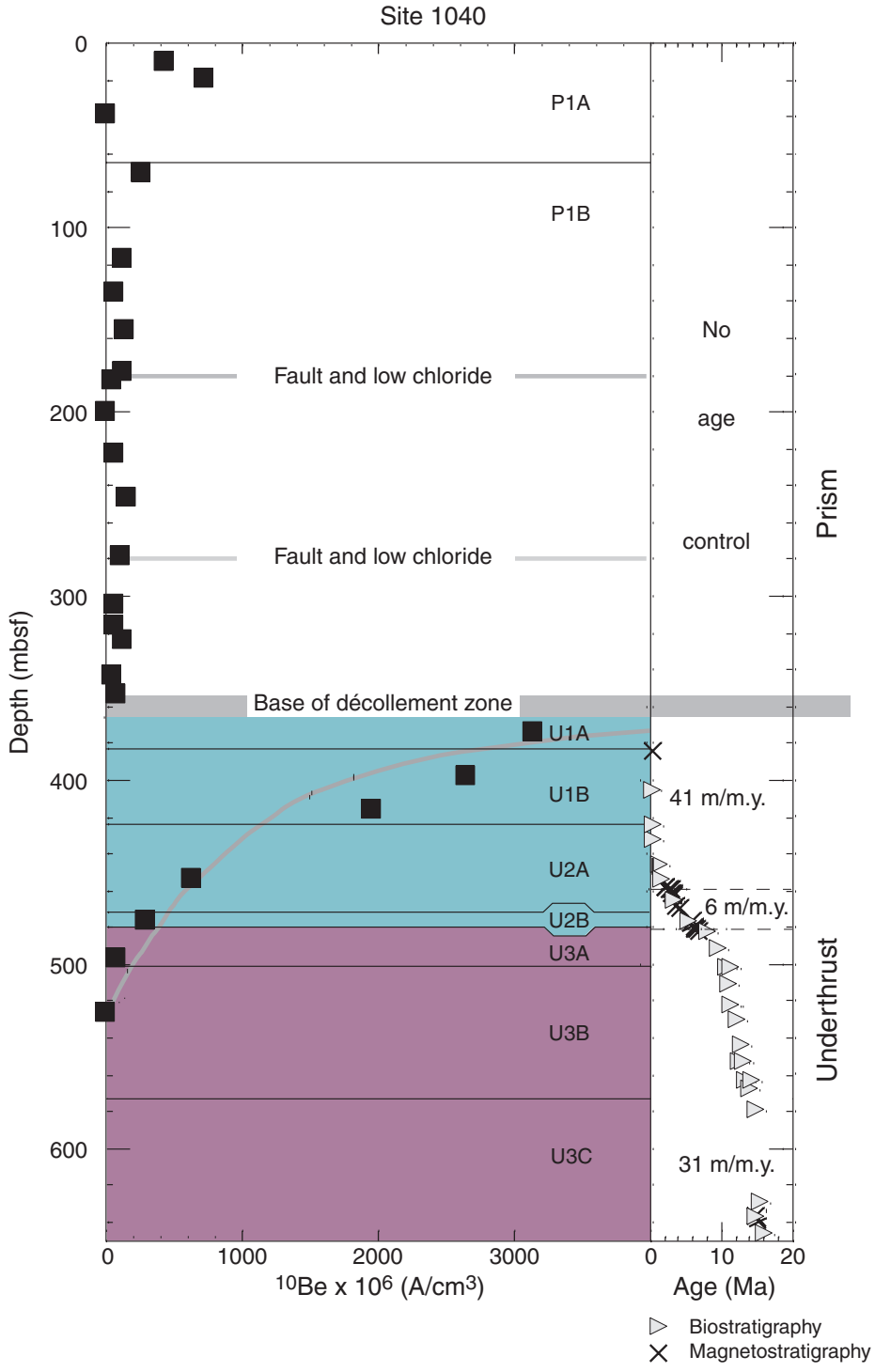
Site 1040
Depth (mbsf)
0
100
200
300
400
500
600
P1A
P1B
Fault and low chloride
Fault and low chloride
Base of décollement zone
U1A
U1B
U2A
U2B
U3A
U3B
U3C
No
age
control
Prism
Underthrust
41 m/m.y.
6 m/m.y.
31 m/m.y.
0
1000
2000
3000
10Be x 10^6 (A/cm3)
0
10
20
Age (Ma)
Biostratigraphy
Magnetostratigraphy

Figure F7

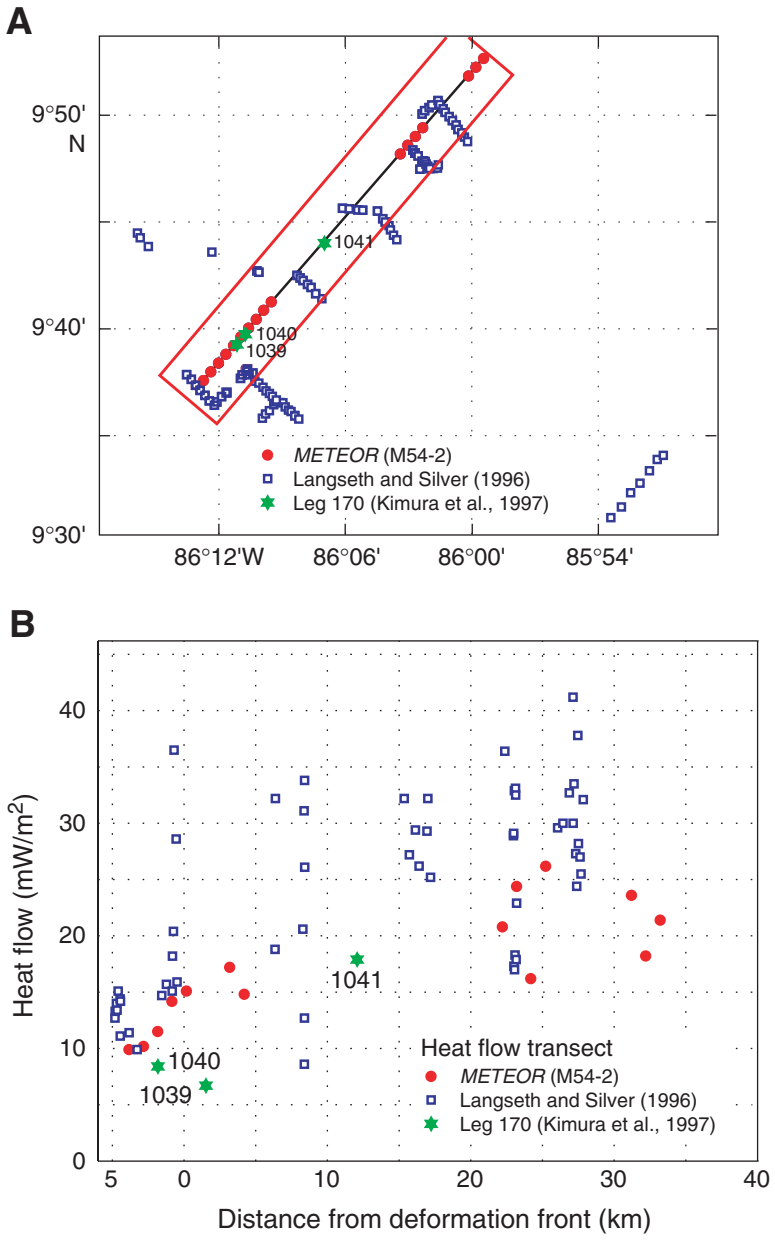
A
9°50'
N
9°40'
9°30'
86°12'W
86°06'
86°00'
85°54'
1041
1040
1039
METEOR (M54-2)
Langseth and Silver (1996)
Leg 170 (Kimura et al., 1997)
B
Heat flow (mW/m2)
0
10
20
30
40
5
0
10
20
30
40
Distance from deformation front (km)
1041
1040
1039
Heat flow transect
METEOR (M54-2)
Langseth and Silver (1996)
Leg 170 (Kimura et al., 1997)

Figure F8

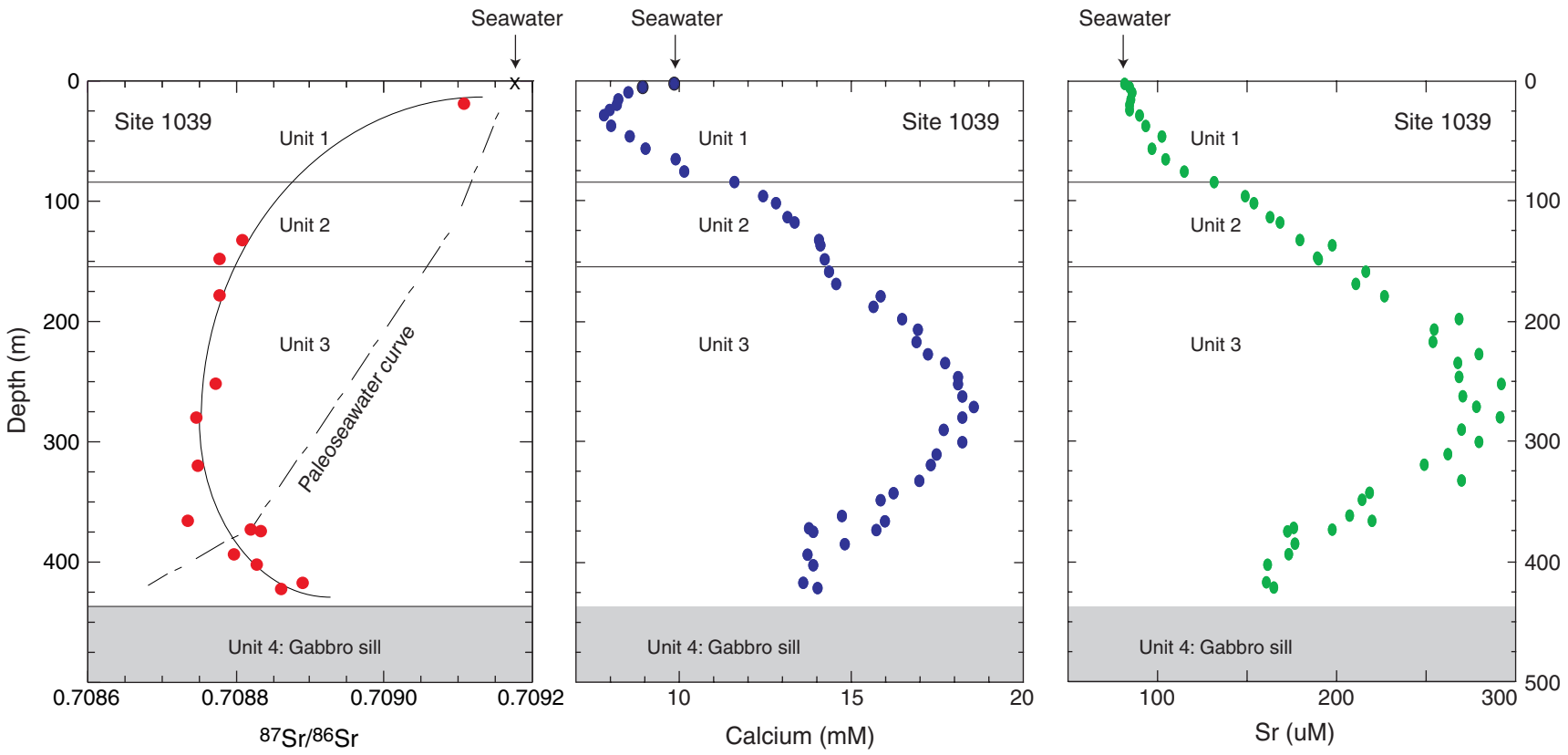
Seawater
Seawater
Seawater
Site 1039
Site 1039
Site 1039
Unit 1
Unit 2
Unit 3
Unit 4: Gabbro sill
Paleoseawater curve
Depth (m)
0
100
200
300
400
500
0.7086
0.7088
0.7090
0.7092
87Sr/86Sr
10
15
20
Calcium (mM)
100
200
300
Sr (uM)

Figure F9

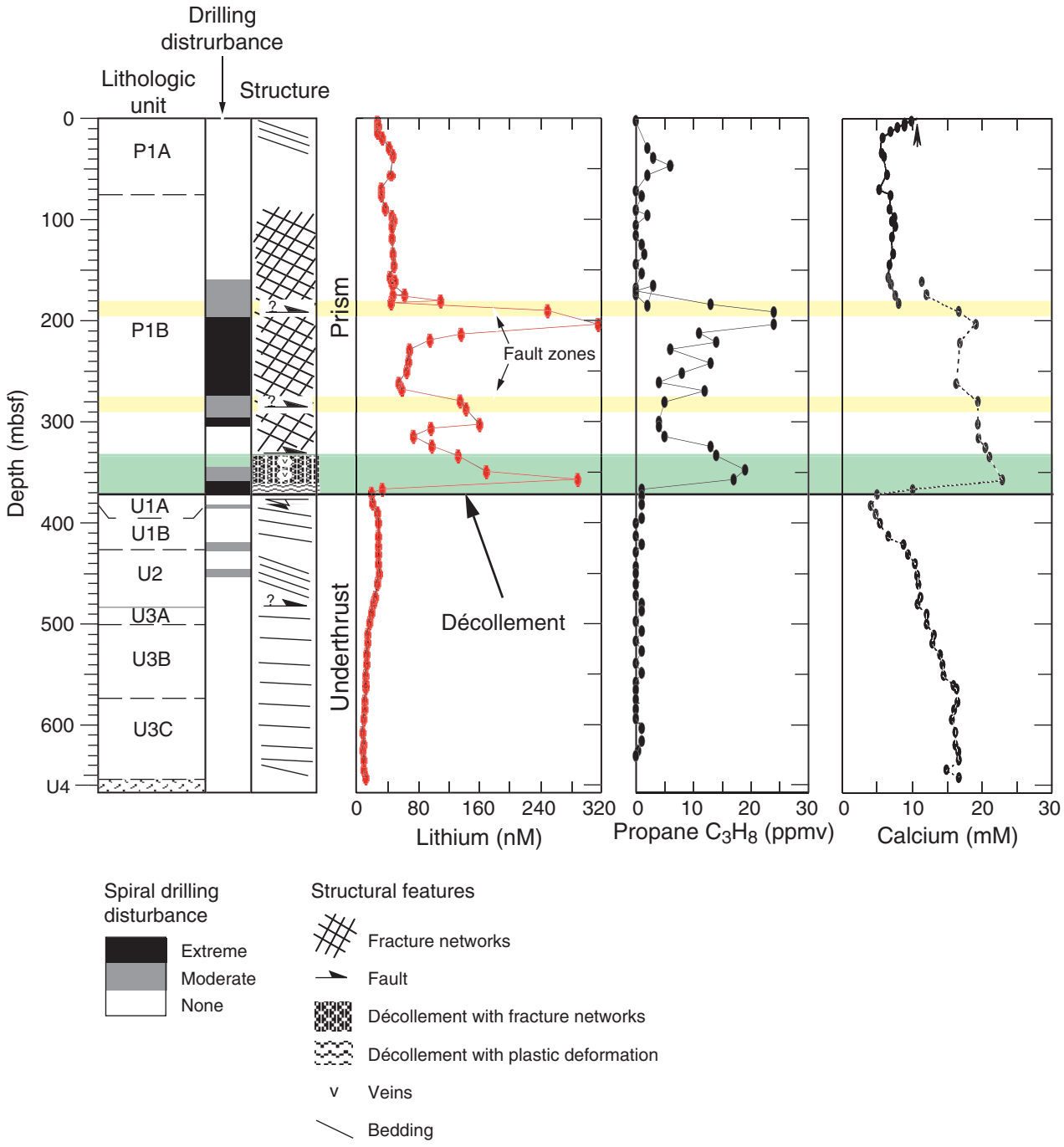
Drilling
distrurbance
Lithologic
unit
Structure
Depth (mbsf)
0
100
200
300
400
500
600
U4
P1A
P1B
U1A
U1B
U2
U3A
U3B
U3C
Prism
Underthrust
Fault zones
Décollement
0
80
160
240
320
Lithium (nM)
0
10
20
30
Propane C3H8 (ppmv)
0
10
20
30
Calcium (mM)
Spiral drilling
disturbance
Extreme
Moderate
None
Structural features
Fracture networks
Fault
Décollement with fracture networks
Décollement with plastic deformation
v
Veins
Bedding

Figure F10

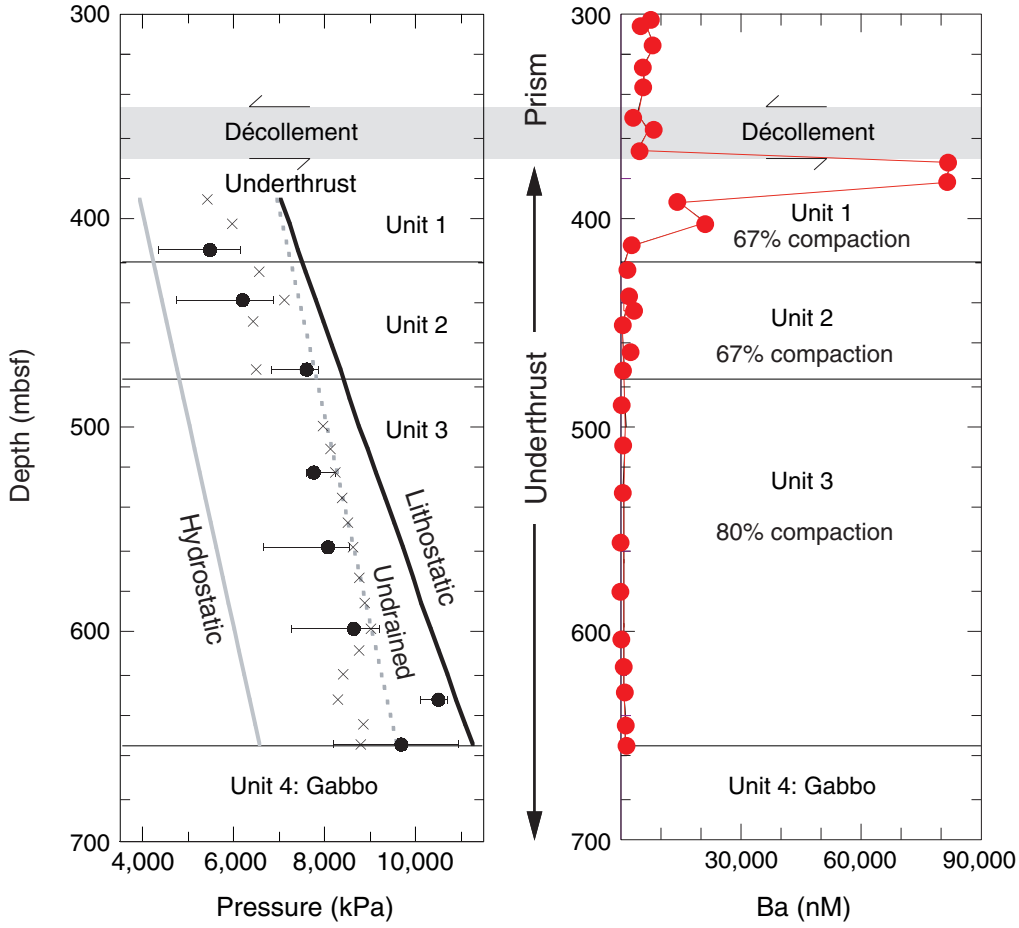
300
400
500
600
700
Depth (mbsf)
Décollement
Underthrust
Unit 1
Unit 2
Unit 3
Unit 4: Gabbo
Hydrostatic
Undrained
Lithostatic
4,000
6,000
8,000
10,000
Pressure (kPa)
Prism
Underthrust
Décollement
Unit 1
67% compaction
Unit 2
67% compaction
Unit 3
80% compaction
Unit 4: Gabbo
30,000
60,000
90,000
Ba (nM)

Figure F11

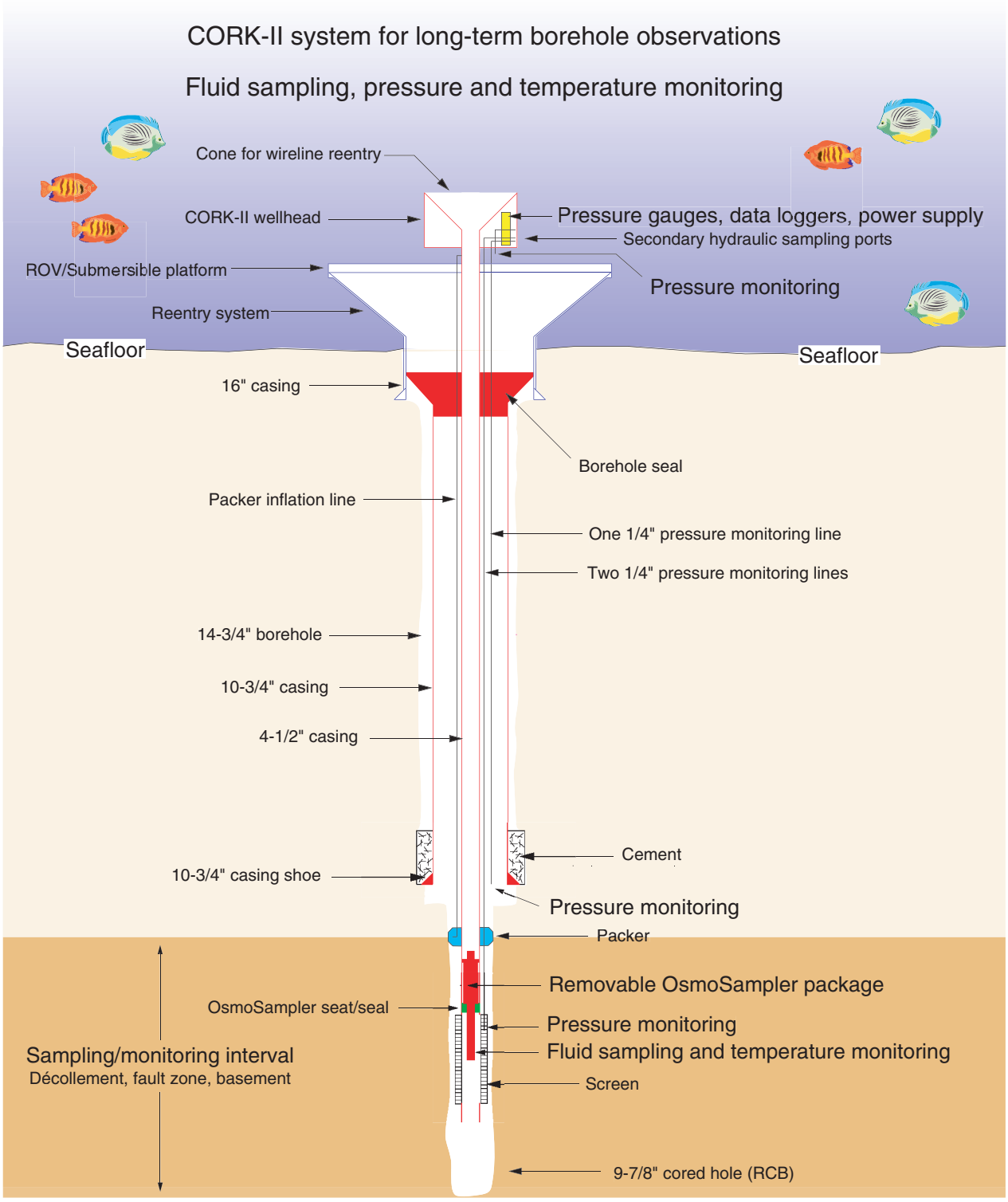
CORK-II system for long-term borehole observations
Fluid sampling, pressure and temperature monitoring
Cone for wireline reentry
CORK-II wellhead
Pressure gauges, data loggers, power supply
Secondary hydraulic sampling ports
ROV/Submersible platform
Pressure monitoring
Reentry system
Seafloor
Seafloor
16" casing
Borehole seal
Packer inflation line
One 1/4" pressure monitoring line
Two 1/4" pressure monitoring lines
14-3/4" borehole
10-3/4" casing
4-1/2" casing
Cement
10-3/4" casing shoe
Pressure monitoring
Packer
Removable OsmoSampler package
OsmoSampler seat/seal
Pressure monitoring
Fluid sampling and temperature monitoring
Sampling/monitoring interval
Décollement, fault zone, basement
Screen
9-7/8" cored hole (RCB)

Figure F12

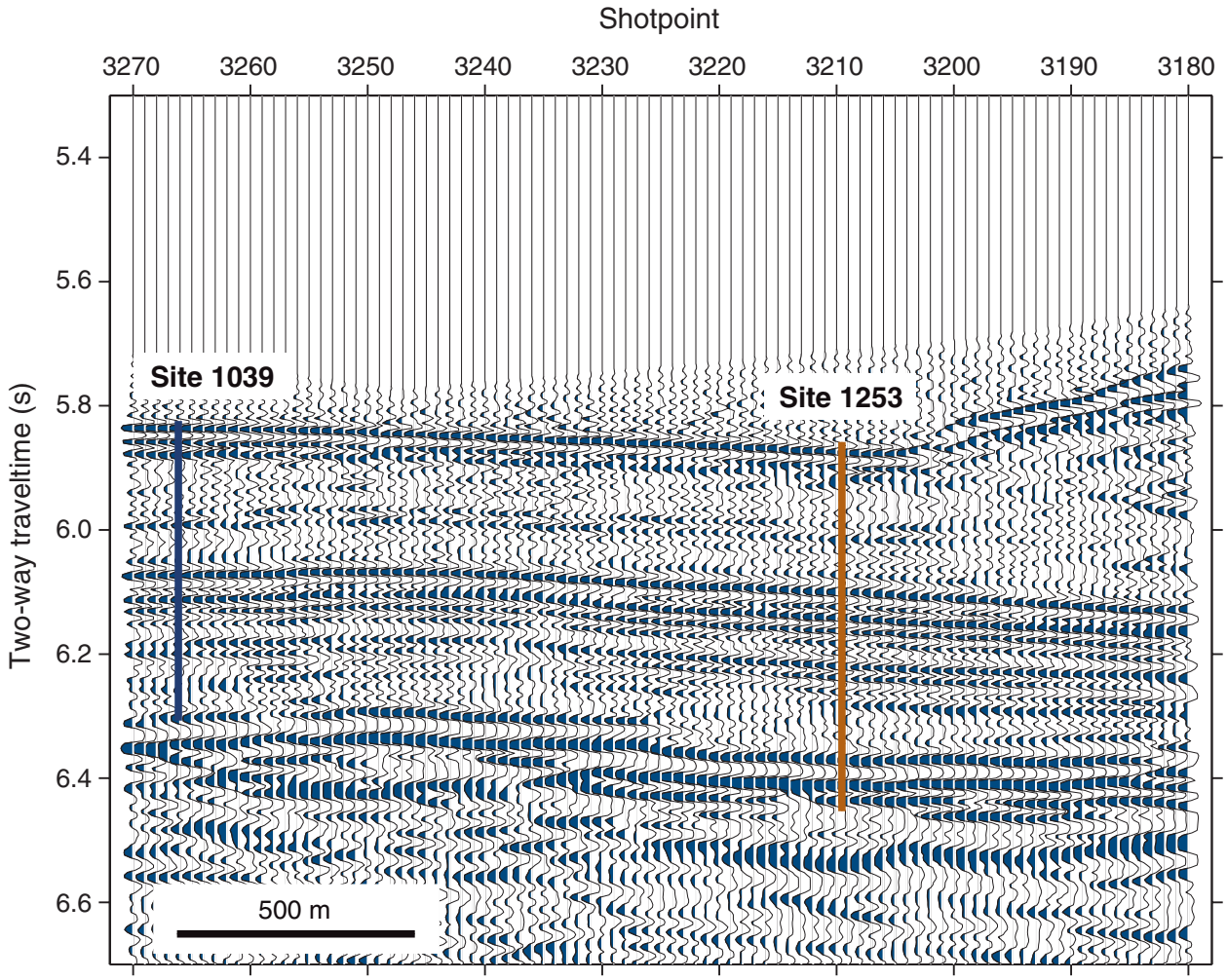
Shotpoint
3270
3260
3250
3240
3230
3220
3210
3200
3190
3180
5.4
5.6
5.8
6.0
6.2
6.4
6.6
Two-way traveltime (s)
Site 1039
Site 1253
500 m

Figure F13

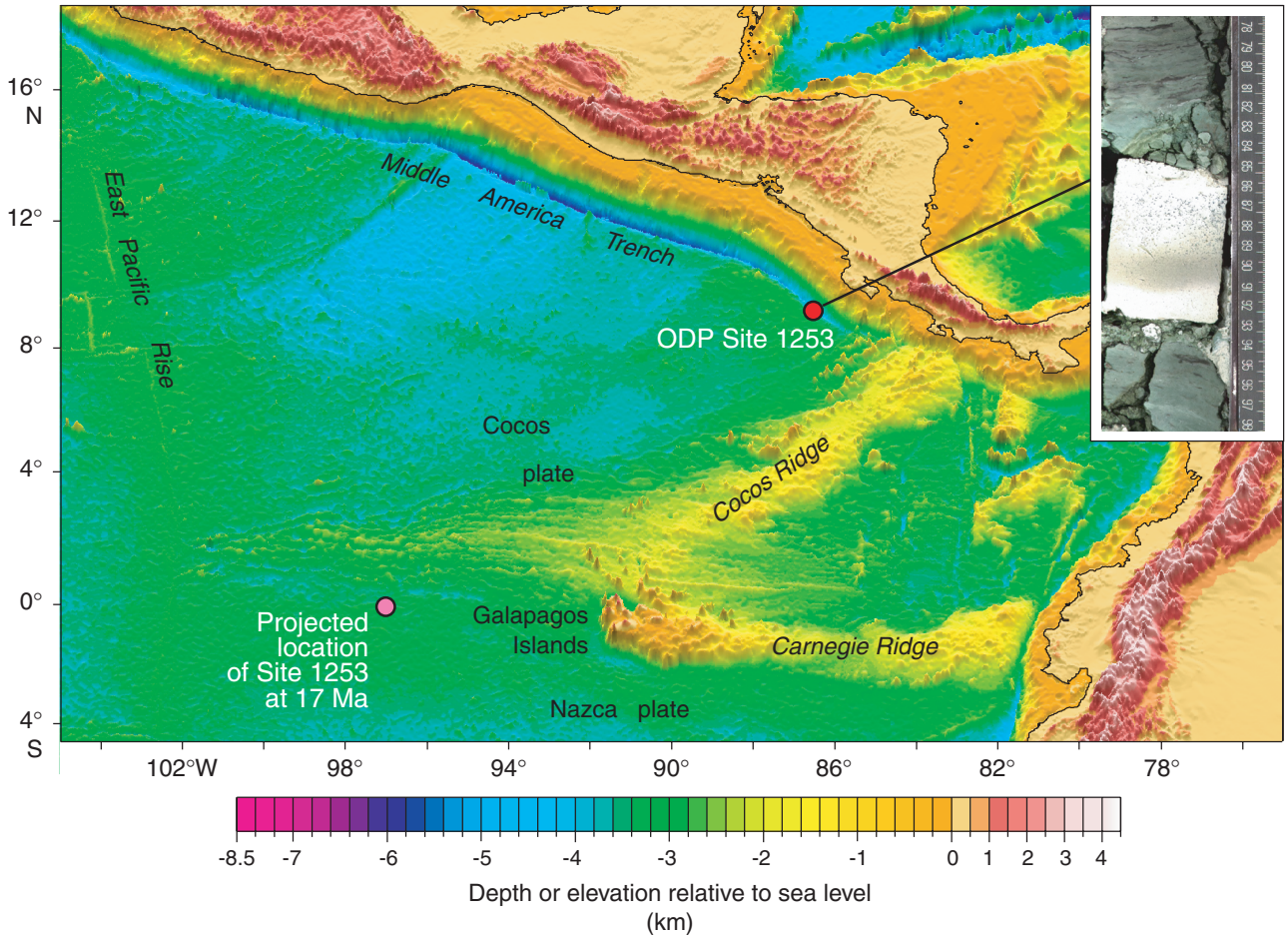
16° N
12°
8°
4°
0°
4° S
102°W
98°
94°
90°
86°
82°
78°
East Pacific Rise
Middle America Trench
ODP Site 1253
Cocos plate
Cocos Ridge
Galapagos Islands
Carnegie Ridge
Nazca plate
Projected location of Site 1253 at 17 Ma
-8.5 -7 -6 -5 -4 -3 -2 -1 0 1 2 3 4
Depth or elevation relative to sea level (km)

Figure F14

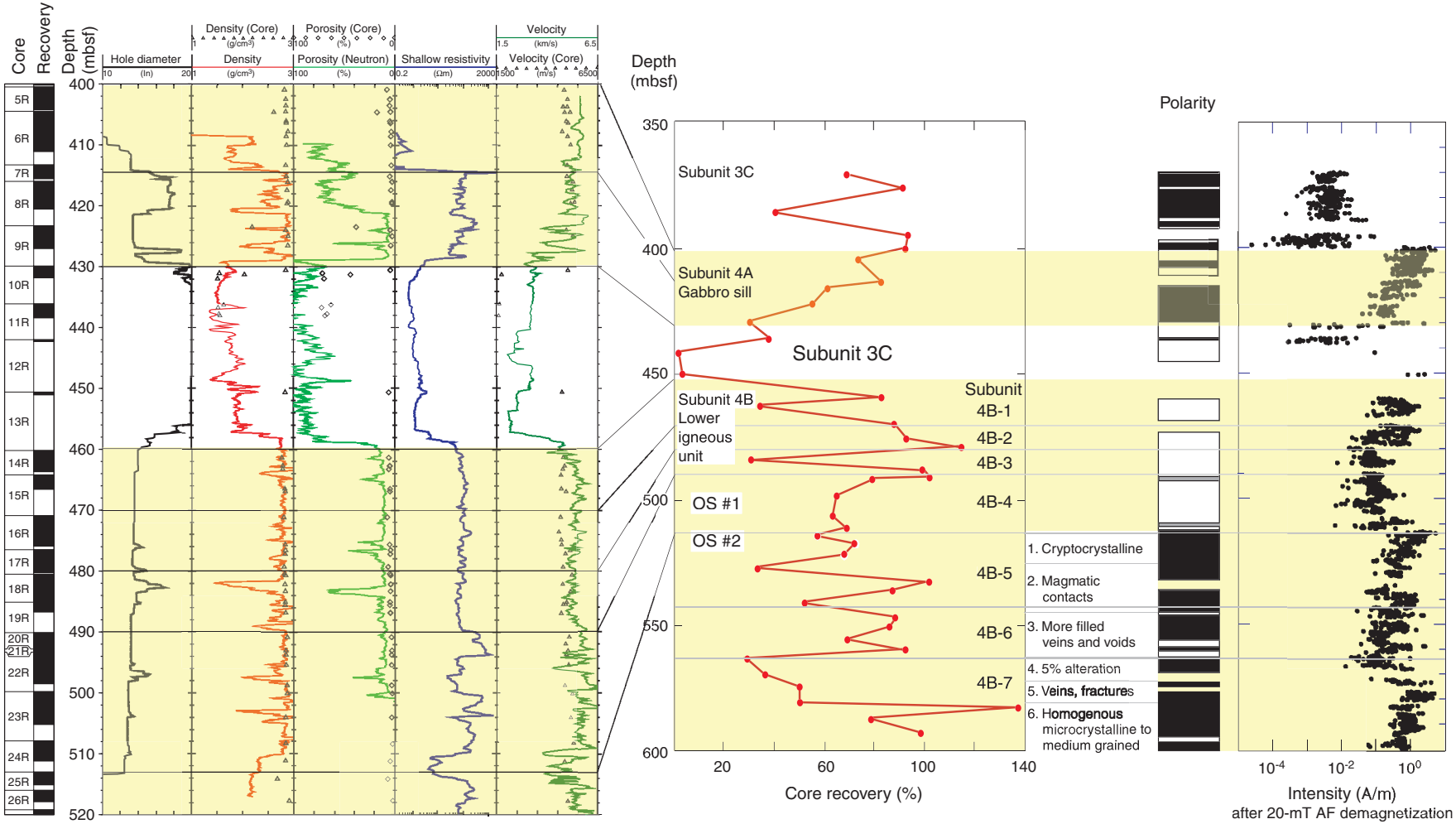
Core
Recovery
Depth (mbsf)
Density (Core)
Porosity (Core)
Velocity
Hole diameter
Density
Porosity (Neutron)
Shallow resistivity
Velocity (Core)
Depth (mbsf)
Subunit 3C
Subunit 4A
Gabbro sill
Subunit 3C
Subunit 4B
Lower
igneous
unit
OS #1
OS #2
Subunit
4B-1
4B-2
4B-3
4B-4
4B-5
4B-6
4B-7
1. Cryptocrystalline
2. Magmatic contacts
3. More filled veins and voids
4. 5% alteration
5. Veins, fractures
6. Homogenous microcrystalline to medium grained
Core recovery (%)
Polarity
Intensity (A/m)
after 20-mT AF demagnetization

Figure F15

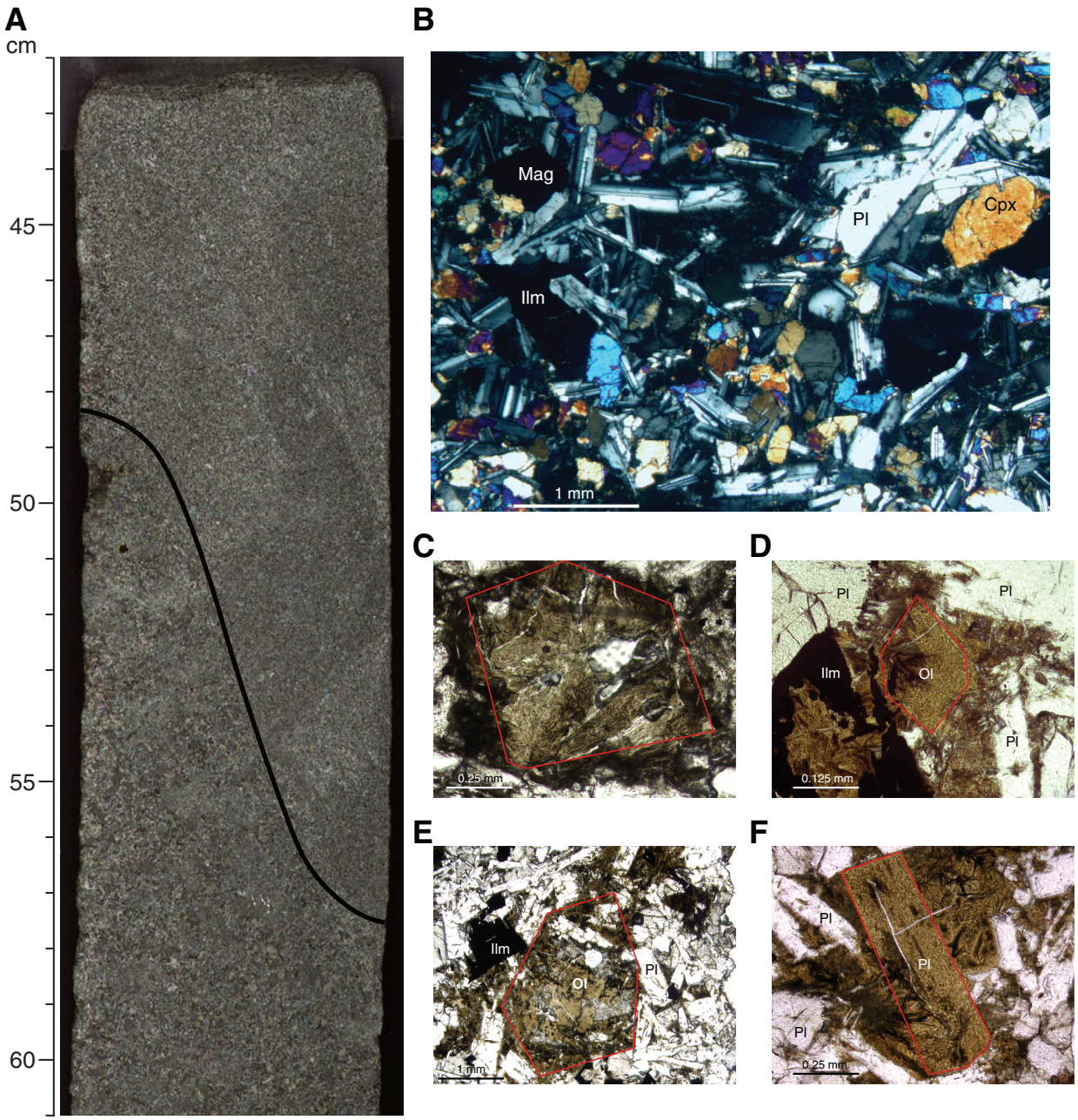
A
cm
45
50
55
60
B
Mag
Pl
Cpx
Ilm
1 mm
C
0.25 mm
D
Pl
Pl
Ilm
Ol
Pl
0.125 mm
E
Ilm
Ol
Pl
1 mm
F
Pl
Pl
Pl
0.25 mm

Figure F16

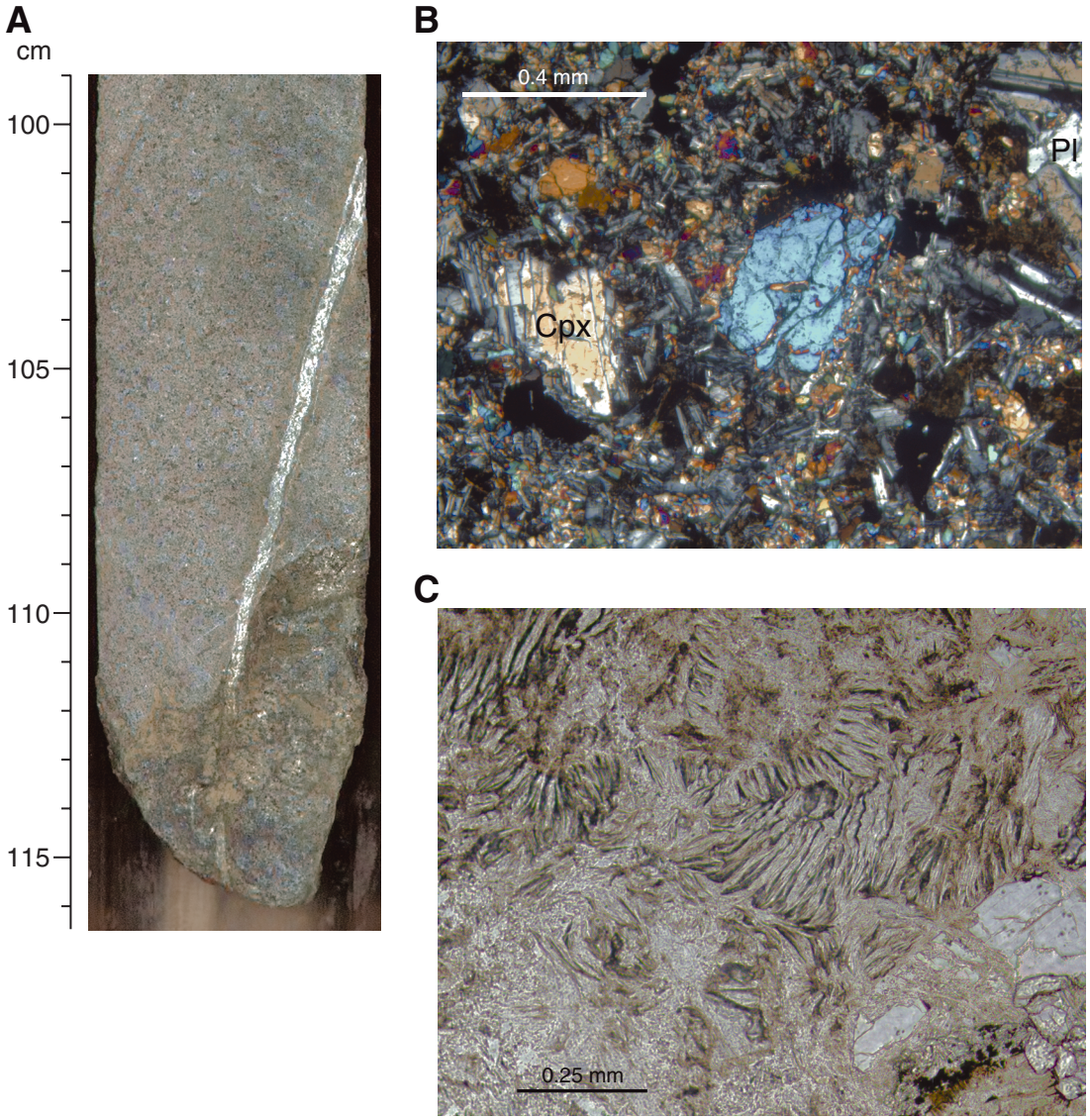

Figure F17

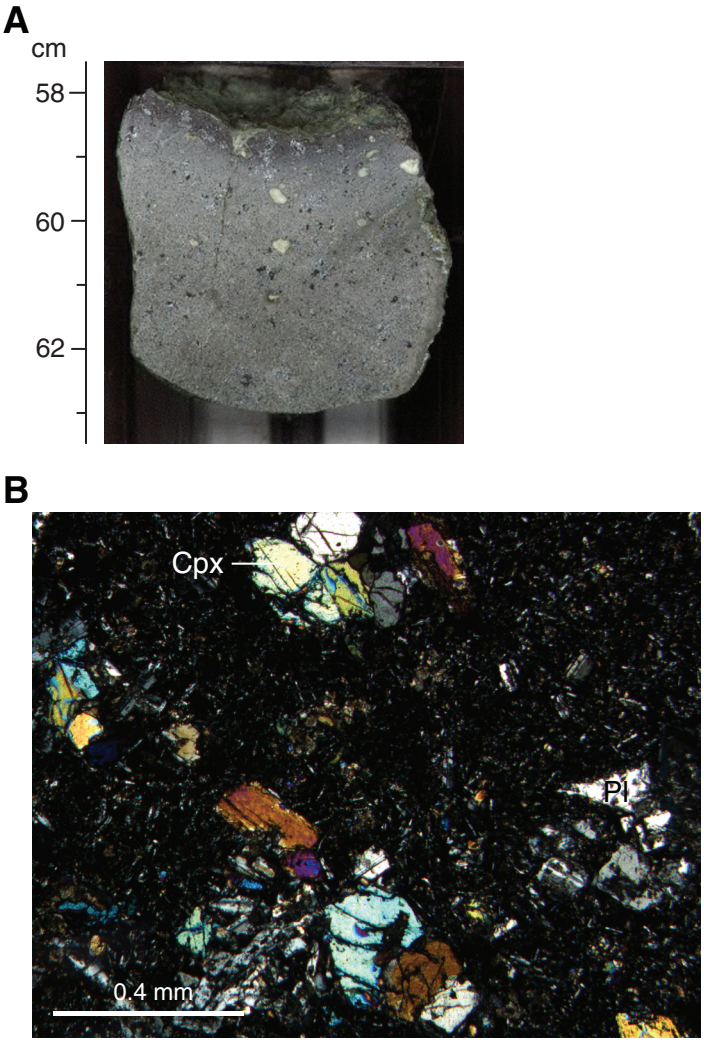

Figure F18

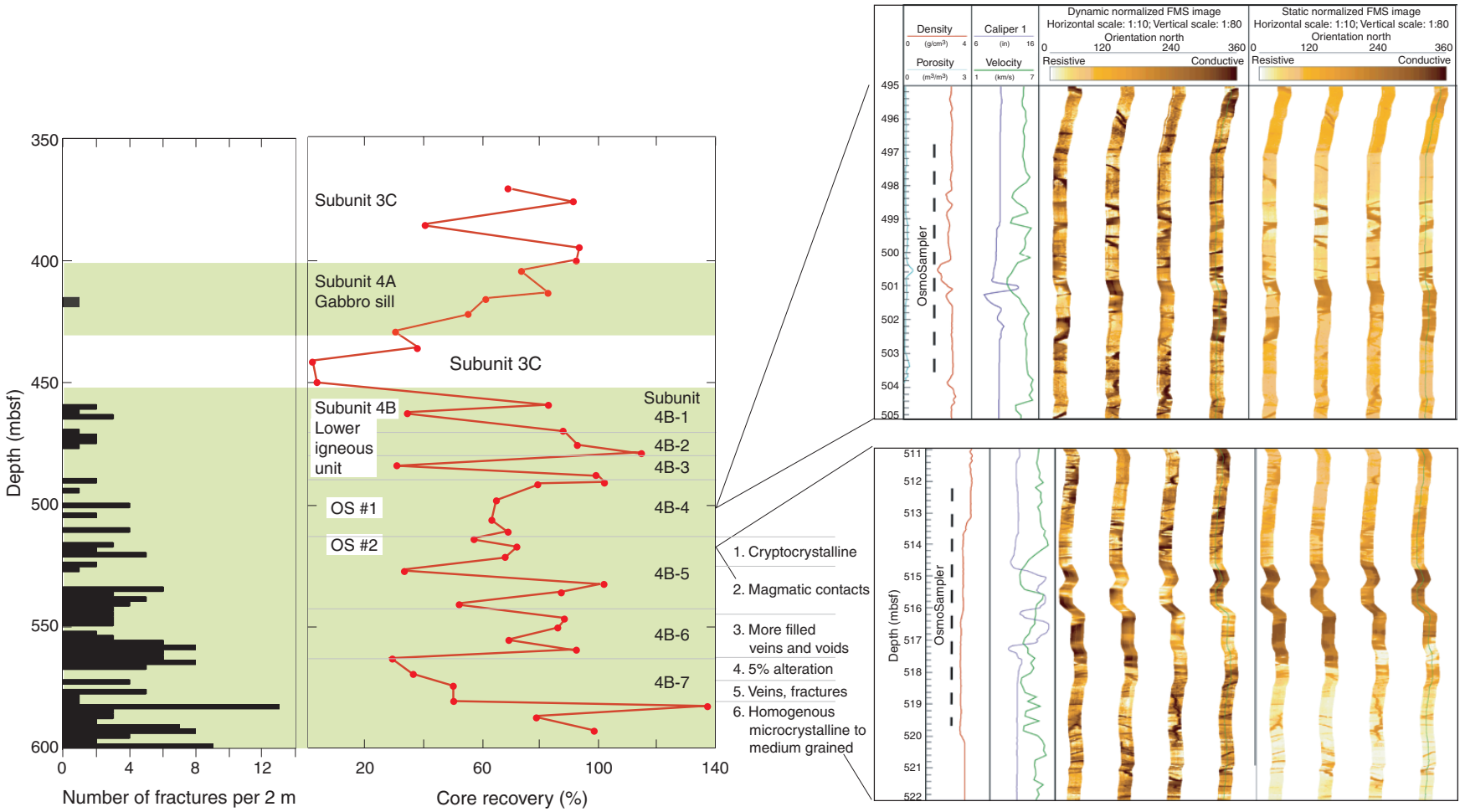
Depth (mbsf)
350
400
450
500
550
600
0
4
8
12
Number of fractures per 2 m
20
60
100
140
Core recovery (%)
Subunit 3C
Subunit 4A
Gabbro sill
Subunit 3C
Subunit 4B
Lower
igneous
unit
OS #1
OS #2
Subunit
4B-1
4B-2
4B-3
4B-4
4B-5
4B-6
4B-7
1. Cryptocrystalline
2. Magmatic contacts
3. More filled
veins and voids
4. 5% alteration
5. Veins, fractures
6. Homogenous
microcrystalline to
medium grained
Density
Porosity
Caliper 1
Velocity
Dynamic normalized FMS image
Horizontal scale: 1:10; Vertical scale: 1:80
Orientation north
Resistive
Conductive
Static normalized FMS image
Horizontal scale: 1:10; Vertical scale: 1:80
Orientation north
Resistive
Conductive
OsmoSampler
OsmoSampler
Depth (mbsf)

Figure F19

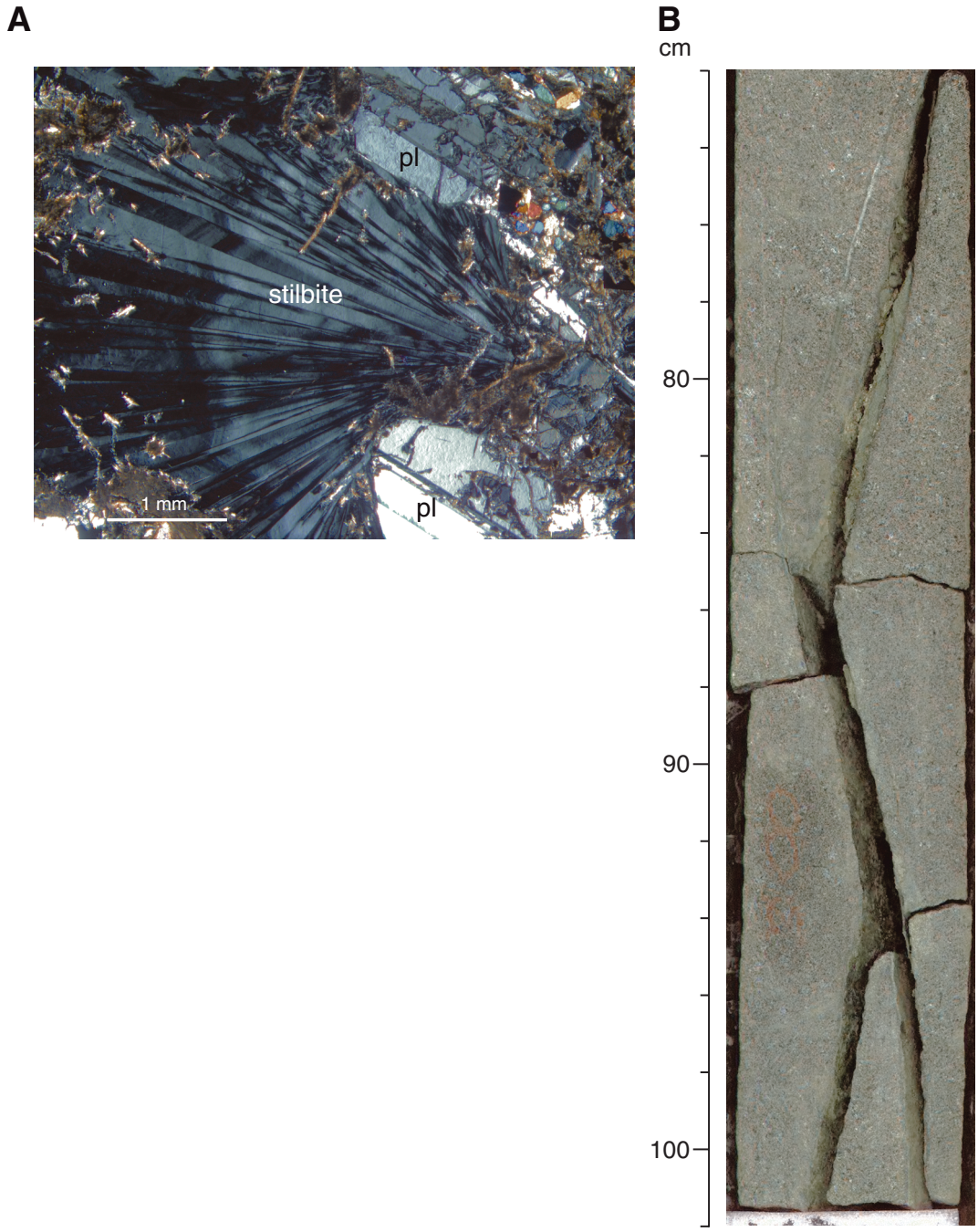

Figure F20

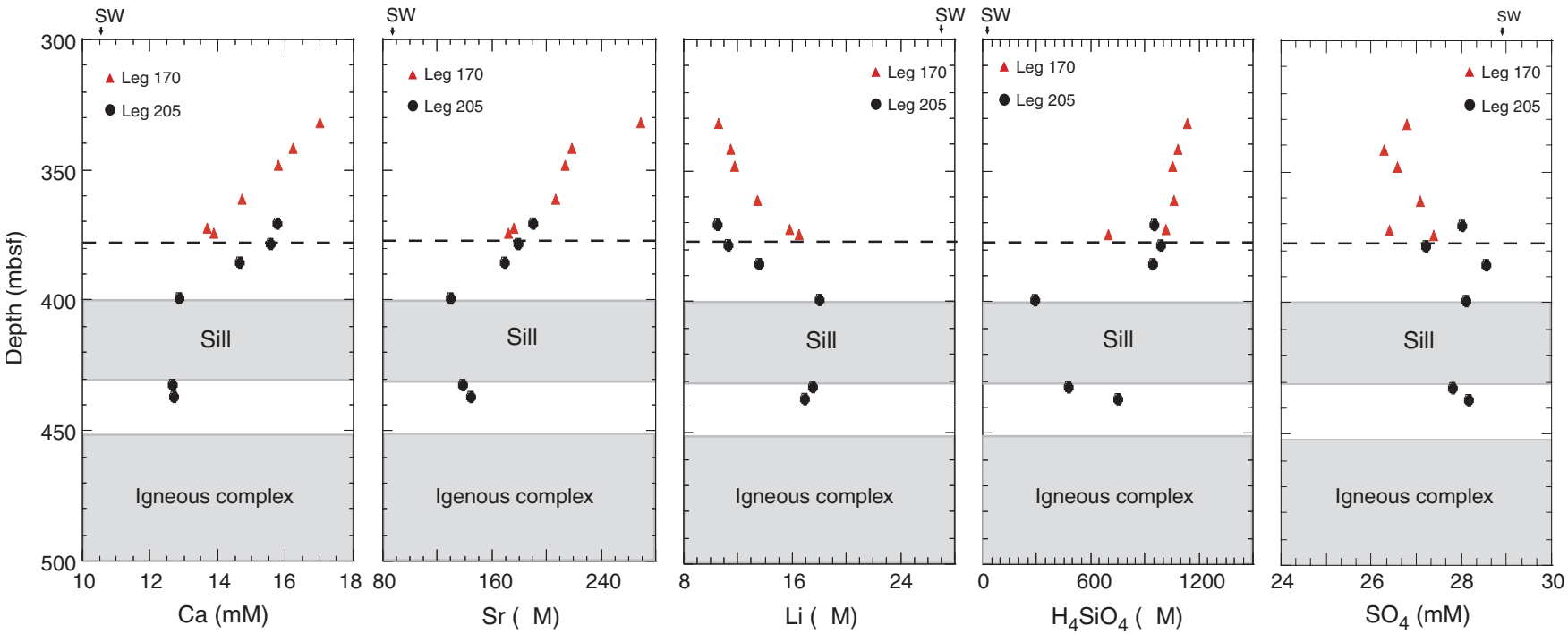
SW
Leg 170
Leg 205
Depth (mbsf)
300
350
400
450
500
Sill
Igneous complex
Igenous complex
10
12
14
16
18
Ca (mM)
80
160
240
Sr (M)
8
16
24
Li (M)
0
600
1200
H4SiO4 (M)
24
26
28
30
SO4 (mM)

Figure F21

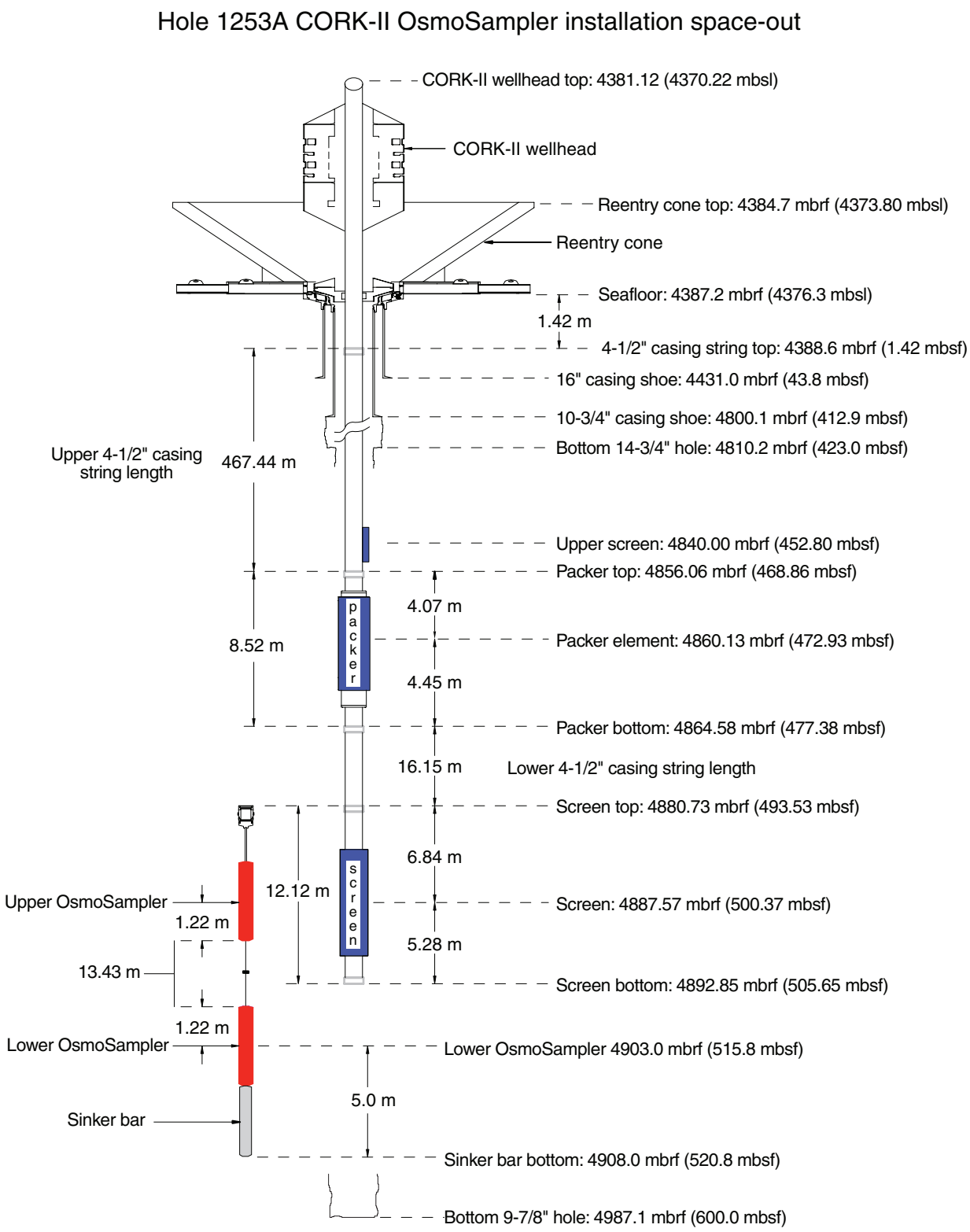
Hole 1253A CORK-II OsmoSampler installation space-out
CORK-II wellhead top: 4381.12 (4370.22 mbsl)
CORK-II wellhead
Reentry cone top: 4384.7 mbrf (4373.80 mbsl)
Reentry cone
Seafloor: 4387.2 mbrf (4376.3 mbsl)
1.42 m
4-1/2" casing string top: 4388.6 mbrf (1.42 mbsf)
16" casing shoe: 4431.0 mbrf (43.8 mbsf)
10-3/4" casing shoe: 4800.1 mbrf (412.9 mbsf)
Bottom 14-3/4" hole: 4810.2 mbrf (423.0 mbsf)
Upper 4-1/2" casing string length
467.44 m
Upper screen: 4840.00 mbrf (452.80 mbsf)
Packer top: 4856.06 mbrf (468.86 mbsf)
4.07 m
packer
8.52 m
Packer element: 4860.13 mbrf (472.93 mbsf)
4.45 m
Packer bottom: 4864.58 mbrf (477.38 mbsf)
16.15 m
Lower 4-1/2" casing string length
Screen top: 4880.73 mbrf (493.53 mbsf)
6.84 m
screen
12.12 m
Upper OsmoSampler
1.22 m
Screen: 4887.57 mbrf (500.37 mbsf)
5.28 m
13.43 m
Screen bottom: 4892.85 mbrf (505.65 mbsf)
1.22 m
Lower OsmoSampler
Lower OsmoSampler 4903.0 mbrf (515.8 mbsf)
5.0 m
Sinker bar
Sinker bar bottom: 4908.0 mbrf (520.8 mbsf)
Bottom 9-7/8" hole: 4987.1 mbrf (600.0 mbsf)

Figure F22

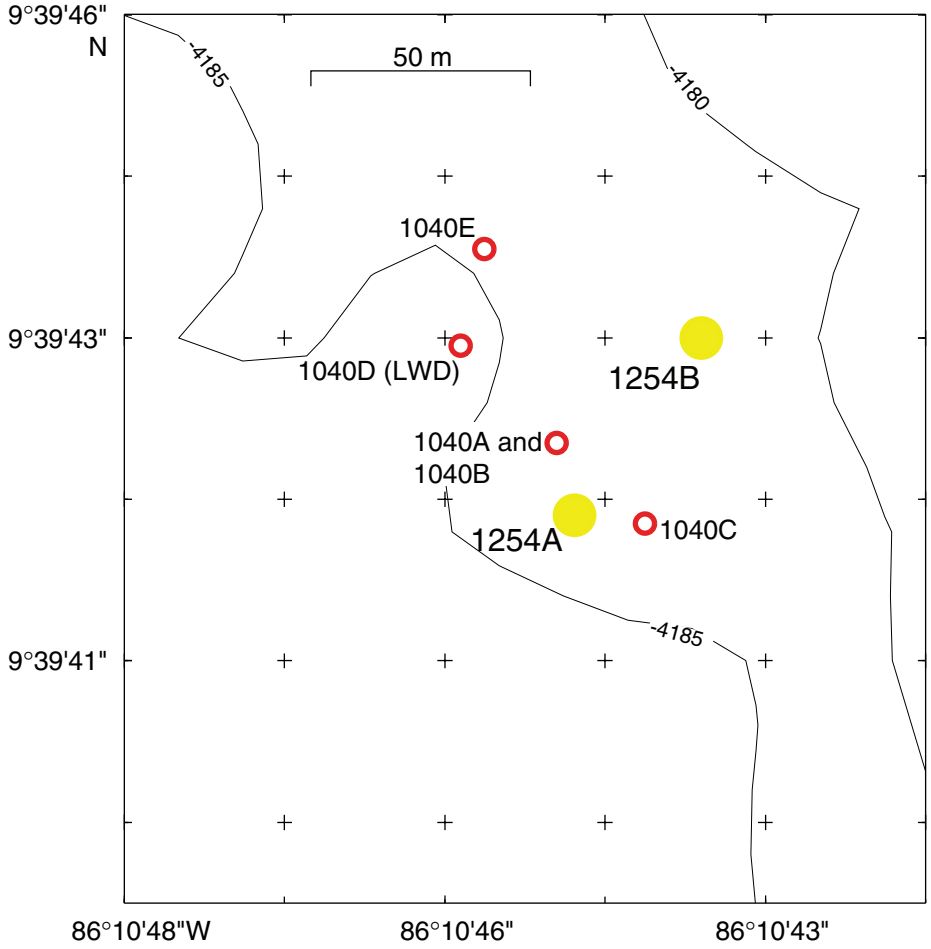
9°39'46"
N
9°39'43"
9°39'41"
86°10'48"W
86°10'46"
86°10'43"
50 m
-4185
-4180
-4185
1040E
1040D (LWD)
1254B
1040A and
1040B
1254A
1040C

Figure F23

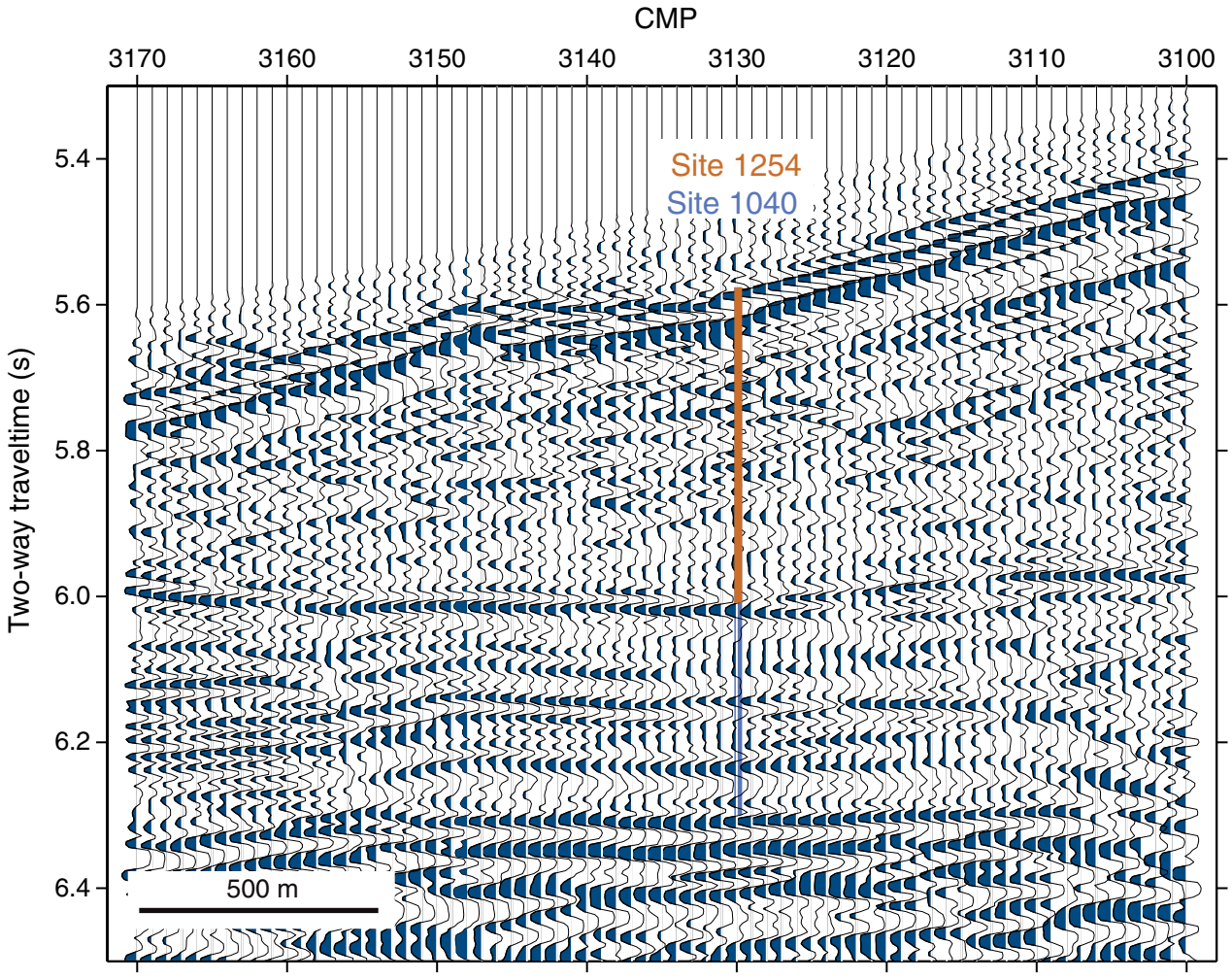
CMP
3170
3160
3150
3140
3130
3120
3110
3100
Site 1254
Site 1040
Two-way traveltime (s)
5.4
5.6
5.8
6.0
6.2
6.4
500 m

Figure F24

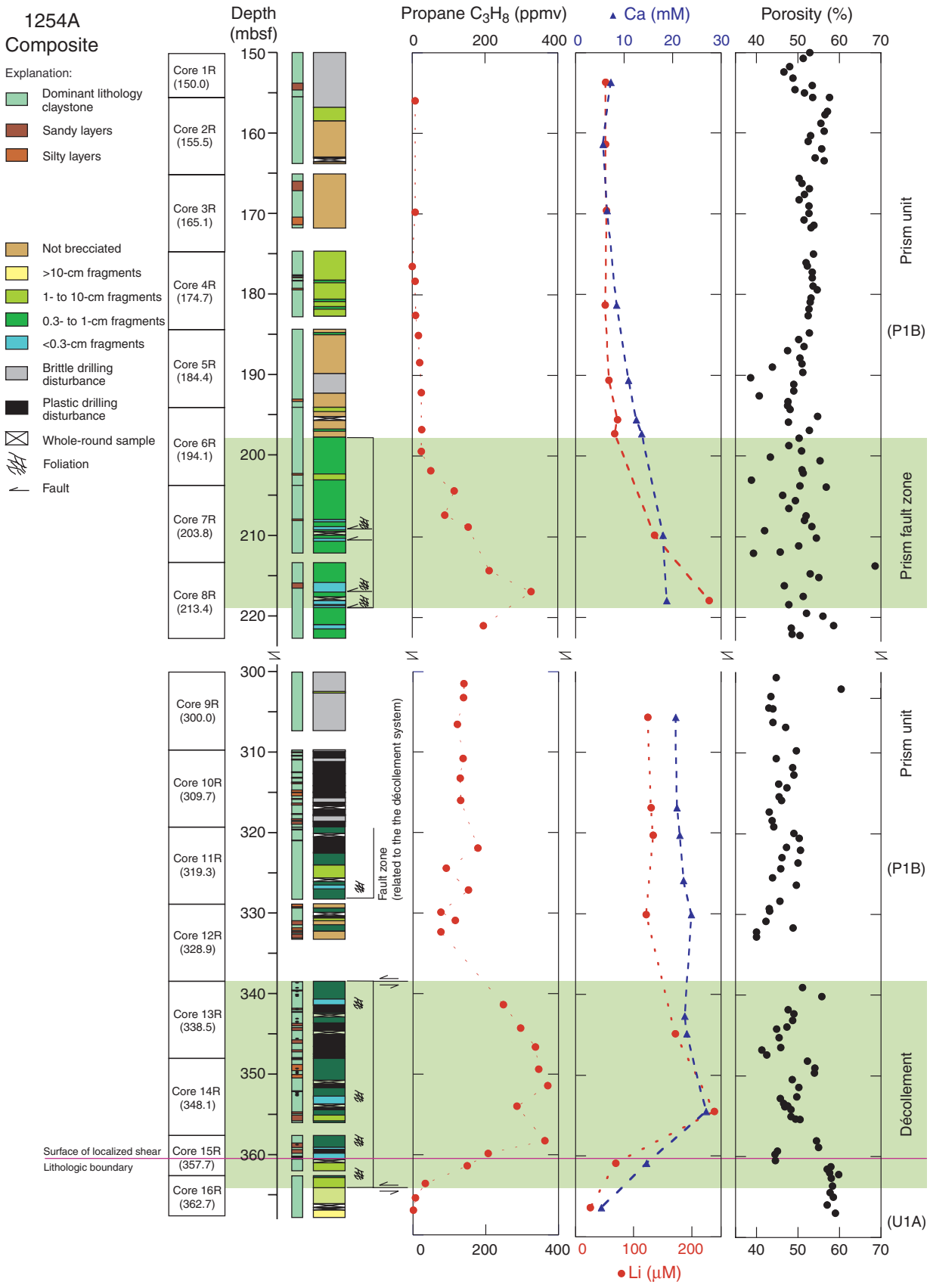
1254A
Composite
Explanation:
Dominant lithology claystone
Sandy layers
Silty layers
Not brecciated
>10-cm fragments
1- to 10-cm fragments
0.3- to 1-cm fragments
<0.3-cm fragments
Brittle drilling disturbance
Plastic drilling disturbance
Whole-round sample
Foliation
Fault
Depth (mbsf)
Propane C_3H_8 (ppmv)
Ca (mM)
Porosity (%)
Core 1R (150.0)
Core 2R (155.5)
Core 3R (165.1)
Core 4R (174.7)
Core 5R (184.4)
Core 6R (194.1)
Core 7R (203.8)
Core 8R (213.4)
Core 9R (300.0)
Core 10R (309.7)
Core 11R (319.3)
Core 12R (328.9)
Core 13R (338.5)
Core 14R (348.1)
Core 15R (357.7)
Core 16R (362.7)
Fault zone (related to the décollement system)
Surface of localized shear
Lithologic boundary
Prism unit
(P1B)
Prism fault zone
Prism unit
(P1B)
Décollement
(U1A)
Li (μM)

Figure F25

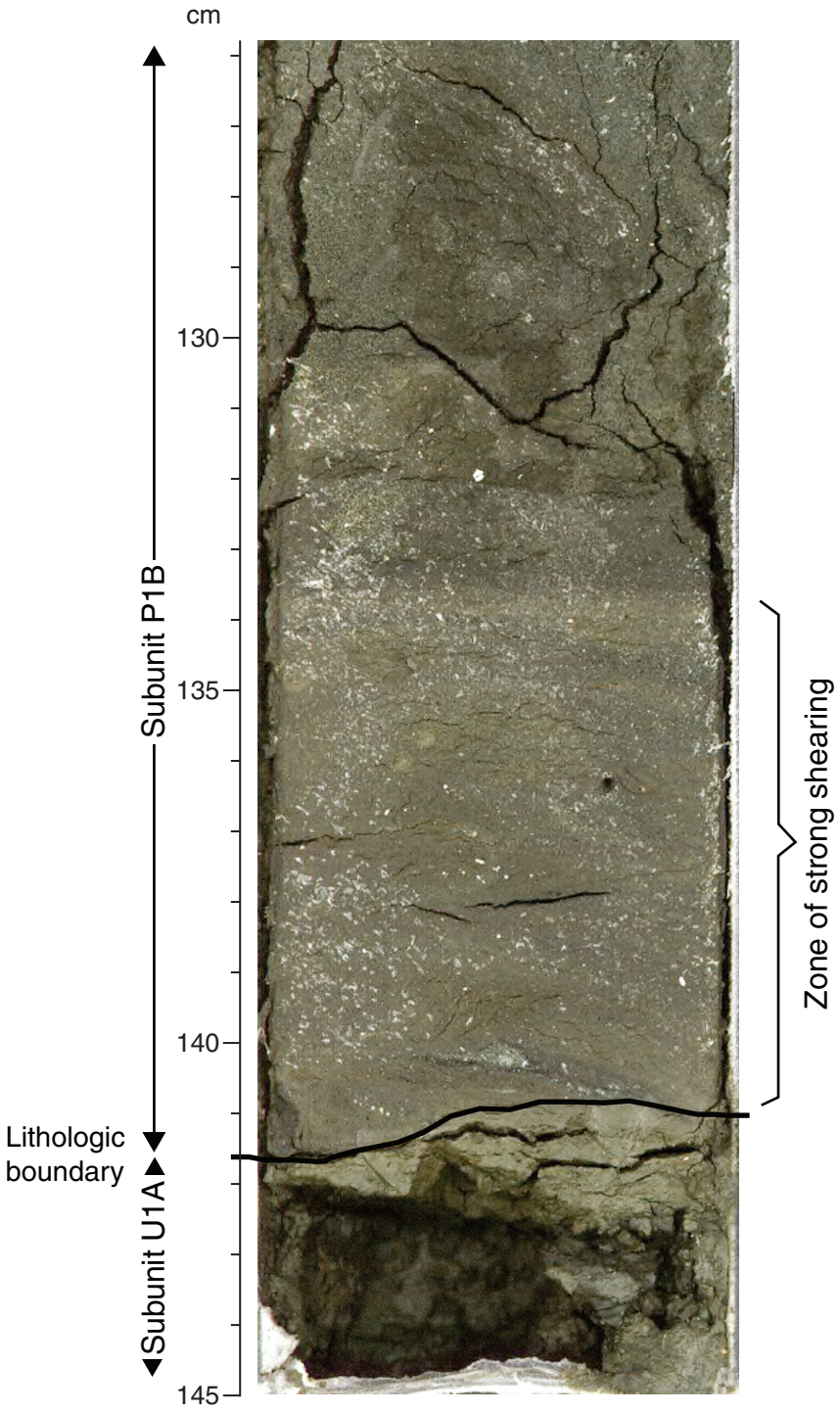
cm
130
135
140
145
Subunit P1B
Subunit U1A
Lithologic boundary
Zone of strong shearing

Figure F26

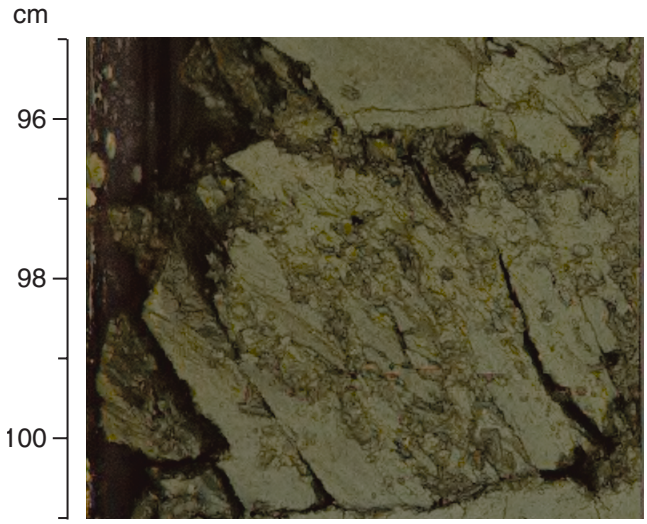

Figure F27

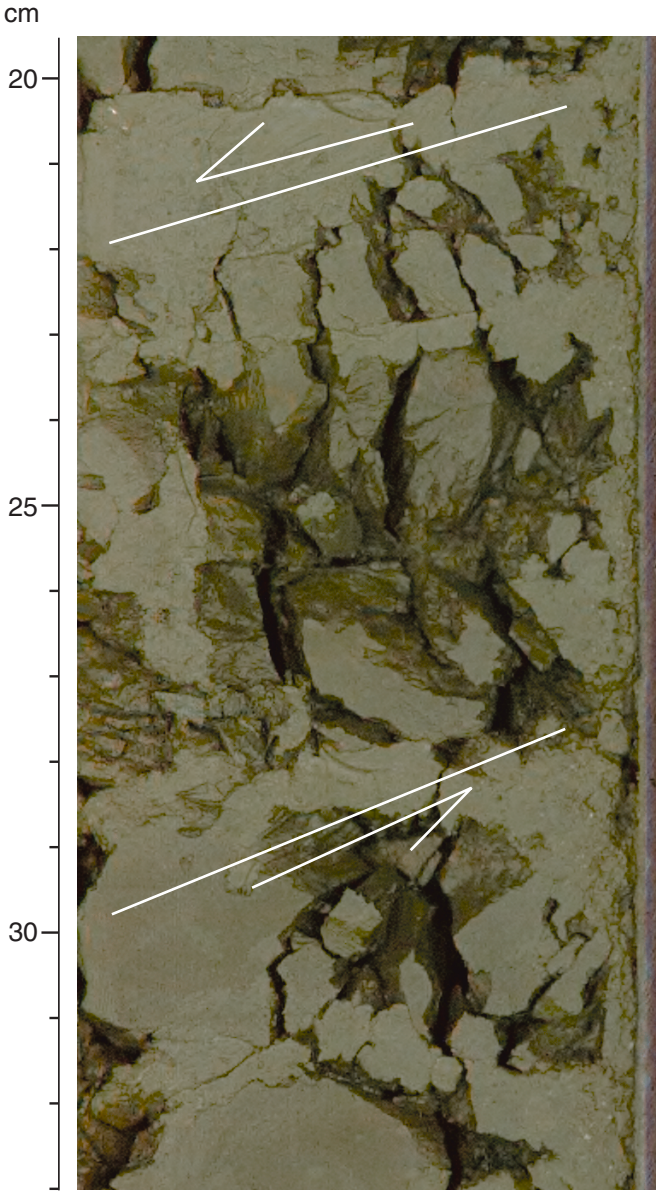

Figure F28

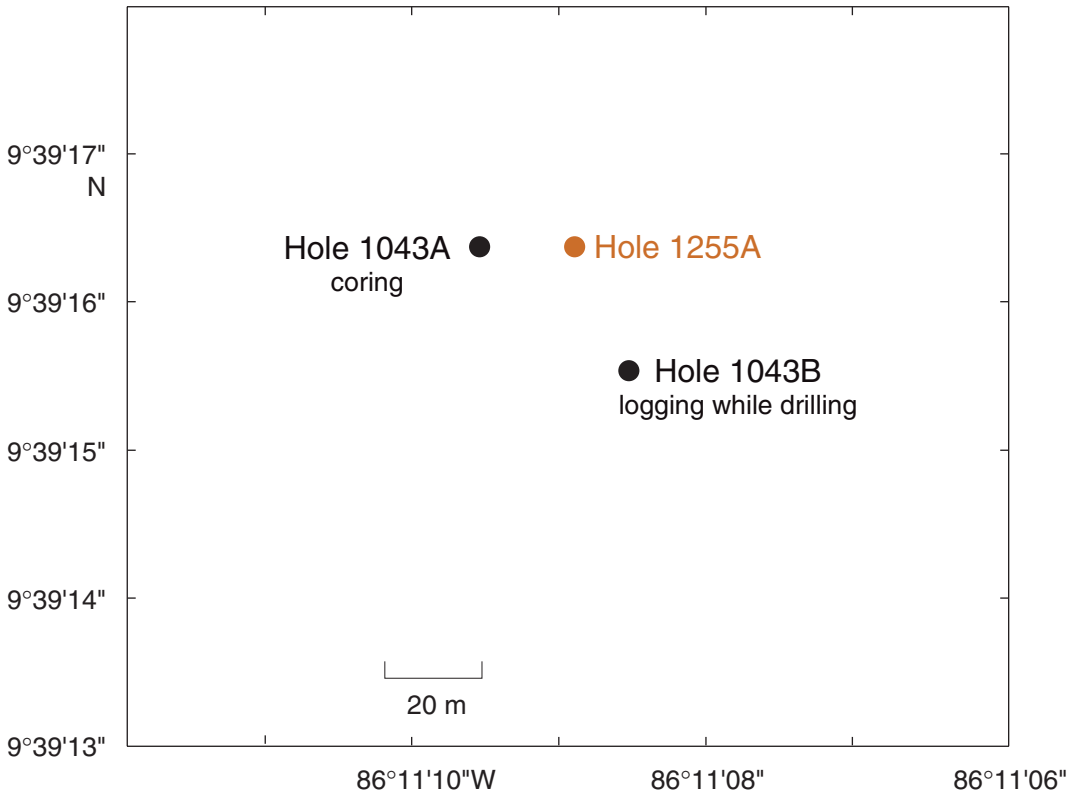
9°39'17"
N
9°39'16"
9°39'15"
9°39'14"
9°39'13"
Hole 1043A
coring
Hole 1255A
Hole 1043B
logging while drilling
20 m
86°11'10"W
86°11'08"
86°11'06"

Figure F29

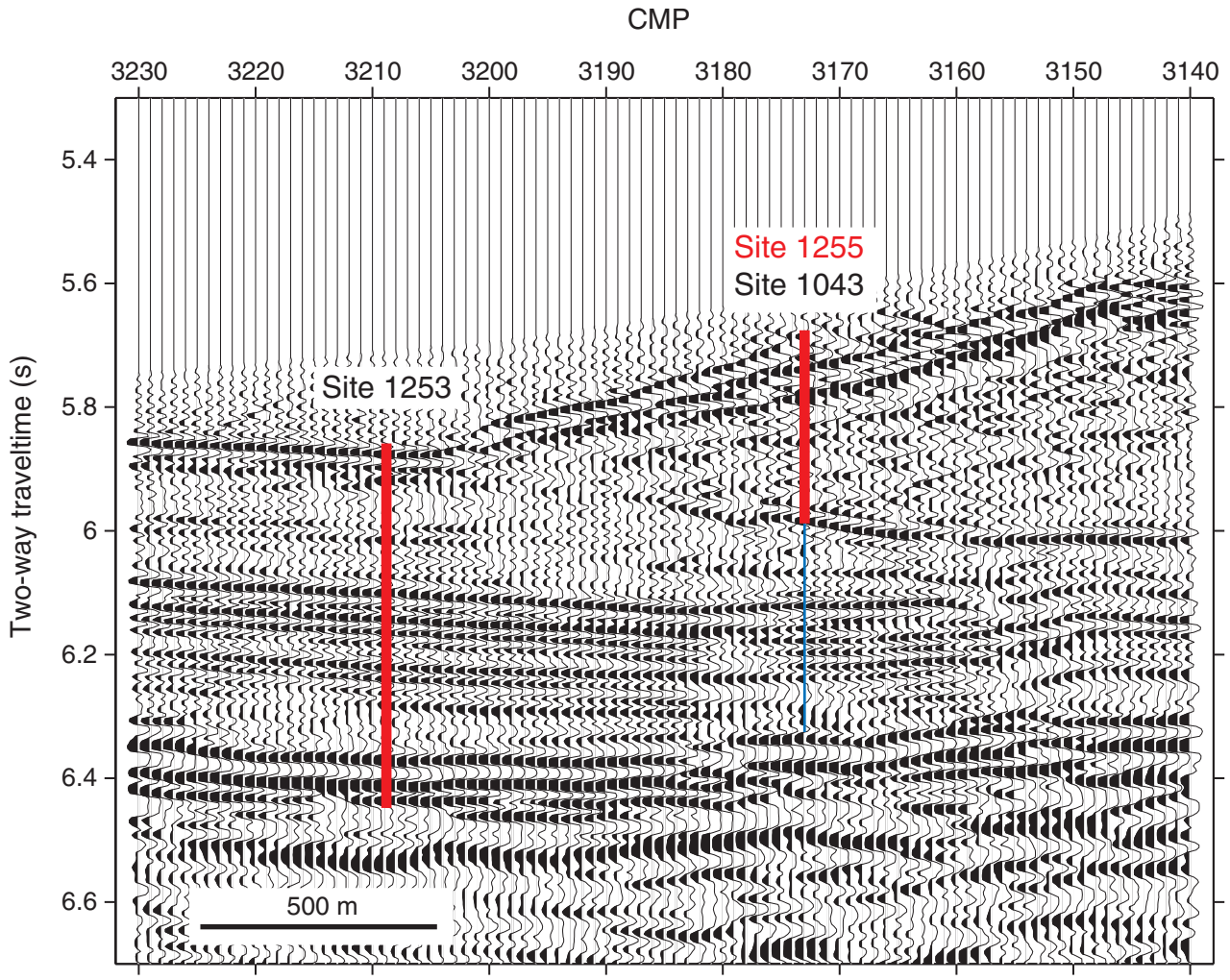
CMP
3230
3220
3210
3200
3190
3180
3170
3160
3150
3140
5.4
5.6
5.8
6
6.2
6.4
6.6
Two-way traveltime (s)
Site 1255
Site 1043
Site 1253
500 m

Figure F30

Hole 1255A CORK-II OsmoSampler installation space-out

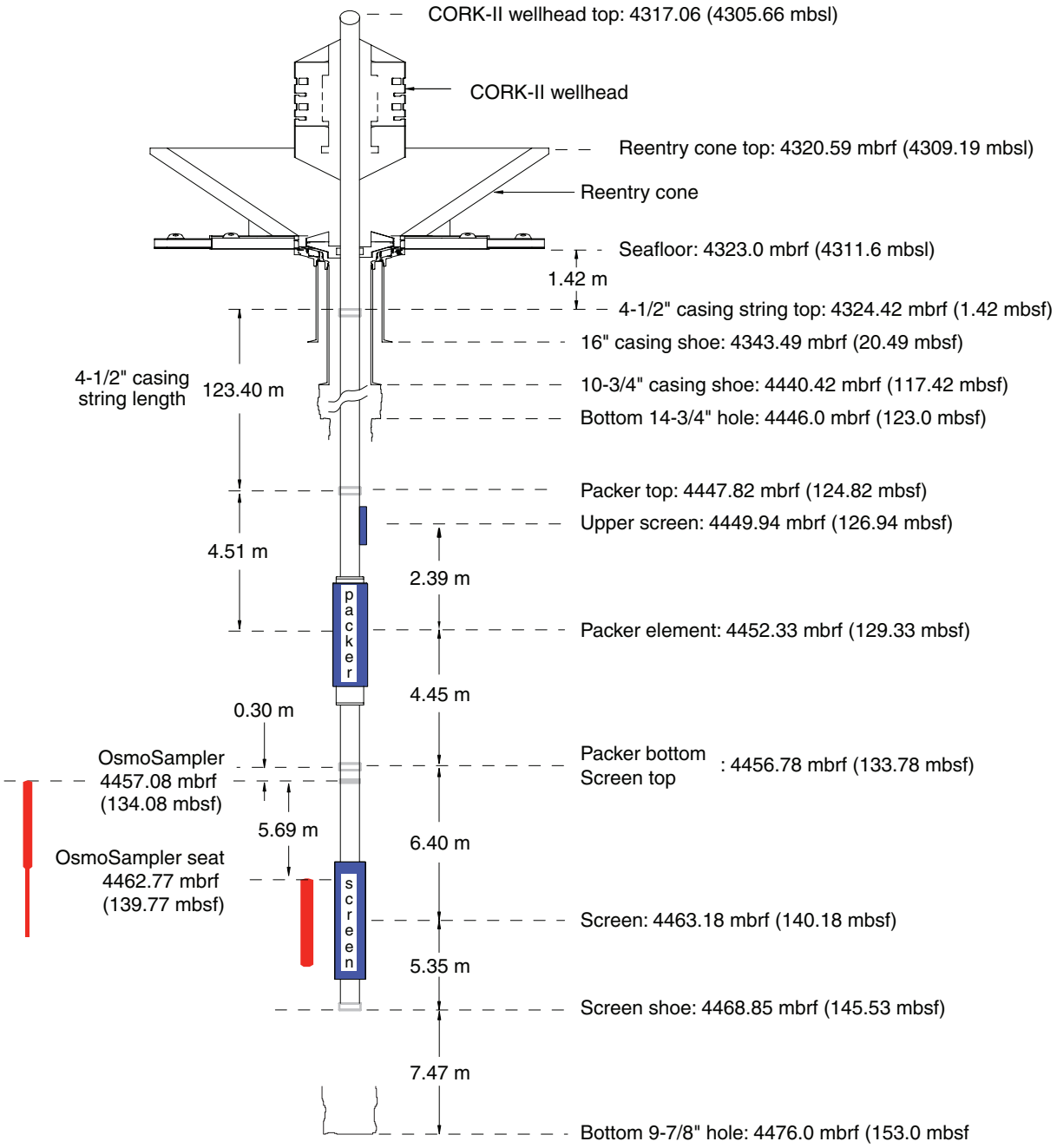

Figure F31